



OTTO VON GUERICKE  
UNIVERSITÄT  
MAGDEBURG

NAT

FAKULTÄT FÜR  
NATURWISSENSCHAFTEN

# Convection and segregation of beads in a flat rotating box

**Dissertation**

zur Erlangung des akademischen Grades

**doctor rerum naturalium**  
(Dr. rer. nat.)

genehmigt durch die Fakultät für Naturwissenschaften  
der Otto-von-Guericke-Universität Magdeburg

von Dipl.-Phys. Frank Rietz  
geb. am 03.10.1978 in Wippra

Gutachter:

Prof. Dr. Ralf Stannarius  
Prof. Dr. Peter J. Thomas

eingereicht am: 27.06.2012

verteidigt am: 12.10.2012



# Contents

<b>1</b>	<b>Introduction</b>	5	<b>6</b>	<b>Single rolls</b>	55
1.1	Selection of topic	5	6.1	General observations	55
1.2	Granular pattern formation	6	6.2	Flow oscillations	57
1.3	Dense granular convection	8	<b>7</b>	<b>Traveling waves</b>	63
1.4	Half-filled rotating drums	10	7.1	Traveling stripes	63
1.5	Densely filled rotating drums	12	7.2	Traveling rolls	69
<b>2</b>	<b>Experimental setup</b>	15	7.3	Comparison with literature	71
2.1	Experimental procedure	15	<b>8</b>	<b>Two-dimensional systems</b>	75
2.2	Experimental control	17	8.1	Spheres	75
2.3	Other setups	20	8.2	Discs	80
2.4	Evaluation methods	23	<b>9</b>	<b>Convection mechanisms</b>	89
<b>3</b>	<b>Convection &amp; segregation</b>	25	9.1	Fluidized zones	89
3.1	Fill level	25	9.2	Model 1: height differences	91
3.2	Axial segregation	27	9.3	Model 2: density differences	92
3.3	Convection rolls	27	<b>10</b>	<b>Conclusions</b>	95
3.4	Convection reproducibility	29	10.1	Roadmap to the future	95
3.5	Transition	33	10.2	Summary	97
<b>4</b>	<b>Influence of driving</b>	35	10.3	Deutsche Zusammenfassung	98
4.1	Rotation speed	35	<b>Appendices</b>		102
4.2	Rotation scheme	35	<b>A</b>	<b>Public outreach</b>	103
4.3	Interstitial medium	36	A.1	Rotating box	103
4.4	Shaking	38	A.2	Sphere packings	105
<b>5</b>	<b>Geometrical influences</b>	41	<b>B</b>	<b>Acknowledgement</b>	107
5.1	Cell aspect ratio	41	<b>Bibliography</b>		109
5.2	Smallest cell size	42			
5.3	Left/right walls	42			
5.4	Top/bottom walls	44			
5.5	Cell thickness	46			
5.6	Cylindrical container	48			
5.7	Initial preparation	50			
5.8	Variation of granulate	51			
5.9	Monodisperse granulate	53			

## Contents

important symbols:

$C$	fill ratio
$C_C$	critical fill ratio
$x, y, z$	cell width, height, depth
$g$	Earth's gravity
<i>Froude</i>	Froude number
[rpm]	rotations per minute

### Statement of autorship

I, Frank Rietz confirm that the work presented in this thesis has been performed and interpreted solely by myself except where explicitly identified to the contrary. I confirm that this work has not been submitted elsewhere in any other form for the fulfilment of any other degree or qualification.

Frank Rietz

Magdeburg, January 30, 2013

### Copyright statement

Some pictures of the thesis have already been published with some modifications in APS journals 'Physical Review Letters' and 'Physical Review E' and in IOP journal 'New Journal of Physics'. Holder of the copyrights are the corresponding publishers.

# 1 Introduction

## 1.1 Selection of topic

The initial scope of the thesis was not set in narrow frames. It had to be based on the pattern formation in rotating drums since there were already some experiences in the laboratory within the department. The system that is investigated in the thesis was discovered accidentally after about half a year of unsuccessful trials. The procedure which nobody had expected anything interesting gave a breakthrough: A flat container was almost completely filled with grains and rotated slowly. If one of the external parameters, for example the amount of grain material, had been slightly chosen differently, coupled with diminishing experimenter's motivation, this thesis would not have exist. The idea to perform these experiments was motivated by a computer simulation [1] however it is still unclear whether the simulation has anything in common with the system that was found (see chapter 8). The results came unexpectedly compared to other experiments known so far. The first picture of the structure dates from February 5, 2006 (figure 1.1).

The grains are arranged in a serpent-like pattern. It became clear that the grains moved in a convective motion and it turned out that this dynamics might be more interesting than the pattern itself. A setup was built in order to observe automatically the development of the convection. Hundreds of experiments were performed to find out the reason for that observation. Instead of approaching to the explanations gradually, new phenomena were discovered one after the other. They appeared to be also far from understanding. In the last years extensive investigations and popularizing among experts were done. Surprisingly there is so far no real clue to the convection mechanism, not to mention any formula. This is surprising and unsatisfying for a thesis and has brought a mysterious atmosphere.

In the thesis the phenomena observed in a flat rotating drum are described in more detail. Examples of pattern formation in granular media that might be related to the discovery are introduced in the next section 1.2. Then experimental setups and main methods are described in chapter 2. The basic underlying effects i.e. segregation and convection are topic of chapter 3. The next chapters 4 and 5 are dedicated to the question how the system depends on external driving and geometrical parameters. The special observation of single rolls and traveling waves was made and described in chapters 6 and 7. After that the

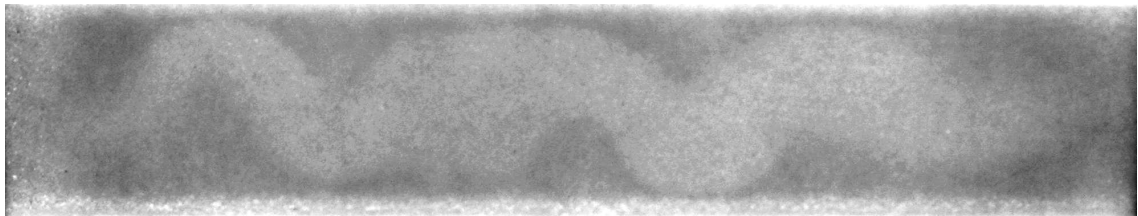


**Figure 1.1:** First photography of a granular convection pattern in a horizontally rotating container. The picture is taken in transmission after  $\approx 10,000$  rotations. The attention of the experimenter was attracted by the unusual pattern at high fill level. Convective motion was concluded and shortly after proven in image series of subsequent experiments. Topic of the thesis is the investigation of the depicted structure. The free space on top of the grains is  $\approx 1$  mm. Top and bottom container boundaries are cut in the image. (container dimensions: width $\times$ height $\times$ depth = 500 mm $\times$ 100 mm $\times$ 5 mm).

results of two-dimensional tests are presented in chapter 8. Ideas about possible convection mechanisms are given in chapter 9. A list of related experiments that should be done in the future and a summary finish the main part of the thesis in chapter 10.

### 1.2 Granular pattern formation

The structure introduced previously belongs to the class of self-organized patterns in granular media. Study of granular media concerns assemblies of macroscopic particles that are large enough so that thermal motion (and depending on definition also van der Waals forces) are negligible in comparison with force due to gravity. This is the case if particles have a minimum size of  $1 - 100 \mu\text{m}$ . If the system is externally driven the only interactions in dry systems are via repulsive dissipative particle collisions. Cooperative dynamics under continuous energy input can lead to structure formation.

Granular media are ubiquitous in everyday life, e.g. in the form of food and pharmaceutical items, in mining, agriculture or in construction trade. In many industrial branches, products are packed, transported and distributed in granular form [2] not forgetting customary beads decorations [3]. Geophysical processes are often related to the granular structure of soil, for example instability of sandbars in Grand Canyon [4] or desert structures [5]. From an engineering point of view, packing properties and granular dynamics under external agitation pose a multitude of problems. Under shearing, vibration or rotation, granular materials in some respect may behave similar to liquids, but often, unexpected and even counterintuitive effects are observed. Unwanted segregation leads to high costs in industry requiring special sophisticated particle technology [6, 7]. In the pharmaceutical industry where optimal mixing plays an important role [8] a powder formulation not meeting uniformity can lead to disposal of the batch that could be worth millions of dollars [9]. A long-standing problem of powder storage is demixing during hopper discharge [10]. Besides achievement of homogeneous mixtures also particle separation is relevant [11, 12]. Research about granular problems in food processing is funded by the EU [13]. Another particle issue is centrifugal fertilizer spreading in agriculture [14].

Simplified experiments have proven to be suitable descriptions for more complex real situations. Chute flow studies with glass beads lead to better understanding of debris flow [15]. Other experiments try to generate artificial Martian-like surface structures [16] or try to get insights in the flow in nuclear pebble bed reactors [17]. The Discrete Element Methods (DEM) have become an essential tool where experimental access is not easily possible [18].

The complexity of granulates has withstood a description within a unified theory so far. The difficult situation was chosen as one of the biggest problems in natural science ever: ‘Can we develop a general theory of [...] the motion of granular materials? So far, such “nonequilibrium systems” defy the tool kit of statistical mechanics, and the failure leaves a gaping hole in physics.’ [19]. Phenomena related to dense flow and jamming have become central topics of research activities [20–25]. During the past decades, there has also been an increased interest in pattern formation of granulates [26–34].

Even relatively simple equipment can produce rich varieties of novel and challenging experimental phenomena that are beyond our current understanding. That is what makes granular science quite exciting. Some examples of granular pattern formation are depicted in figure 1.2. With minimal effort one reproduces the pattern in figure 1.2a. Slowly pouring a particle mixture into a narrow cell results in a stratification pattern [35]. Such a self-sorting might have similar reasons as layered textures of sandstones [36]. More complex patterns emerge when a shallow bed of particles is strongly vertically shaken. During

vibration the surface corrugations can for example look like spirals (figure 1.2b) or spiral defect chaos (figure 1.2c). The latter pattern is originally known from heated shallow fluid layers [37]. The liquid-like behavior of granulates is also manifested in convective motion that is phenomenologically similar to Rayleigh-Bénard convection [38,39]. Figure 1.2d shows a box filled with monodisperse beads. After vertically shaking the box four convection rolls form (red arrows in figure 1.2e). In this experiment the rolls are visualized by dark tracers which initially cover the white beads. When agitated the tracers move along the convection streams and leave a trace. Granular convection<sup>1</sup> is commonly observed in shaken experiments [41]. Vibration plays also a role in recycling of electronic waste [42] or in future laser applications [43]. Another way to add energy is by rotation. If a half-filled cylinder is filled with a bidisperse mixture it is known that axially demixed bands can emerge (figure 1.2f). The flat rotating container is to some extent related to the rotating cylinder. More details will be given in section 1.4.

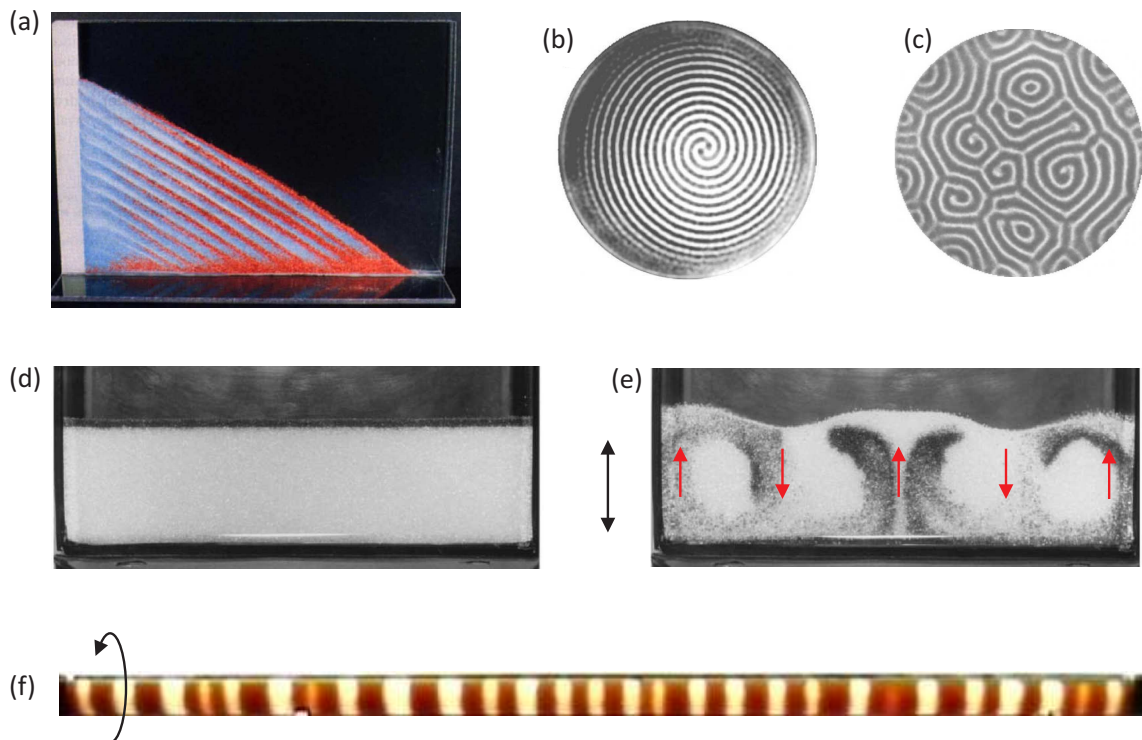


**Figure 1.2:** Typical examples of granular patterns. (a) Stratification of beads poured from the left side into a narrow cell. A mixture of three kinds of beads is used (white 0.15 mm, blue 0.4 mm, red 0.8 mm), from [35]. (b,c) Shaken shallow bead layers can exhibit (b) two-armed spirals (15.4 layers at 2.81 g) or (c) spiral defect chaos (6.7 layers at 3.13 g). Bright/dark indicates elevation/depression of the particle bed, particle size 165  $\mu\text{m}$ , from [44]. (d,e) Convection rolls in a bulky granular bed. (d) Initial state, a few black colored layers are on top of white beads. (e) Shaking in direction of the black arrow drives four convection rolls, visible by the dark tracers. (bead size 0.61 mm, 50 Hz, 6.4 g, after 8 s shaking, bed height: 5 cm, width: 20 cm, depth: 3 cm), from [45]. (f) Rotation of a half-filled drum separates initially mixed granulate into bands of large (orange, 1.5 mm) and small (white, 0.6 mm) particles. The particles are immersed in water. (cylinder length: 1 m, diameter: 3.7 cm, 20 rpm).

<sup>1</sup>The term ‘granular convection’ is also used in astrophysics for convection cells (so called ‘granules’) on the sun [40]. Inflow and outflow of plasma leads to a granulated appearance of the sun’s protosphere.

### 1.3 Dense granular convection

For the case of the convection in figure 1.2e, grains are strongly fluidized i.e. the whole granulate expands during agitation. Particles can collectively rearrange and flow. In contrast, in the almost completely filled flat container only low fluidization is possible. In the following, subsurface situations are mentioned, where convection under limited fluidization takes place or where it is at least assumed. It is known that slow fluxes occur in deep layers where the grains do not have individual degrees of freedom for positional changes [46]. Only a few situations with convection at restricted fluidization were found in the literature. They are partly governed by hydrodynamic laws but interactions with grains play also a role. Similarities to the rotating flat cell might be speculative. However, insufficient explained systems that are only partly comparable might have a common solution.

In periglacial climate zones daily freeze-thaw cycles lead to convection rolls in the soil. If a frozen soil thaws at the surface the density anomaly of water causes water to descend from the surface. Water in deeper layers is lighter and ascends and convection begins through the porous soil moving the thaw front upwards (figure 1.3b). The subsurface rolls carry stone material that imprint a polygon, stripe or circle pattern (figure 1.3a) on the surface [47]. There are also competitive theories claiming different heat conduction between stones and soil as the main reason [48].

Offshore piles for wind turbines are periodically exposed to lateral forces of water waves and wind. In a small scale experiment [49] several million times lateral force cycles were applied on a pile that is grounded in sand. Cyclic load resulted in convection around the pile (arrows in figure 1.3c) that might have consequences for the long-term stability of offshore piles.

Convection in the Earth's mantle was simulated in a small-scale experiment with putty layers that contain small particles. Six putty layers were horizontally stratified in a disc. Layers were sorted in increasing order of density. Then the disc was strongly centrifuged in a way that forces act in the direction of the density gradient. Inertial forces made the stratification unstable and convection rolls are formed. A cut through the disc shaped putty (figure 1.3d) is depicted in figure 1.3e.

Salt domes contain layers of pure white halite interbedded with layers of black halite and anhydrite. Overburden denser sediments create buoyancy forces and the layers are complexly folded. The dark pattern in figure 1.3f looks like a serpent.

Diffusive transport in the upper crust of the Earth is assumed (figure 1.3g). In the higher porosity region the solubility of the fluid is higher than in the surrounding region. Therefore the density of the fluid increases and the fluid descends. Loss of solutes leads then to an ascent of the fluid. It is speculated that by addition of chemical reactions and gradients in temperature these processes can result in a kilometer-scale convection roll with velocities in the order of 1 cm/year [50, 51].

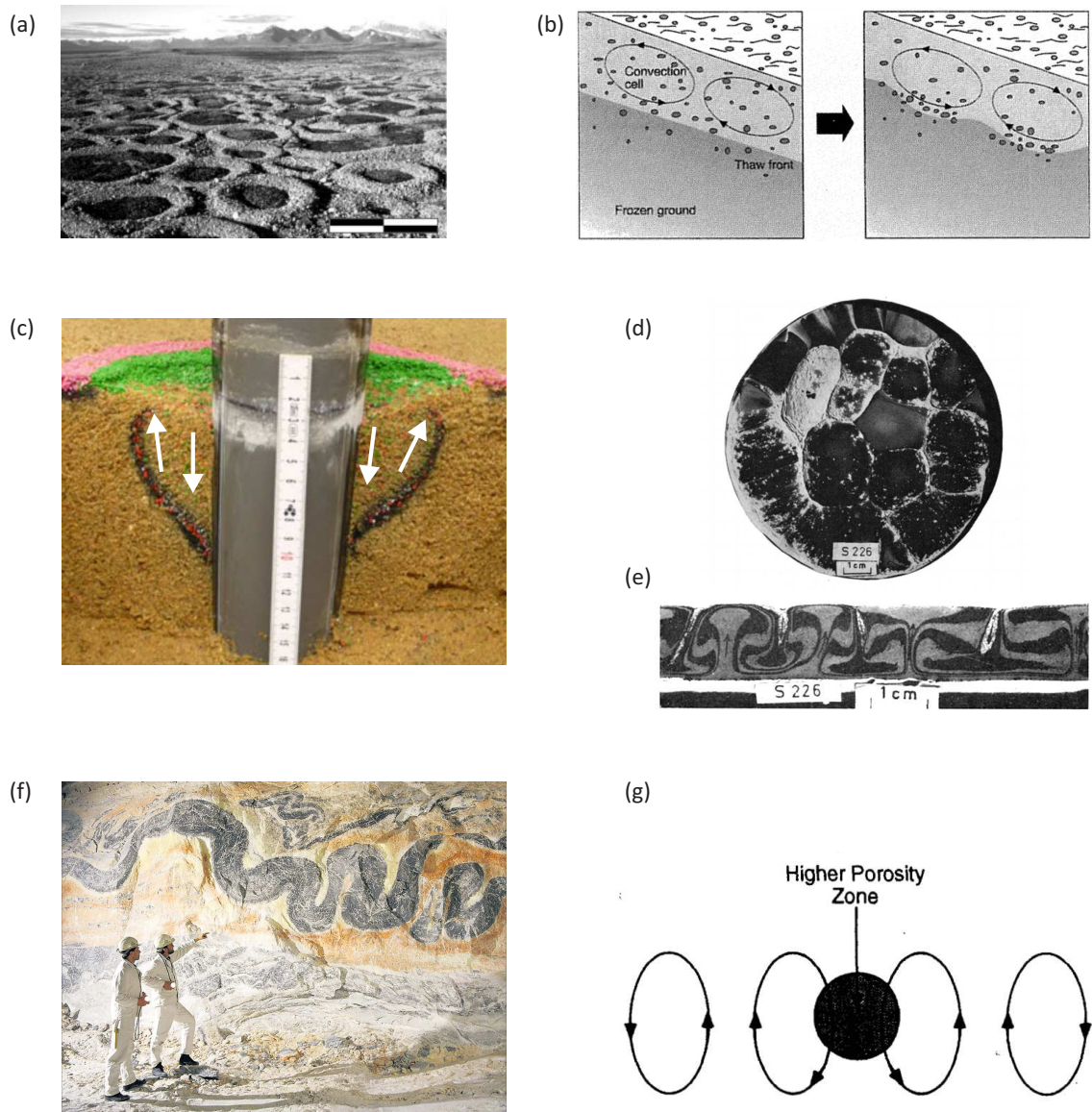


**Figure 1.3:** Subsurface convection under low fluidization. (a) Stone circles in Spitsbergen (diameter 2 m, from [48]), caused by density inversion. (b) Sketch of contributing processes. Ice at the thaw front melts and water rises upward whereas denser water at  $\approx 4^{\circ}\text{C}$  sinks from the surface, from [33]. (c) Convection roll due to cyclic pile load. The pile was partly excavated afterwards. The black contour are tracers that were initially at the surface. The convection zone lies between pile and black line, flow is indicated by arrows, from [49]. (d,e) Centrifuged stratification of six putty layers with different density. (d) Top view of the disc. Cellular convection cells are visible. (e) Cut through the disc. Dome-shaped flow after centrifuging at  $800g$ , height: 12 mm., from [52]. (f) Overburden denser sediments lead to folding of lighter salt layers, from [53]. (g) Supposed kilometer-scale convection in the upper crust of the Earth. Porosity fluctuations lead to different solubility and density inversion, from [51].

## 1.4 Half-filled rotating drums

If the drum is rotated in the continuous avalanching regime [54], the surface forms a constant angle of repose with the horizontal (green lines in figure 1.4a). Only in a shallow surface layer, particles tumble down (red zone in figure 1.4b). The remaining granulate rotates together with the container. The rotation rates are small enough to neglect inertial forces which is expressed using the *Froude* number. The *Froude* number is the ratio of inertial to gravitation forces and in a rotating system  $Froude = \omega^2 r / g$ , with  $\omega$  the angular velocity,  $r$  the farthest distance of the cell interior to the rotation axis and  $g$  gravity. Inertial forces are negligible if  $Froude \ll 1$ .

If a bidisperse mixture of differently sized grains is rotated horizontally in a cylindrical drum, a complex scenario of segregation processes is found. Small particles chute down the surface and are trapped easy in interstitial voids than large particles. The smaller particles form a core in the central drum area (red encircled in figure 1.4a). This sieving process is called radial segregation. Axial segregation can be observed at longer timescales. The segregated components form axial stripe patterns after circa 100 rotations (figure 1.2f). Merging of these stripes (coarsening) can follow on even in longer time scales. Axial demixing in a horizontal rotating container was first described by Ôyama [55] in 1939. However the effect had been known to engineers even earlier (see discussion in reference [26]). Nowadays the rotating drum represents a standard system to study granular segregation. The rotating drum model serves as a system for mixing studies [56, 57], for rotating bioreactors [58, 59] and has applications in the form of rotary kilns [60] or sorting of ore particles [61]. For a general review of pattern formation in rotating drums please refer to reference [34].

Radial segregation in the rotating drum is easily explained by sieving. However axial segregation and coarsening are not well understood. Formation of axial bands can be seen as follows: The initial mixed state has some concentration fluctuations along the rotation axis. Larger particles have a smaller angle of repose than the mixture as the latter has a higher packing density, and is more resistant against shear. Due to height gradients of different angles of repose, large particles from the mixed region flow down to the lower regions that are enriched with large particles. In this way small fluctuations self-amplify and bands form. End wall friction might also play a role due to the collection of small particles at the side walls [62]. The validity of the model was supported by systematic variations of the angle of repose. At lower speed, the angles of repose for both species are identical and no segregation took place. At higher rotation rate, the difference in the angles of repose increases accompanied by segregation [63, 64]. Other theories assume fluctuations in the radial core that might couple with the angle of repose [65]. There is no model that explains coarsening. One might speculate whether the interfaces between demixed phases can be considered as a kind of ‘surface tension’. Analogous to liquids the system tries to reduce surface tension by band merging [66]. No axial segregation by pure density differences could be found [67], but probably pure elasticity differences are sufficient [68].

Theoretical models have been conceived to explain axial segregation [69–72]. They can only be applied on a very simple level. The observed experimental effects are too complex and often contradict postulated theories. Information about single particles can be obtained in simulations. Discrete Element Methods (DEM) can currently only simulate a few drum rotations in a useful time period. To give an example, 200 drum rotations filled with 50,000 particles required 6 weeks of calculation time [73]. However the dynamics in the thesis are in some cases observable only on time scales from at least 10,000 rotations.

At higher fill ratios, the fluidized area shrinks (small red zone in figure 1.4c) and the majority of the grains rotate in a jammed state. In contrast to cylinders there is no continuous flow in the flat cell geometry. Only every  $180^\circ$  rotation chuting occurs if the container exceeds an angle similar to the angle of repose (figure 1.4e,f). For the most time the beads only redistribute among their neighbors. Flow measurements of chute flow [74] have revealed the velocity profile along the cell depth (figure 1.4d). There is higher friction and smaller flow speed at the lower granulate edge because of pressure by overburden material. If the cell is continuously rotated, the shear gradient produces a vortex motion in the sense of driving.

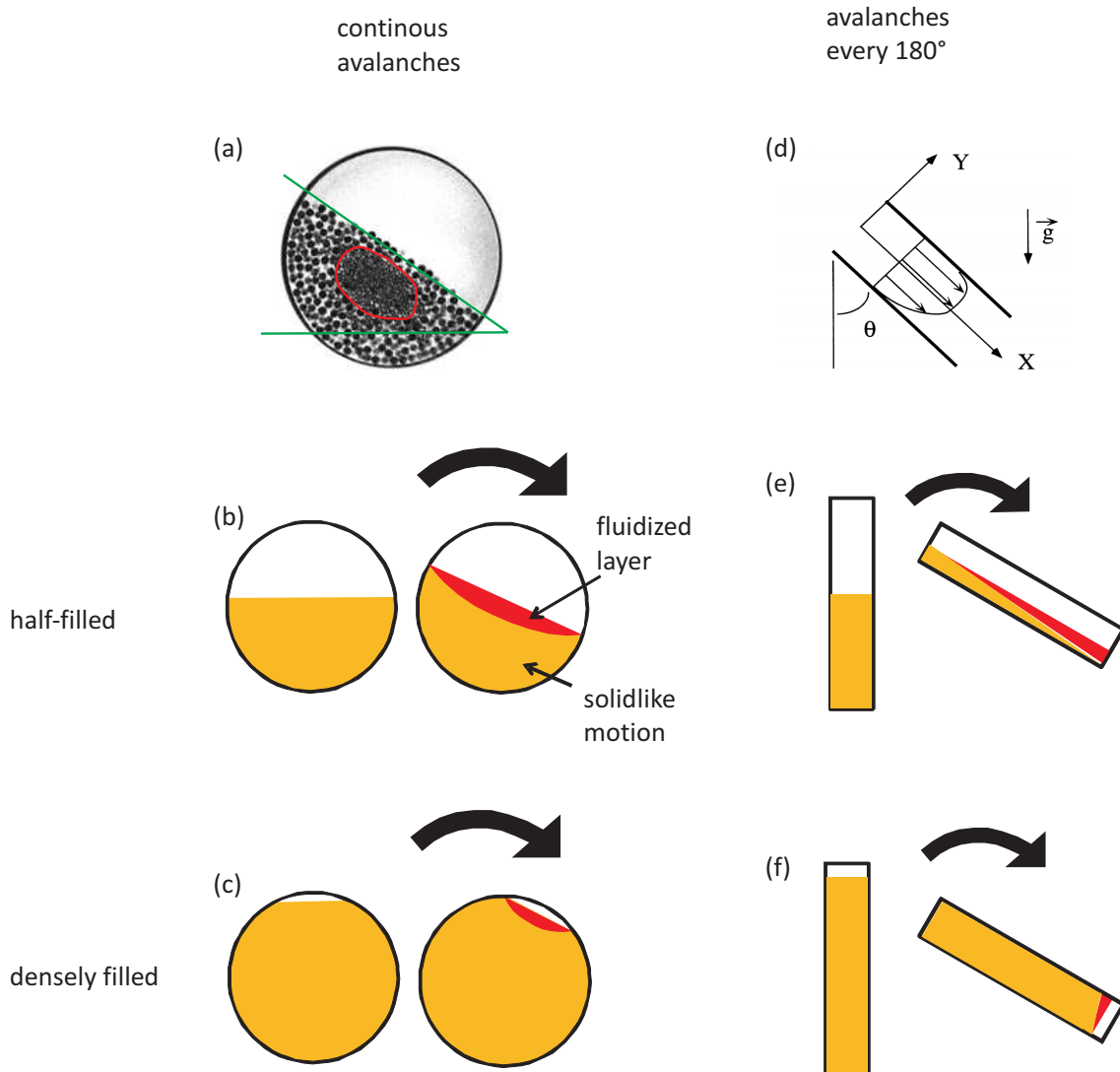


**Figure 1.4:** Flow in boxes with circular and rectangular cross sections for half and almost completely filled cases. Pair wise, the non-rotating and rotating states are sketched. (a) Radial slice along the tube from a reconstruction by Magnetic Resonance Imaging (MRI). Small particles are radially segregated (confined by red zone). Green lines span the angle of repose with the horizontal, adapted from [75]. (b) Flow regimes in a half and (c) densely filled cylinder. Material in the red marked area flows continuously. (d) Qualitative velocity profile for confined chute flow. The velocity is lowest at the sliding plane, from [74]. (e,f) Corresponding flow regimes for the flat container. Chute flow takes place only every half rotation.

## 1 Introduction

Besides in cylinders (figure 1.5a, [26, 65, 76–85]), axial segregation was also observed in boxes with square cross sections (figure 1.5d, [76, 84]) or spherically shaped tumblers (figure 1.5c, [86, 87]). Mixing studies were done using conical (figure 1.5h, [88, 89]), double-conical (figure 1.5b, [90, 91]), V-shaped (figure 1.5e, [92]) or two-dimensional containers (figure 1.5g, [93–95]). Two-dimensionality in this case means a short drum expansion along the rotation axis. Whereas the two-dimensional type is the most prominent shape, when one considers the number of publications, there are no experiments with containers that exhibit two-dimensionality perpendicular to the rotation axis (figure 1.5f). Hence, this geometry is used throughout the thesis.

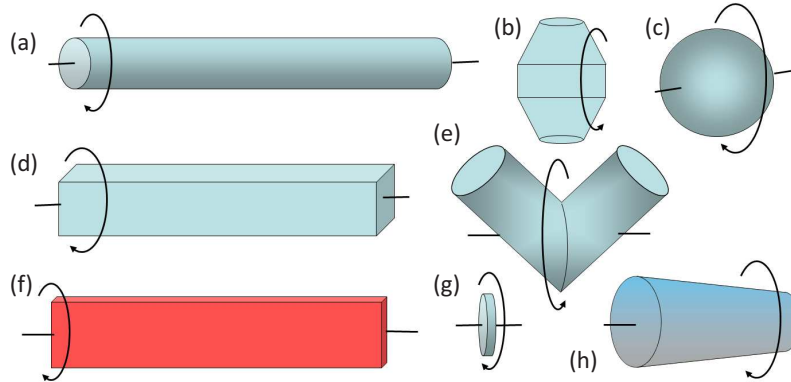


**Figure 1.5:** For the rotating drum there are following typical container shapes: (a) cylindrical, (b) double-conical, (c) spherical, (d) square (e) V-like, (h) conical. Concerning two-dimensional boxes there are two possible realizations. Often type (g) is used but no other study deals with flat containers like (f).

## 1.5 Densely filled rotating drums

The majority of these experiments deal with rotating drums that are approximately half full (but  $\geq 80\%$  fill level for drums like figure 1.5g [95–98]). There, fluidization of the granulate surface plays the most important role in the emergence of axial segregation patterns. In densely packed systems, geometrical restrictions prevent the independent motion of particles, and slow and collective dynamics are observed. Access to the inner structure of the granular bed is often limited to invasive methods, and conclusions on subsurface convection have to be derived indirectly.

However, there are a few experiments [80, 81, 99] and simulations [1] dealing with horizontally rotated drums that are almost completely filled with granulate. Contrary to expectation, these studies demonstrate that pattern formation can even occur when fluidization is strongly inhibited.

In simulations of a truly two-dimensional cell [1] (reprinted with slight changes in [99–101]) segregation and global convection at high fill level were reported. Rotations of bidisperse packings of 750 particles were simulated. Depending on the rotation rate, different phases can be found. At low speed, small particles assemble along the drum center. At higher rotation rate, the situation reverses (figure 1.6a,b). This can be explained as follows: at low speed, the outer regions are diluter because of particle rearrangements during sliding. Larger discs move easier in diluter outer regions than to the more compact core. At higher speed, particles are driven outwards and smaller discs easier find easier voids for passing.

The situation in figure 1.6a is not stable and develops toward a situation as in figure 1.6c. There, particles are axially segregated and the interfaces between small and large discs are tilted. Small particles cannot penetrate this interface and they move along the interface forming a global convection roll. Large particles cannot find voids in the central region that is rich by small particles. They are dragged by the smaller species and form a similar roll motion (figure 1.6d).

There are three experiments that deal with rotation experiments using highly filled long cylindrical drums [80, 81, 99]. Nakagawa *et al.* [99] (similar in [102, 103]) used Magnetic Resonance Imaging (MRI) to discover particle migration at almost completely filled cylinders (the exact fill height is not stated). A cylinder with axially demixed components was prepared and then rotated. MRI revealed radial ring-like segregation and axial migration of particles inside the drum (figure 1.6e).

Kuo *et al.* [80] ‘froze’ and cut drums that had been rotated at fill levels up to 90%. The cutting procedure is shown in figure 1.6f. The cuts show more complex patterns than expected by usual radial segregation. Therefore, the authors indirectly conclude on the existence of some kind of convective currents: ‘there are convective currents within the core that strongly affect segregation, even at large fills (whereas current dogma says that the core, once formed, is static)’.

Inagaki and Yoshikawa [81] rotated a cylinder with initial demixed phases at 96% fill level (figure 1.6j). Traveling waves on the granular surface were observed ((figure 1.6(k-n)). By cutting the cylinder similarly like in the previous study a global convection roll inside the granular bed was conjectured from the segregation structure (see section 7.3). In addition to these experiments at high fill level, Losert *et al.* [85] also speculate that slow convective currents occur in axial segregation bands in half-filled rotating drums. In all mentioned experiments convection rolls were never directly observed. They were concluded as possible explanation of the results.

To summarize, no direct observation of convection had been made in a rotating drum so far. There are many convection studies with fluidized granulates and some subsurface scenarios at low fluidization. The latter are difficult to observe. It seems that the flat cell combines features so far known only from rotated or strongly agitated granulates. In the succeeding chapters, comparisons of the cell with other related granular phenomena will be made.

## 1 Introduction

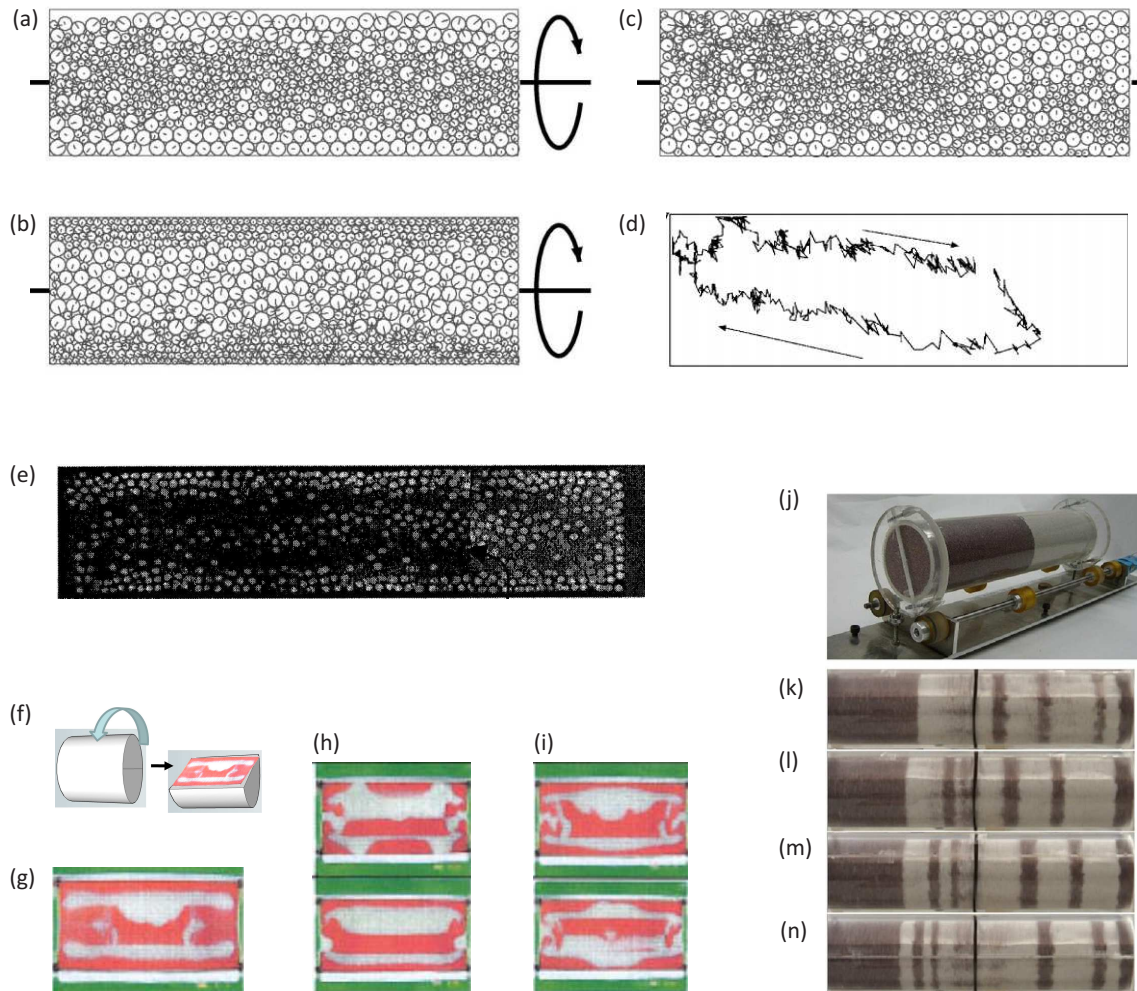


**Figure 1.6:** Summary of all previous studies on highly filled long rotating drums. (a-d) Simulation of a flat container filled with a monolayer of bidisperse discs at 84% area density. (a) At slow rotation, small particles collect in the center ( $Froude = 0.31 < 1$ ). (b) At fast rotation, large particles settle in the center ( $Froude = 1.78 > 1$ ). The situation in (a) is not stable and it develops to an axial segregated state (c). Particles form a global convection roll and move along the tilted disc interfaces. (d) Representative large particle trajectories for 1,600 rotations. Arrows show the main flow directions. Small particle trajectories are analogous. Cell aspect ratio: 3.2, particle diameter ratio: 1:2, from [1]. (e) MRI of pharmaceutical particles after 1.5 hours rotation in an almost completely filled drum. Larger particles (bright, 4 mm) that were initially on the right half have moved to the left. Small particles (dark, not individually resolvable, 1 mm) that were initially on the left side have simultaneously moved to the right forming ring-like segregation. Cylinder length: 27 cm, diameter: 6.9 cm, rotation rate 11.4 rpm, from [99]. (f-i) Rotation of a 90% filled cylinder. (f) A sketch demonstrates cutting of the container after the packing was frozen. The interior reveals complicated structures of small (white, (0.25-0.42) mm) and large (red, (0.59-0.84) mm) glass spheres, (g) at 30 rpm, (h) two experiments at 10 rpm, (i) two experiments at 20 rpm. Each experiment after 2 hours rotation. The green and touching white stripes do not belong to the container interior. (g-i) from [80]. (j-n) Traveling wave segregation at  $\approx 96\%$  filling fraction. (j) Initial demixed state of large (dark,  $\approx 1$  mm) and small (bright,  $\approx 0.15$  mm) sand. (k,l,m,n) Outer pattern after 1,216 min., 1,224 min., 1,232 min., 1240 min., respectively. The stripe positions are not fixed, they drift. The cylinder can also be opened similar to (f) in order to investigate the inner structure. 30 rpm, cylinder length: 32 cm, diameter: 8 cm, from [81].

# 2 Experimental setup

## 2.1 Experimental procedure

The simple experiment is depicted schematically in figure 2.1: A flat transparent container is slowly rotated about its central horizontal axis. In the flat cell geometry, the main effect of the rotation is a periodic modulation of the effective gravitational acceleration, in combination with friction of the granulate at the two plates of the Hele-Shaw cell.

In most experiments, the cell is filled with a mixture of  $(300 \pm 50) \mu\text{m}$  and  $(900 \pm 100) \mu\text{m}$  diameter almost spherical shaped soda-lime glass beads of density  $\rho = 2.490 \pm 0.002 \text{ g/cm}^3$  (Quantachrome Ultrapycnometer 1000) in 50%/50% volume ratio (figure 2.2). In some experiments different mixtures are used. The principal effects do not depend on the exact mixture compositions. Beads are separated before the experiment by a sieving machine ('Retsch AS200 basic') or in fewer cases by manually built sieves that are made from milling mesh. The cell is filled with the mixed granulate, sealed, and thereafter rotated about the long horizontal axis. Of course during filling, demixing always takes place and will be considered in section 5.7. The results depend strongly on the amount of filled granulate (section 3.1) but hardly on the initial mixing state.

Containers that are flat in the direction perpendicular to the rotation axis are necessary to allow clear observation of convection rolls (figures 2.1,2.3b). Their front and back walls consist of acrylic glass (PMMA) that were either glued or screwed to an aluminum or PMMA frame. Containers were constructed in different sizes and aspect ratios. Paddings can be used to modify the size of a given cell (figures 2.3b,5.3c and section 5.4). The cell depth  $z$  is fixed to 0.5 cm (order of 10-15 bead layers). Other cells thicknesses are discussed in section 5.5. The boxes are not airtight. The relative air humidity was protocolled for some experiments where periodical modulation of the flow velocity played a role (chapter 6,7). Humidity in air might form liquid bridges between particles and may influence the flow speed.

The container rotates on bearings and is connected to the motor via a Cardan joint to balance deficiencies in the rotational symmetry. The cell is adjusted horizontally by a self leveling laser line. For slightly tilted cells, convection structures develop only in the

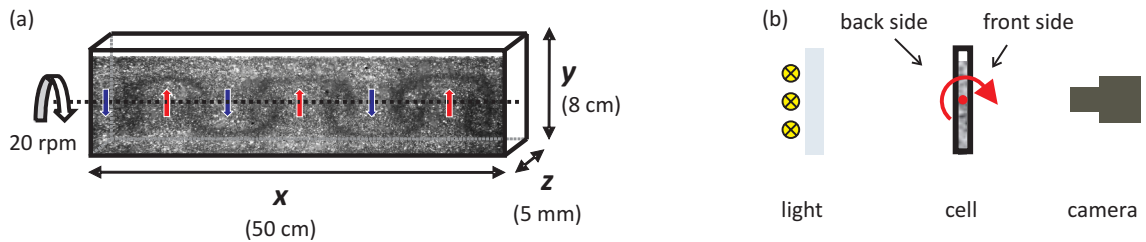


**Figure 2.1:** (a) Schematic drawing of the flat container that rotates along a horizontal axis (dashed line), with a typical sample image pasted on the front (camera) side. The convective motion is indicated by red (upward) and blue (downward) arrows. Dark and bright regions are enriched with small and large particles, respectively. Standard cell dimensions i.e. width  $x$ , height  $y$ , and depth  $z$  are given in brackets. (b) Definition of the standard rotation sense (red arrow) in profile view. The edge, which is currently on top moves towards the camera. For image taking always the front side is directed to the camera. The setup is backlit by three fluorescent tubes blurred by a frosty glass plate.

## 2 Experimental setup

axial cell range where the granular bed has the required fill height. The box is horizontally rotated at 20 rpm. Inertia forces are negligible because  $Froude < 0.02 \ll 1$ . Higher rotation rates are explained in sections 4.1 and 8.1. One arbitrary side of the cell is defined as the front side that always faces the camera during imaging. The upper edge of a cell rotates from an upright orientation towards the camera (figure 2.1b). This will be considered as standard rotation sense.

In contrast to other studies where conclusions about the flow can only be made on the basis of costly devices like MRI [104], the flatness of the cell permits direct observations. The cell is observed in transmission with uniform background illumination. Lighting is achieved by three stacked horizontal 1.20 m long fluorescent tubes that are blurred by a frosted glass plate. Typically every 20 full turns, the rotation is gradually slowed down until the cell stops in an upright position. Then a picture of the front side is taken by a scientific gray scale high resolution CCD camera ( $3072 \times 2048$  pixels) with an exposure time of  $\sim 50$  ms at medium objective aperture. Pattern formation and dynamics are extracted from these images. A typical experiment runs for more than 10,000 rotations (one to a few days) and sometimes even longer (a few weeks). No qualitative influence of the stopping procedure on the pattern formation was observed.

In a nutshell, one can say that the qualitative result is quite insensitive to different experimental parameters. It can be repeated by any reader at ease. However, the onset of convection demands a high fill level and flat container shape. Also crystallization must be suppressed by a sufficient size distribution of particles. *The settings in table 2.1 shall be taken as standard if other parameters are not explicitly stated.* Deviations from default parameters are given in the corresponding images.

granular material:	glass spheres, type Ballotini MGL, Eisenwerk Würth, Bad Friedrichshall, Germany
small particle sieve fraction:	250-355 $\mu\text{m}$ , appears dark in images
large particle sieve fraction:	800-1000 $\mu\text{m}$ , appears bright in images
specific gravity of particles:	$\rho = 2.490 \pm 0.002 \text{ g/cm}^3$
particle ratio:	equal weight fractions
cell dimensions:	width $x$ : 50 mm, height $y$ : 80 mm, depth $z$ : 5 mm
driving:	continuous rotation at 20 rpm, every 20 rotations gradual stops for image taking rotation sense: upper edge moves towards camera
experimental duration:	>10,000 rotations, typical one to a few days, sometimes up to two or four weeks

**Table 2.1:** Parameters that shall be taken as standard if they are not explicitly stated. Deviations from default parameters are given in the corresponding images. For a definition of the rotation sense and cell dimensions see also figure 2.1.



**Figure 2.2:** Photography of small and large species of used standard glass beads. They are not ideally spherical with aspect ratios typically from 0.7 to 1.3.

## 2.2 Experimental control

In contrast to visualization of flows in rotating cylinders, the pattern must be captured at a constant cell orientation. As the trigger of the camera is not sufficiently reliable and also to avoid blurring motion, the cell must gradually stop in regular intervals. There are two main setups. The first was used from 2006 to 2008 and the other from 2009 to 2011. The first one is quite cumbersome in construction and usage. The second setup is more convenient. The reason for building the complicated setup at first, is based on the fact that ‘Labview’ support was not available previously.

**From 2006 to 2008** This setup allows rotation in uniform direction. The current orientation and speed of the container is indirectly concluded by a feedback mechanism. The bottleneck was the frame grabber (‘Roadrunner PCI-12’ from ‘BitFlow’) supported only by a C++ library that had to run on a ‘Windows NT 4.0’ system with ‘Microsoft Visual C++ Pro’ version 6. The C++ program is based on code from reference [105]. Commands are sent and received via serial interfaces using the measurement device language ‘Standard Commands for Programmable Instruments’ (SCPI) and special camera commands. The control scheme is depicted in figure 2.3c. The control computer sends a command to a device that outputs the requested voltage that is afterwards amplified. The voltage signal drives the gear motor which is connected with the cell. At the rotation axis, a control unit is fixed for the measurement of the momentary rotation speed (enlargement in figure 2.3a). There a photo diode measures the light interruption by a slit disc. The frequency of the diode’s TTL-signal is measured and sent back to the control computer. A proportional-integral-derivative controller (PID) measures the deviation from requested rotation speed and calculates the new output voltage. In this way, the variation of the rotation speed lies within  $\pm 0.5\%$ . A magnet at the rotation axis triggers a reed switch once per full rotation. The switch is connected to a button of a computer mouse. The control computer registers mouse events. The number of mouse clicks corresponds to the number of rotations. These feed back processes take place in quasi real time. In the last round, the cell is gradually slowed and stops at low speed when the magnet influences the reed switch. A trigger command is then sent to the camera and the frame grabber reads the image that is transferred to another computer. Then the cell is gradually accelerated again.

## 2 Experimental setup

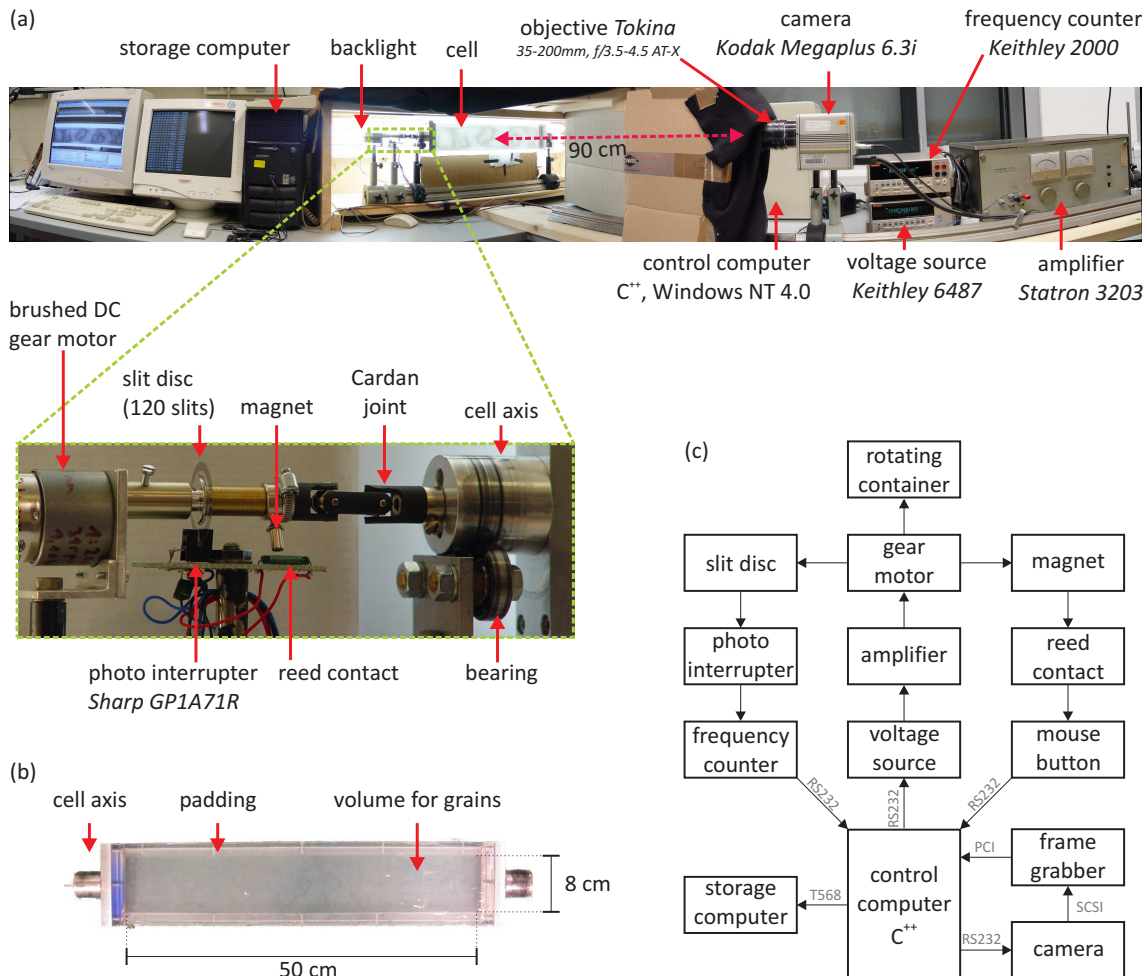


**Figure 2.3:** (a) Panoramic view of the setup with enlargement of the rotation control unit that was used from 2006 to 2008. During a run the setup is sealed by a black curtain to avoid reflections by day light. (b) Example of an empty cell. (c) Flow chart of the experimental control. Labels at arrows stand for common data protocols. See text for a description of the motor control.

**From 2009 to 2011** This setup allows rotation in any rotation sense and any combination of rotation protocols. The current orientation and speed of the container is directly controlled by output of stepper motor pulses. Availability of frame grabber driver for ‘Labview’ (‘BitFlow SDK 4.50’ [106]) motivated reorganization of the former motor control. ‘Labview’ allows communication with different interfaces in half-graphical programming style with a graphical user interface for adjustment of settings. In the ‘Labview’ program stepper pulses that are necessary to drive a stepper motor at constant and accelerating rotation rates were generated. Calculation of an accelerating step sequence describes figure 2.4(a-c). The pulse sequence is transmitted to a USB sound card. The sound card is controlled via the sound card interface ‘WaveIO’ version 0.42 [107]. The capacitors of the sound card output are shortcut to avoid signal deformation. The sound card delivers at 20,000 Hz sampling rate TTL voltage sequences for the stepper motor control. The motor control handles the motor coils to allow 3,200 steps/360° in a 16 micro steps mode. In irregular periods (within a day or month) the sound card can crash without reason. The graphical interface (figure 2.4e) allows manual picture taking and manual cell rotation for positioning. Arbitrary automated rotation schemes are also possible.

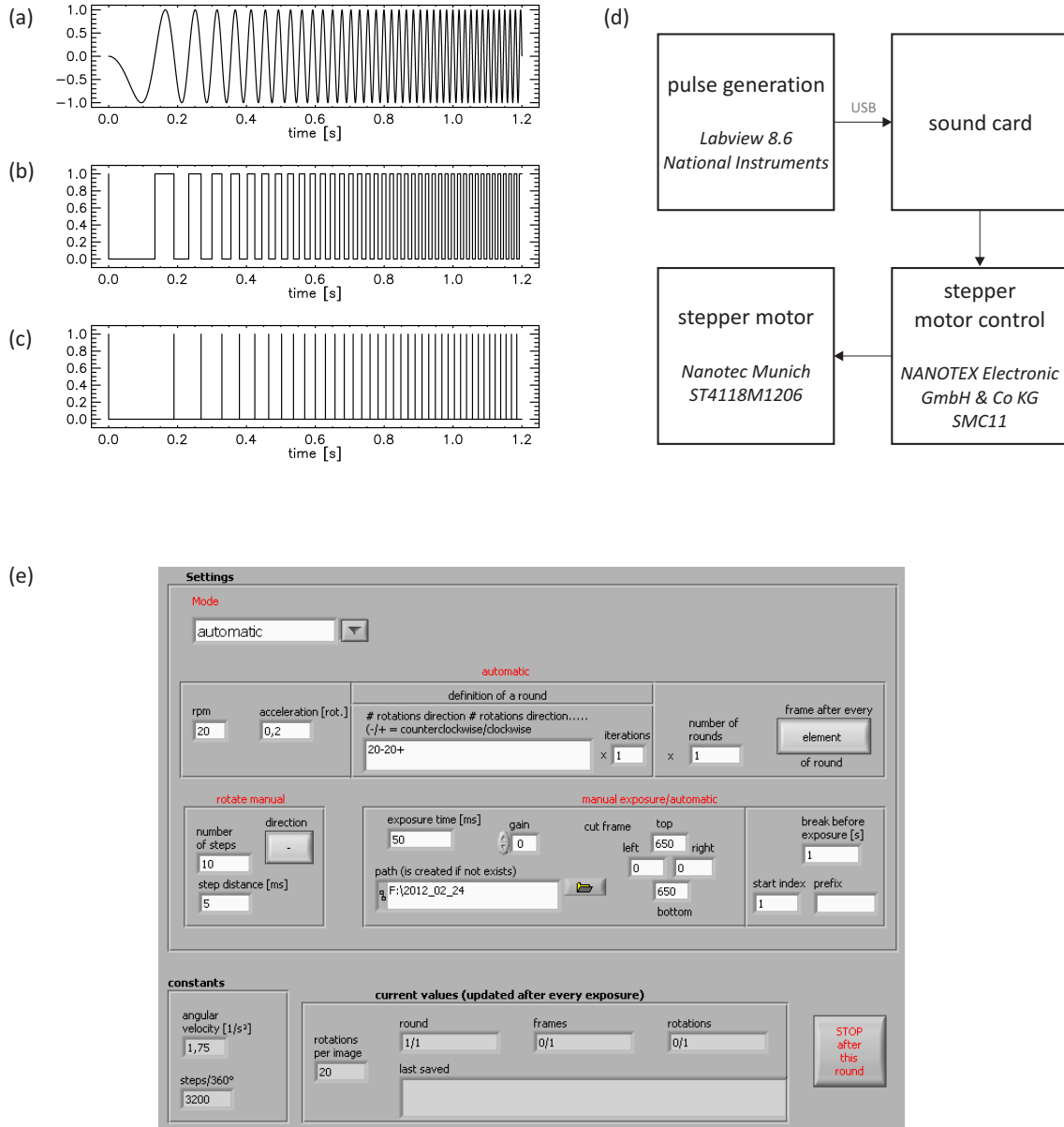


**Figure 2.4:** Improved rotation control with stepping motor for the period 2009-2011. (a-c) Graphs demonstrate how a uniformly accelerating step sequence is generated. Real experimental settings are used, i.e. the acceleration path is 0.2 rotations and the final rotation rate is 20 rpm. Here, for better display micro steps are neglected and the motor resolution is assumed to be 200 steps/rotation. From these values follow a constant angular acceleration  $\alpha = 1.75 \text{ s}^{-2} = 55.56 \text{ steps} \cdot \text{s}^{-2}$  and acceleration time 1.2s encompassing 40 steps. The number of steps  $n(t)$  after accelerating time  $t$  shall obey  $n(t) = 0.5 \cdot \alpha \cdot t^2$ . Following procedure leads to the requested step series: (a) A function  $f$  is constructed that is periodical after every full step:  $f(n) = \sin(2\pi \cdot n - \pi)$ . (b) Now the signs from  $f$  are extracted:  $0.5 \cdot (\text{sgn}(f) + 1)$ . (c) Falling edges from the step function give the 40 moments for the motor pulses. (d) Scheme of the rotation control. Camera and frame grabber are directly controlled by 'Labview' and neglected in the scheme. (e) Graphical user interface of the 'Labview' program for control of motor and camera. The user can select corresponding rotation schemes.

## 2.3 Other setups

**X-ray** X-ray measurements at five different devices were done in order to get deeper insights of the packing. They are summarized in table 2.2. X-rays were used for absorption measurements to estimate the average packing density along the container depth. Computer tomography was used to measure the three-dimensional particle distribution. However, the quality was too bad to resolve the smaller particles (figure 3.4c) but the segregation structure can be identified. Preliminary tests at another tomograph led to promising results (figure 2.5c,d). All particles can be detected and measurements are to be continued in the future.

device	description	results
‘Small Animal In vivo Scanner’, NanoSPECT/CT, Leibniz Institute for Neurobiology Magdeburg	animal tomograph, X-ray tube rotates around the probe, resolution $\geq 200 \mu\text{m}/\text{pixel}$	figures 2.5a,3.4c,5.7
Radioskopiesystem GS 220, Sauerwein GmbH, 32 keV, Institute of Materials and Joining Technology, University at Magdeburg	for radioscopy of metals, used for absorption measurement	figure 3.5b
‘CT Alpha ProCon X-Ray’, 160 keV, Faculty for Process and System Engineering, research group NaWiTec, University at Magdeburg	tomograph, used for absorption measurement	section 3.3
‘Phoenix Nanotom’, 180 keV, Max-Planck-Institute for Dynamics and Self-Organization Goettingen	tomograph, probe rotates, resolution $50 \mu\text{m}/\text{pixel}$	shield: figure 2.5b test: figure 2.5c,d
‘Siemens Artis Zeego’, Experimental Factory Magdeburg	fast medicine tomograph, X-ray tube rotates around probe	resolution too low

**Table 2.2:** X-ray devices that were used to measure material absorption and packing structure.

**Co-moving frame** There is an alternative way to observe the cell. The granular displacement during rotation can be recorded by a co-moving camera. Stopping of the container is no longer required. A preliminary setup was built (figure 2.5e) but no usable information could be extracted till date. More elaborated studies are planned for the future.

**Vacuum setup** A setup was built to allow evacuation experiments (figure 2.6(a-c)). Direct evacuation of the cell would require quite robust cell walls. Therefore a container ( $x \times y \times z = 140 \text{ mm} \times 35 \text{ mm} \times 5 \text{ mm}$ ; with small slits at top and bottom sides to allow degassing) is enclosed in an outer vessel consisting of a large glass cylinder (inner diameter 20 cm, length 20 cm, borosilicate glass of 7 mm wall thickness) and two 15 mm thick aluminum side walls. These rubber coated side walls are initially fixated with threaded

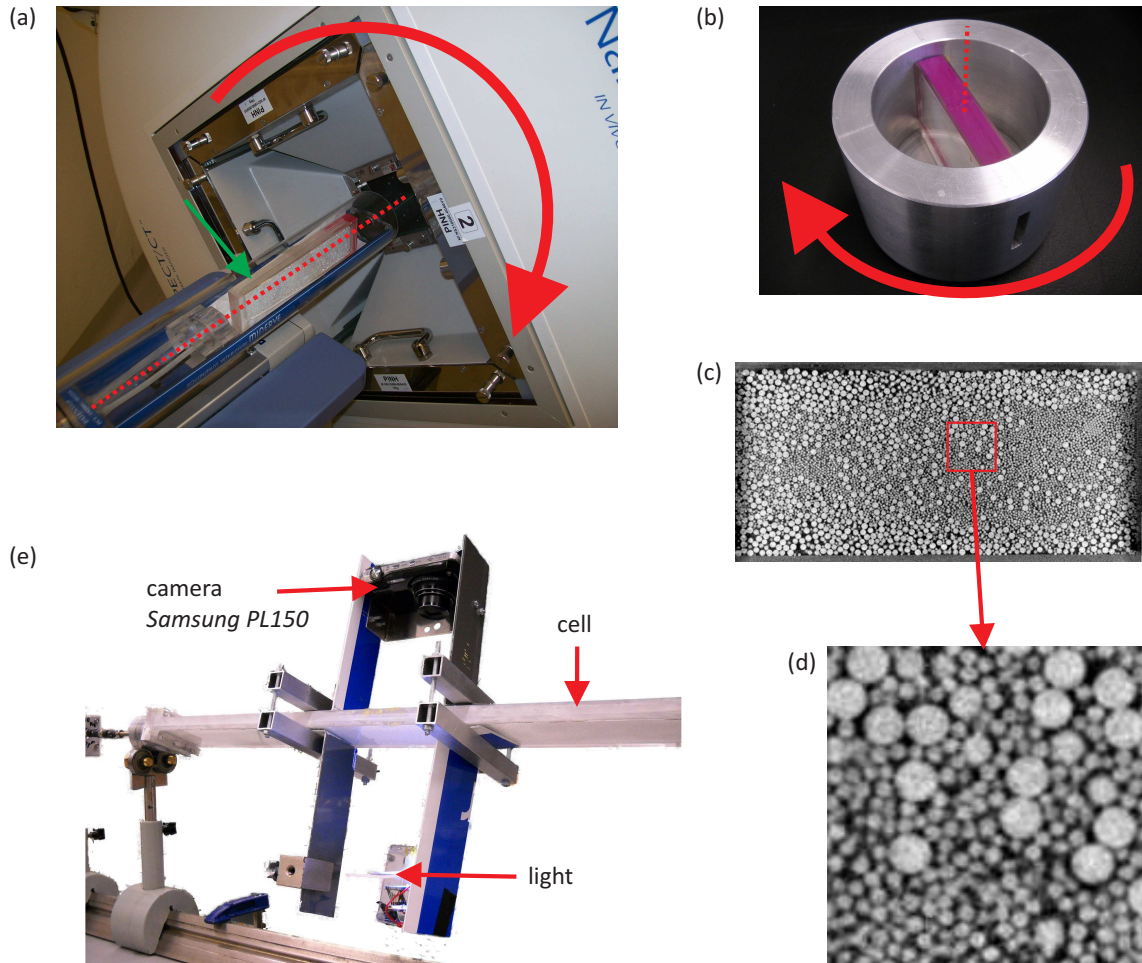


**Figure 2.5:** (a) Tomography with ‘NanoSPECT’. The cell (green arrow) is inserted into the tomograph and an X-ray tube rotates around the cell on a helical path. Rotation direction and rotation axis of the tomograph are indicated by the red arrow and dashed line, correspondingly. (b) Because the probe itself rotates in the X-ray beam of the ‘Phoenix’ tomograph a cylindrical aluminum shield was built that contains the cell (violet top surface). The shield absorbs beams that pass the short container axis but does not absorb beams that pass the long axis (visible is one of two slits of the shield). In this way absorption contrasts during probe scanning are reduced. The shield with the cell rotates horizontally along the arrow around the dashed line. Irradiation is by a horizontal conical beam. (c) Slice of a test scan and (d) zoomed part of precision beads ( $1.01\text{ mm} \pm 0.01\text{ mm}$ , ‘Glass sphere s.r.o.’ and sieved  $400\text{--}425\text{ }\mu\text{m}$ , ‘Mo Sci’). Any particle is detectable.  $x \times y \times z = 60\text{ mm} \times 30\text{ mm} \times 5\text{ mm}$  (maximum allowable size for the device). Compare the image of ‘Phoenix’ (c,d) with the lower quality of ‘NanoSPECT’ in figures 3.4c,5.7! (e) Setup for a co-moving camera. A camera rotates with the cell opposed by a light source.

rods on the glass cylinder edges. After pumping out air from the cylinder the atmospheric pressure seals the construction by pressing the parts against each other. The side walls contain an orifice for the vacuum pump and a pressure gauge (figure 2.6b). The rotating cell in the vacuum chamber is driven from the outside by a motor. The driving axis transmits rotation via a vacuum feedthrough (figure 2.6c). As in any granular experiment, the local pressure inside the granular bed cannot be measured. The actual pressure may be somewhat higher than the pressure given by the gauge because of continuous degassing of the large granular surface. The setup was evacuated for a few hours until a sufficiently low inner pressure level was established.

## 2 Experimental setup

**Underwater setup** Trapped air bubbles are always present if the container is filled with only water which would inevitably disturb the grain's motion. The following procedure was found useful: The vacuum setup was modified to immerse the complete container and the granulate in water (figure 2.6d). As in the vacuum experiment, the setup was evacuated before the start of the experiment, and simultaneously water with a small amount of detergent was soaked into the cylinder enclosing the experiment. A radial shaft seal allows transmission of rotation and simultaneously seals the container. The reason for constructing the setup was to avoid electrostatic charging. To achieve this, one can find other ways, not only the underwater experiments. Presence of indium tin oxide (ITO) or transparent conductive oxide (TCO) coatings, antistatic powder or spray, conducting granulates and containers, high energy radiation by a UV lamp or sufficient air humidity also might help. A similar setup was used to immerse the cell in sunflower oil. The handling and evacuation of the oil filled setup made experiments almost unmanageable.

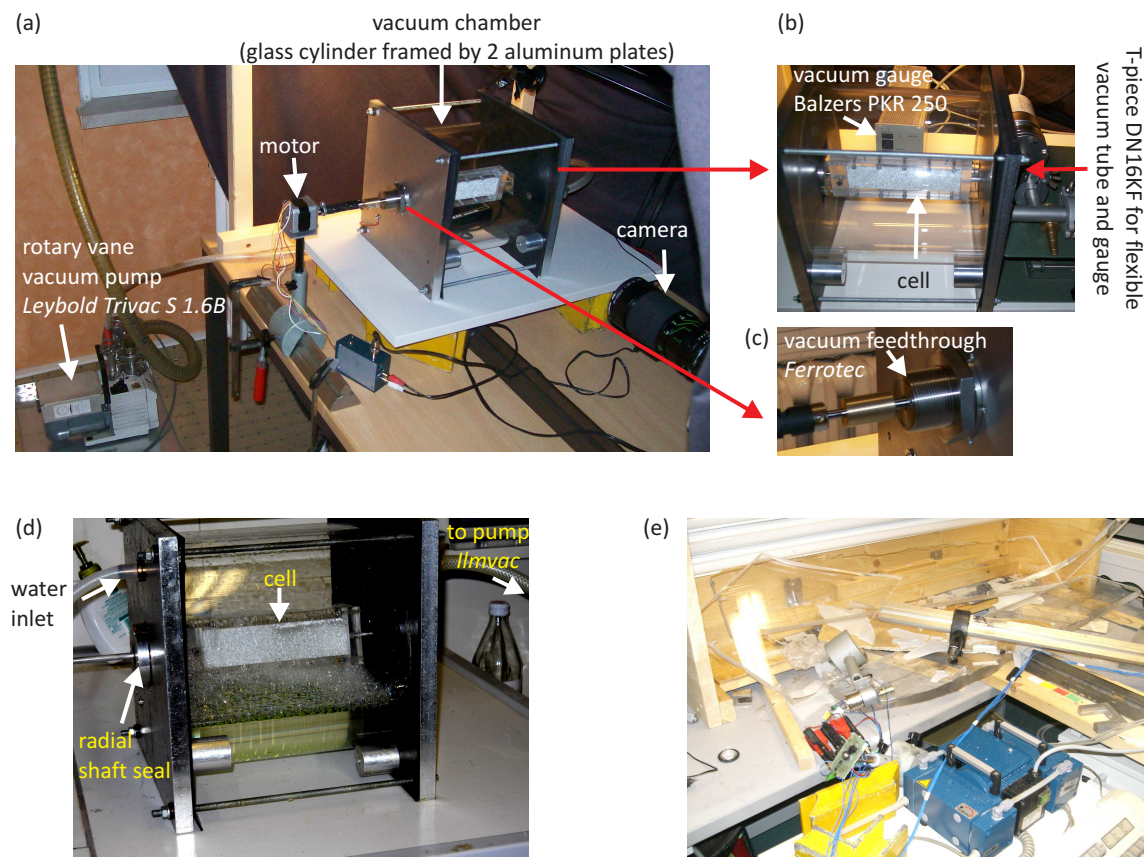


**Figure 2.6:** (a-c) Vacuum setup. (a) Total view. Experiments took place in a separate room in order to avoid unwanted incidents. (b) Front view of the vacuum box containing the cell. (c) A magnetic fluid rotary vacuum feedthrough transmits rotation in the vacuum chamber. (d) Modified vacuum setup for under water experiments. (e) Beware the vacuum! (preceding vacuum setup after becoming unusable).

## 2.4 Evaluation methods

In general, transparent glass beads are used. Opaque materials like food grains do not allow observations in transmission. The optical signal hitting the camera consists of light that had been refracted at about 20-40 glass-air interfaces. Regions that are enriched with small particles along the depth of the cell have more interfaces. Therefore in these regions the light is scattered to a larger extend and they appear darker than zones with predominant large particles. This stands in accordance with investigations about light transmission in a granular bed [108].

The contrast of most pictures are enhanced and corrected for temporal and spatial inhomogeneities in illumination intensities. Illumination gradients are negligible compared to the different brightness levels of the segregated phases. Usually, the better contrasts were gotten with higher exposure time under the expense of overexposure of the upper granular surface. In cases where the surface layer was relevant, a lower exposure rate was chosen.

In general, the mixtures are doped by a few black tracers in the range 780-820  $\mu\text{m}$  (Sigmund Lindner, type P), however, tracers were tracked only in a few studies (figure 7.2, section 9.1). One can follow the tracers only for a few rotations and single particles cannot be optically resolved on a reliable basis. However, for post processing it is sufficient to observe local particle clusters that move principally in the same direction. To a large extend the pattern that is seen on the front side is also observed from the back. The transmission technique reflects the pattern inside the packing (visually proven in figure 3.4). Furthermore, the relation between the local transmission intensity and granular composition has been established in separate experiments.

Convective motion is visible for the naked eye if series of consecutive images are played at least 100 times faster than the real time. Final movies are sped up by a factor of 1,000-10,000. They can be downloaded from the corresponding journal websites (p. 103).

The collective particle motion is exploited for the determination of local cluster velocities. Images are subdivided into evaluation squares of the order of 8 mm  $\times$  8 mm and, within each segment, the principal cluster displacement (maximum cross-correlation vector) is determined from the analysis of consecutive images with sub-pixel accuracy (figure 2.7(a-e)). Particles should move maximum 1-3 pixels between two images. This condition is in general fulfilled if there are 10-100 rotations between two pictures. The method allows a reconstruction of the local granulate motion in the cell plane. In order to restrict spurious vectors the area is oversampled i.e. partly the interrogation cells overlap. Particle Image Velocimetry (PIV) algorithms can be found in reference [109]. From the reconstructed vector field, a time-space plot is constructed from the data along the horizontal granular center. Only the vertical components are considered as horizontal motion can be neglected in the center. Throughout the thesis, red/blue in time-space plots stands for upwards/downwards flow. Upwards/downwards flow is defined with positive/negative sign. The construction procedure demonstrates figure 2.7(f-i). Upwards or downwards flow means the resulting grain displacement after a full rotation. In the reference system, upwards flow corresponds to motion against the rotation sense and downwards flow to motion in the rotation sense. From the time-space plots, the mode number can be calculated. Time-space plots of the brightness of the segregation patterns are made analogously.

In some cases, especially if no segregation pattern is visible, convection can only be derived from consecutive frames (movie). Convection can then still be visualized by overlaid vectors or by brightness fluctuations. For any pixel position the fluctuation is defined as  $\sum_{i=0}^n |g_i - g_{i+1}| / (g_i + g_{i+1})$  where the difference between the gray values  $g$  is normalized

## 2 Experimental setup

by their intensities. Summation goes over  $n$  consecutive pictures. After repeating the procedure for every pixel the resulting fluctuation picture is then normalized (in the range that is spanned by 2% and 98% of the cumulative histogram distribution) to achieve higher contrasts. Brightness fluctuations reflect particle displacements i.e. fast and slow moving regions. A useful side effect of such a definition is the fact that the visual results partly resemble streak lines.

All image processing routines are written in the ‘Interactive Data Language’ (IDL) versions 5.4 and 6.3.

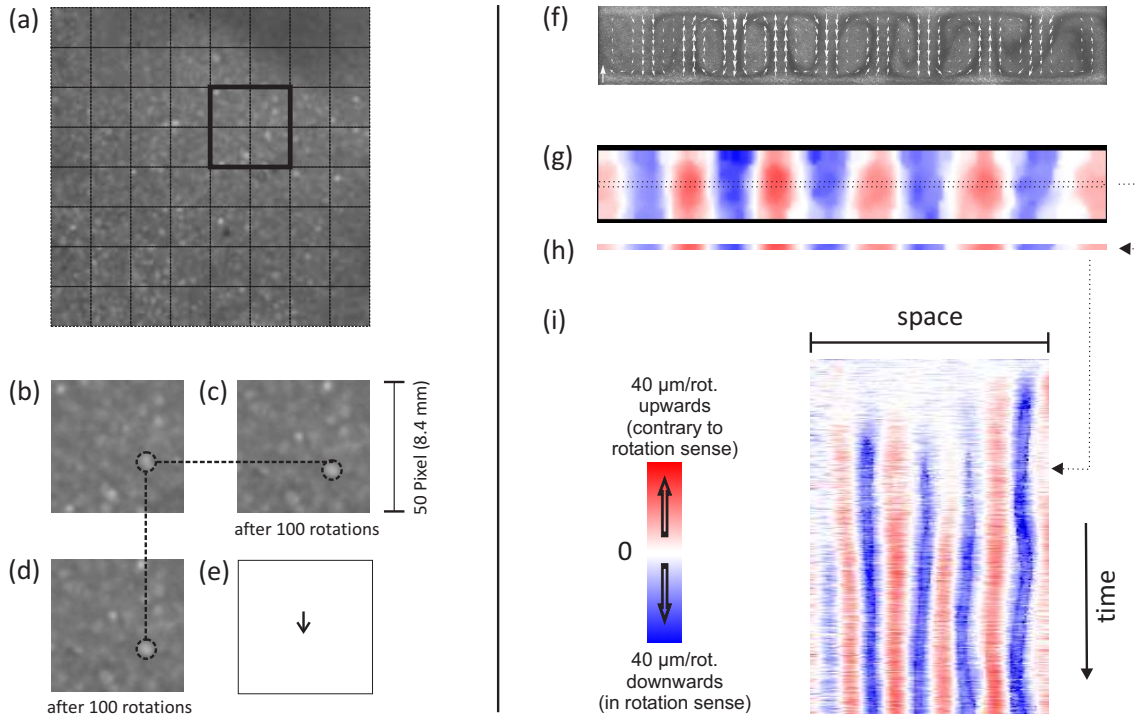


**Figure 2.7:** (a-e) Measurement of mean displacements from brightness patterns. (a) The original picture is split into smaller square cells (thinner lines). Displacement is calculated for the area of four squares that share a common vertex (thicker lined square). (b) Image content of the thicker lined square in (a). (c,d) After 100 rotations the particles have shifted a little bit. For better impression a bright spot is encircled and its displacement is recognizable by reference lines. (e) Resulting mean displacement vector for the whole square. (f-i) Construction of time-space plots from a vector field. (f) Original picture with overlaid vectors. (g) Vertical vector components in colored representation (smoothed by interpolation). Red/blue stands for upwards/downwards motion. (h) Extracted horizontal line from the center of the granular bed. For all moments the lines are combined to a time-space plot (i).

# 3 Convection & segregation

The main focus of the thesis is the observation of a twofold granular scenario in a rotating flat container. By changing the fill level one can switch between two regimes that differ completely in the resulting segregation patterns and in the motion of granulates. One of the two regimes was not known so far.

## 3.1 Fill level

First, it is necessary to define a quantitative measure for the fill level. The motional degrees of freedom of the granular particles are controlled by the available space above the granulate. However, this free volume is not a practicable parameter, since the height of the granular bed depends on the filling procedure, and it is not exactly preserved during the experiment. Therefore the granulate is weighed before filling. Using the mass  $m$  and known material density  $\rho$ , the fill ratio  $C$  is defined as the proportion of the net volume of glass beads to the entire volume of the box  $V$ , i.e.  $C = m/(\rho \cdot V)$ . If the container is half-filled with the bimodal mixture, the fill level is  $C \approx 0.33$ . For a cell completely filled, without and with additional manual tapping, one finds  $C \approx 0.66$  and  $C \approx 0.70$ , respectively. Granular motion reduces with increasing  $C$ . A thin fluidized layer that is necessary to have any dynamics forms only when  $C$  is smaller than  $\approx 0.66$ . Two distinct phenomena are observed in the flat cell. The transition between them is found at a critical fill height  $C_C \approx 0.60$  i.e. at relatively high fill ratio where fluidization is almost impossible.

Note that, by this definition of the fill level, the free volume above the granulate for a given  $C$  increases with container height. The values for  $C$  and  $C_C$  depend on the cell and bead parameters. The values given here correspond to a box with default dimensions and granular composition as defined in table 2.1. For other experimental settings the critical fill ratio  $C_C$  was not determined. However for any geometry  $C_C$  can be expected slightly below the maximum fill ratio where collective fluidization is still possible. As a rule of thumb, one finds convection if the free vertical space on top of the granulate settles in the range  $\approx 0.3$ -3 mm after it was agitated by rotation. Corresponding convection velocities can be expected in the order of 1-100  $\mu\text{m}$  per rotation. The definition of the fill level should not be mistaken with usual definitions of the packing density [110] where the occupied volume is related to the bulk of the particles. The occupied volume is related to the complete container that on top of the granulate is empty. In some cases where the exact granular quantity is not vitally important, only the initial percentage of the fill height is given. It varies slightly during the experiment.

The redistribution of particles during cell rotation is basically restricted to the sliding of the granulate, driven by gravity, when the cell plane tilts out of the horizontal. Below the critical fill ratio  $C_C$  axial segregation patterns of alternating stripes of small and large particles form. If the fill ratio exceeds  $C_C$ , convection rolls associated with another type of segregation emerge. The two different scenarios are summarized in a scheme in figure 3.1. The main focus of the thesis lies on highly filled containers where convection is observed. Except of section 3.2, axial segregation is only considered in chapter 7 and subsidiary in section 8.1.

### 3 Convection & segregation

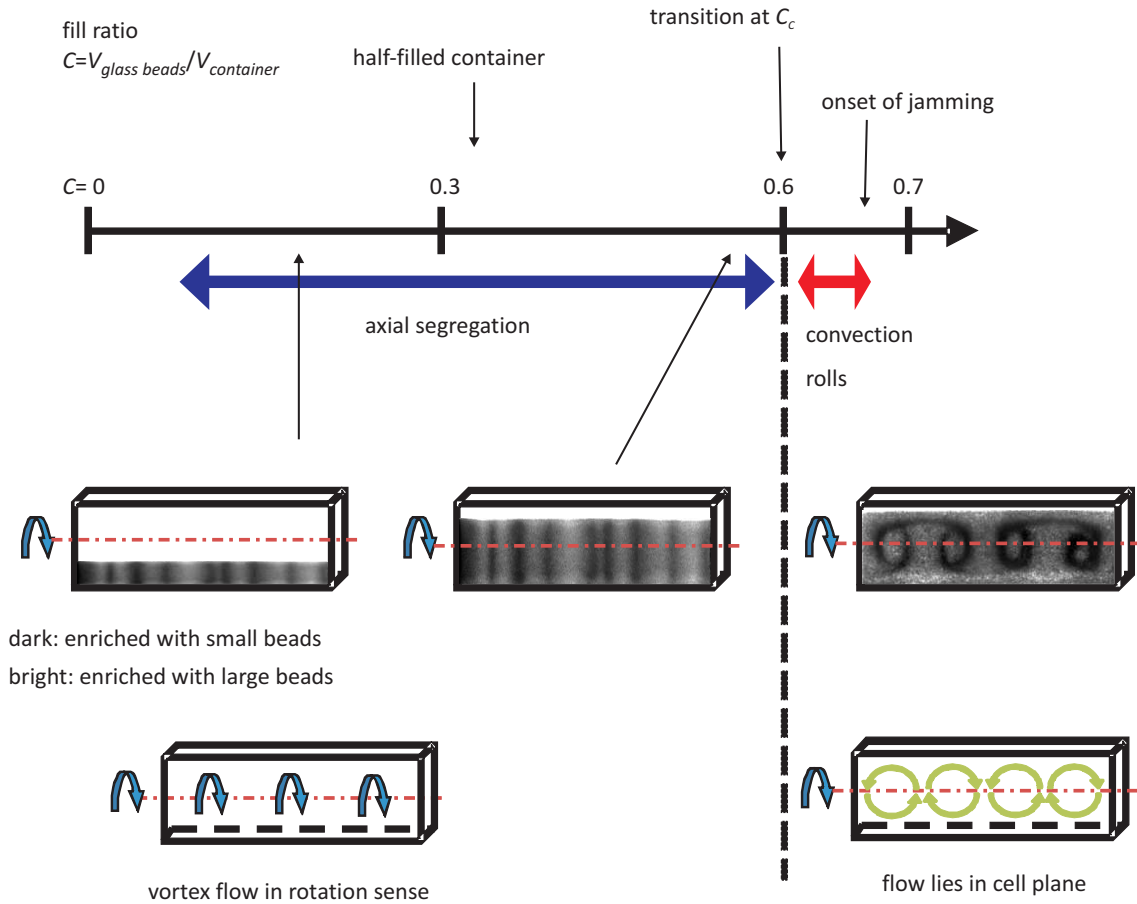


**Figure 3.1:** The scheme shows patterns that are observed for different fill levels  $C$ . Below the critical value  $C_c$  axial segregation and above  $C_c$  convection rolls are found. Dark/bright areas in the containers are areas with predominant small/large particles. At the bottom, particle motion is indicated. For axial segregation it follows the sense of rotation whereas for convection the vortex flow lies in the cell plane. For a description of flow directions see also section 9.1.

## 3.2 Axial segregation

At lower fill ratios  $C < C_C$ , chute flow occurs every time the cell plane passes a certain tilt angle (roughly the angle of repose) during rotation. This leads to an axial segregation which is connected with a local modulation of the fill height like in usual cylindrical drum experiments (figure 3.8a and for drums [69,77,78]). At long time scales, the stripe pattern coarsens. Figure 3.2 shows five experiments at slightly subcritical fill level. In the figures (left column), initially 6 to 9 stripes of small particles (dark) can be distinguished. In the course of the experiment these segregation patterns slowly coarsen and only 4 to 5 stripes remain (right column). Finally two or three well segregated regions persist to the end (figure 3.2f). Stripe positions vary between the experiments. Lateral edges can be occupied by the small or large species. Radial segregated cores of small particles develop (for one exposure dashed in figure 3.2e) similar to radial segregation in cylindrical mixers. In contrast to cylinders, the dynamics are limited to two avalanches during a full rotation ( $360^\circ$ ). The flow speed is an order higher than for convection (top right panel). The situation can also become unstable and traveling waves form (chapter 7). An intermediate state between axial segregation and convection is depicted in figure 3.2g. The fill ratio is 2% higher than in the cases of figure 3.2(a-e). The bands are deformed and small particles collect at the top and bottom edges (similar to convection in figure 3.3a). Flow is tilted from the vertical but still follows the sense predefined by the rotation. This situation is maintained for the whole experimental time (6,000 rotations). The lowest fill height where axial segregation experiments were done was  $\approx 30\%$ . The minimum necessary particle volume for these structures has not been determined in the studies.

## 3.3 Convection rolls

If the fill level is further increased, the chute flow disappears and the granulate jams. At fill ratios above  $C_C$ , one observes the formation of characteristic zones after the start of the experiment (figure 3.3a). The described patterns and dynamics are qualitatively different from those at lower fill ratios (section 3.2).

In shallow layers, that are within a few mm of the top and bottom cell edges, the particles' motion is fast and relatively uncorrelated. This region becomes enriched with large size beads, indicated in figure 3.3(a-d) by the bright horizontal stripes. Except for these regions, the grains can maneuver only in compact clusters. Within the next few mm, narrow bands of jammed small size beads develop along each edge, while the central part of the cell contains mixed granulate (figure 3.3a).

This initial structure becomes distorted by the onset of convective flow so that small particles from the outer bands are advected towards the center (figure 3.3b), and a serpentine structure develops (figure 3.3c). The emerging rolls are decorated by small particles (figure 3.3d). Whereas optically brighter regions contain a nearly balanced mixture of large and small beads, dark regions contain a noticeable excess of small beads. The periodicity of the convection pattern, once it has formed, is persistent, and there is no coarsening. The spatial period of the flow structures is not sensitive to the fill ratio above  $C_C$ . Convection can start anywhere in the container (section 5.3).

The limited free space allows the formation of only two shallow fluidized zones on top and bottom edges (marked by dashed lines in figures 3.3c,3.4b). These fluidized areas sandwich the zone where convection is observed and there the main horizontal particle transport takes place. The particle motion is there one to two orders of magnitude faster than in

### 3 Convection & segregation

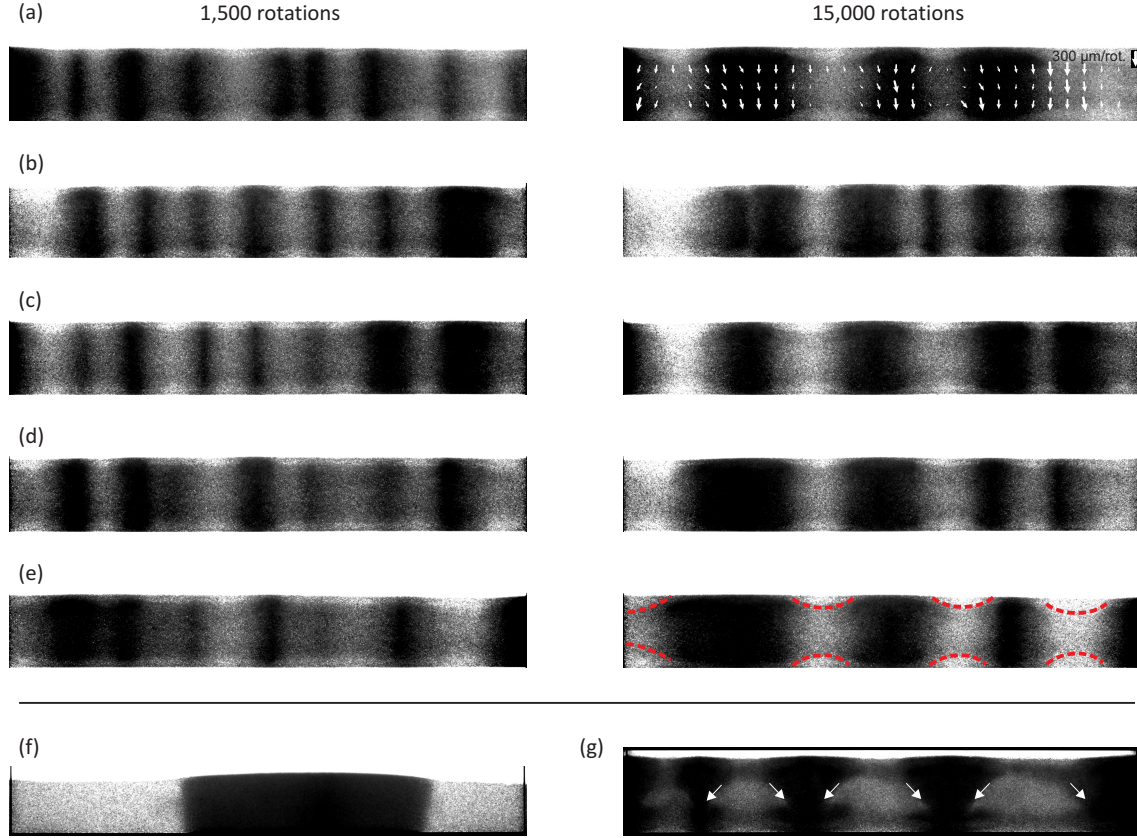


**Figure 3.2:** (a-e) Axially segregated stripe patterns in the chute flow regime for 5 experiments at  $C = 0.581 < C_C$ . Dark/bright indicate enrichment of small/large particles after formation of the segregation bands at 1,500 rotations (left column), and coarsening at 15,000 rotations (right column). In (a) arrows symbolize the flow on the front side measured by particle image velocimetry. The flow is opposite on the backside (not shown) i.e. there is vertex flow in sense of rotation as expected for a rotating drum. In (e) the radial core of small particles is indicated with dashes. Band positions are different in experiments but coarsening always takes place. (f) Long-term behavior at 50,000 rotations for lower fill ratio,  $C = 0.4$ . The mixture is completely segregated in two bands of large particles that confine small particles. The pattern is stable for the remaining run (in total 184,000 rotations). (g) Pattern with a slightly higher fill ratio than in (a-e). The structure is an intermediate state between axial segregation and convection, at 1,500 rotations. Visible flow on the front side is manually marked by arrows. Flow is tilted from the vertical. The upper container edges are cut for (a-f).

the convective core (this is reflected by the red color in the fluctuation plot figure 3.3e). Fluidized layers are considered as main driving mechanism and discussed later in section 9.1.

From the fluctuations (figure 3.3e), qualitative character of the flow can be derived. Along the rotation axis circular and vertical motion alternate (curved and straight streak lines). For a more quantitative analysis, the velocity field is determined from the displacement of clusters as described in section 2.4. Figure 3.3f shows the vector field overlaid over figure 3.3d. In the two fluidized layers at the top and bottom edges, the flow is too fast to be determined. Figure 3.3g,h shows the vertical velocity and the local composition of the mixture obtained from the optical transmission intensity in the middle part of figure 3.3f, vertically averaged between the dashed lines.

The convection is overlaid by a vertex motion in the  $yz$  plane in the sense of rotation (for a definition of the coordinate system see figure 2.1). The vertex is one order of magnitude

smaller than the convection flow maxima. This means that, in the selected reference system (figure 2.1b), downwards/upwards streams on the defined front side are slightly faster/slower than the corresponding downwards/upwards streams on the rear side. Under continuous reversals of the rotation sense (section 4.2), the offset vanishes and the front and back side velocities are equivalent.

Another example of a convection roll array is shown in figure 3.4. Four rolls are decorated by dark bands enriched with small beads. Fluidized regions are seen at the bottom and top edges. The flow and composition patterns seen on the front extend through the whole cell depth and there are only minor differences between front (figure 3.4a) and back textures (figure 3.4b). Whereas the optical transmission pictures (figure 3.4a,b) result in a brightness distribution that is averaged along the cell depth, X-ray tomography shows the pattern inside the granular bed directly. A tomogram from the vertical midplane between front and back cell walls is shown in figure 3.4c. Notwithstanding the very low image resolution, the X-ray image confirms the visual content of the transmission pictures.

In order to explore the granular packing in more detail, X-ray transmission measurements on a fully developed convection roll were performed. Figure 3.5 shows an optical image of a typical segregation structure (a) and an X-ray transmission image (b) of the same region. As one can see, the X-ray transmission image is very sensitive to the local composition of the granular mixture.

In the X-ray image, the optically darker regions appear systematically brighter than the rest, i.e. the absorption is lower. In a control experiment, it was verified that small and large beads have the same absorption characteristics in monodisperse samples. This indicates that the regions enriched with small beads must have a lower packing density than the optically brighter regions containing a more balanced mix of small and large beads. It is well known that a bidisperse mixture of spherical grains will always have a higher packing than a monodisperse ensemble of spheres (e.g. [110] and references therein). Here, the packing of the regions enriched with the smaller beads are obviously closer to the lower packing density of monodisperse grains than the rest of the cell. There are two reasons for this: First, the packing density curves as a function of mixture composition are in general asymmetric, with the maximum shifted to a higher content of large particles. Second, the dark regions cover less than 25% of the cell area, whereas the brighter regions cover the rest. Thus the 50 volume percent of small beads are enriched to a higher extent in the dark regions than depleted in the rest of the sample.

### 3.4 Convection reproducibility

Five experiments under same conditions were performed (figure 3.6, labeled (a-e), added numbers distinguish different representations). Concerning with their segregation textures, all the experiments look different. The blue dashed lines cut either centers or edges of rolls in different experiments (a1-c1,e1) or for the same experiment (d1,d1').

From a Fourier analysis of the vertical flow amplitude along the rotation axis, the mode selection is monitored. Boundary conditions require that rolls end with up or down flow at lateral cell sides. Only half-integer and integer modes can therefore be observed. To give an example, a selected wave number of 4.5 in figure 3.3g corresponds to 4.5 roll pairs i.e. 9 rolls. The spectra for modes 0-10 are plotted in figure 3.6(a2-e2). Brighter intensity means faster flow. In most cases, the fastest growing mode dominates from the beginning and determines the wavelength of the succeeding pattern (figure 3.6(a2-c2)). The selected wavelength can fluctuate between neighboring modes (figures 3.6d2,5.1). The mode can be constant for several 10,000 rotations but the longer the experimental duration the likelier

### 3 Convection & segregation

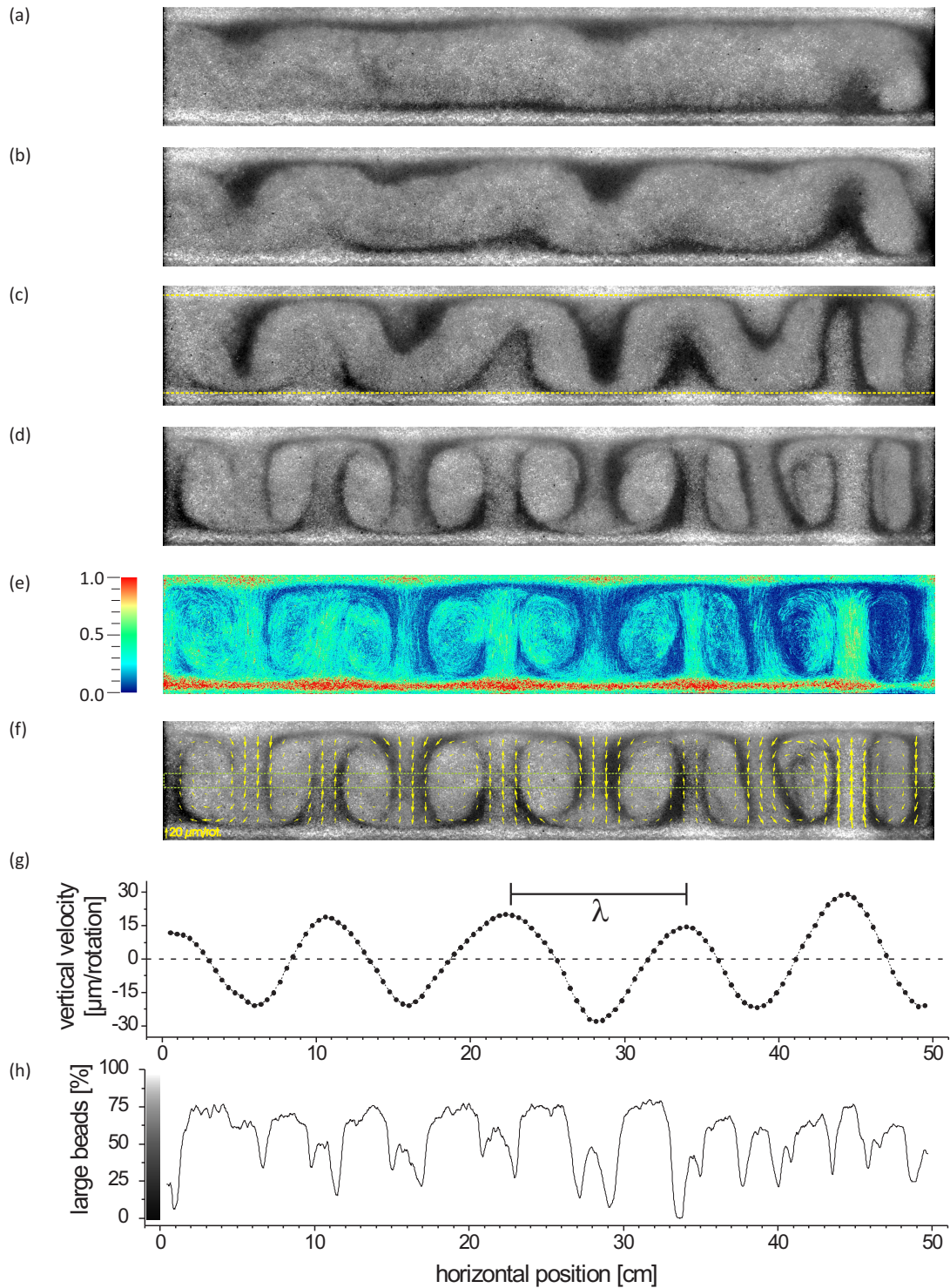


**Figure 3.3:** Convection pattern in a densely filled cell. Development of the pattern after (a) 2,000, (b) 4,000, (c) 6,000 and (d) 12,000 rotations. Regions enriched with small particles appear darker, regions enriched with large particles appear brighter. The optical transmission reflects an average particle concentration through the cell depth. Fluidized zones and convection streams are separated by dashed lines in (c). (e) Brightness fluctuations (normalized) of (d) reveal streak lines (averaged over 400 rotations (20 images)). (f) The pattern of (d) with superimposed arrows (yellow) of the flow field, i.e. the mean displacement of clusters per rotation, as detected from velocimetry. (g) Vertical flow velocity for the central region of (f) (greenly dashed). The wavelength  $\lambda$  of the flow pattern is indicated. (h) Corresponding composition of the mixture.  $C = 0.647 > C_C$ .

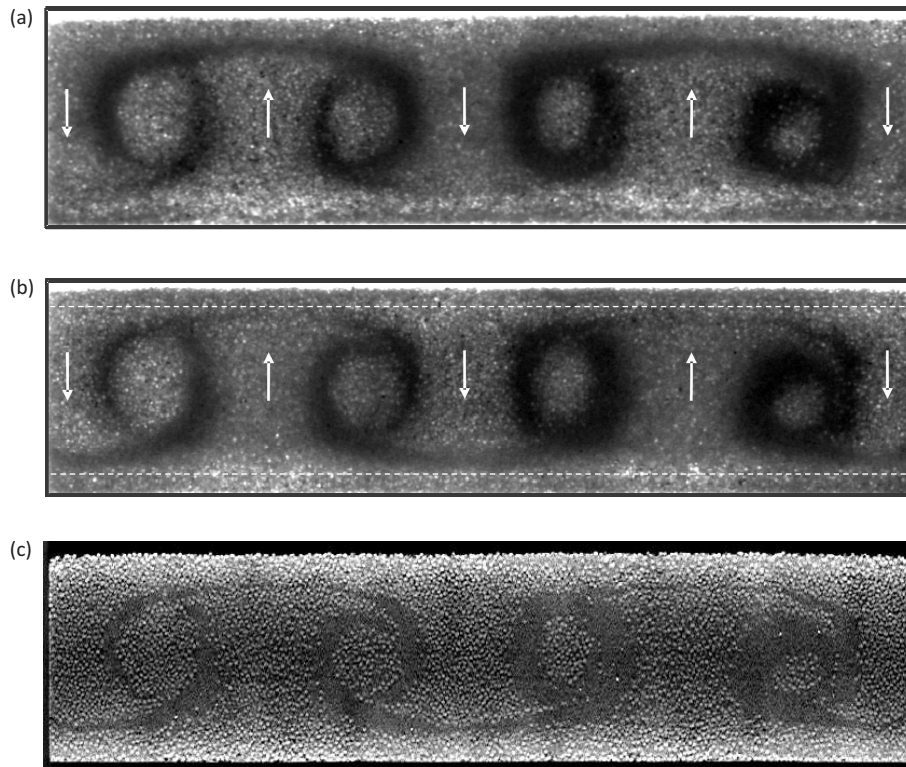


**Figure 3.4:** Example of convection rolls in a densely filled container after 18,000 rotations. (a) Front view and (b) corresponding rear view of the same experiment. The rear view has been mirrored horizontally to facilitate direct comparison of the patterns. Only minor differences are seen between front and back. The horizontal dark bands, enriched with small particles and located between circular shapes, evidence slight differences of both container sides in regions where the flow is upwards/downwards. The container border is indicated by a black frame. The small gap on top of the granulate corresponds to the free space in the container cell (the real gap height is smaller as there is a slight overexposure). Dashed lines separate the fluidized regions along the outer edges from the central convection region. (c) Computer tomography of the same experiment. Shown is the central slice between front and back sides. Single small particles (dark areas) are not resolvable. The resolution is  $200 \mu\text{m}/\text{pixel}$ . Transmission and reconstructed X-ray images show the same patterns and therefore optical transmission is considered as a reliable method. ( $x=160 \text{ mm}$ ,  $y=40 \text{ mm}$ ,  $C = 0.625$ ).

the mode will change. A mean ‘survival’ time of a selected mode was not determined. For three cases, the strongest mode is selected and their growth rate for the first 6,000 rotations was determined (figure 3.6(a3-c3)). During this time all modes grew approximately linearly. The strongest modes for the three experiments are (a) 4.5, (b) 5, and (c) 4, respectively. The growth rates vary by a factor of 2.2. There seems also no relation between growth rate and mode number. The stronger a mode the narrower is its distribution in the mode diagram (compare weak mode in figure 3.6e2 with strong modes in figure 3.6a2,b2). Small differences during the initial filling processes – that cannot be easily controlled – seem to cause large differences in the mode selection. However, it is later shown (section 5.7) that the way of filling is not the reason for convection itself.

### 3 Convection & segregation

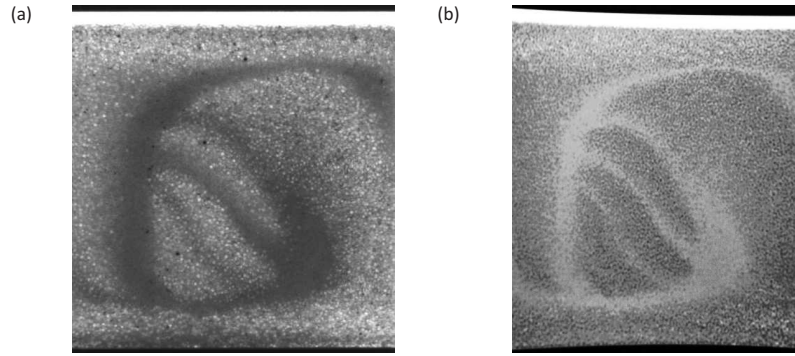


**Figure 3.5:** Convection roll both times seen in transmission by either (a) visible light or (b) X-ray (strongly contrast enhanced,  $\lambda = 0.05$  nm). The sense of convection is clockwise. Brightness indicates in both frames the amount of photons that hit the detector. In the optical image, regions enriched with small particles appear dark as light is scattered more intensely. In the X-ray image, regions enriched with small particles appear brighter indicating lower absorption. Both pictures show roughly the same global pattern. The slight warp in the X-ray image is a device artifact.

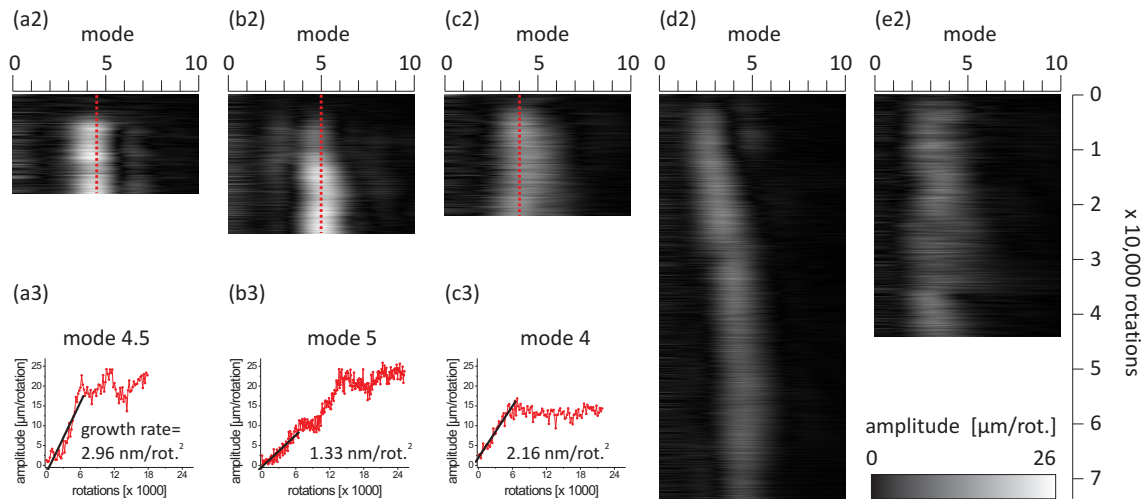
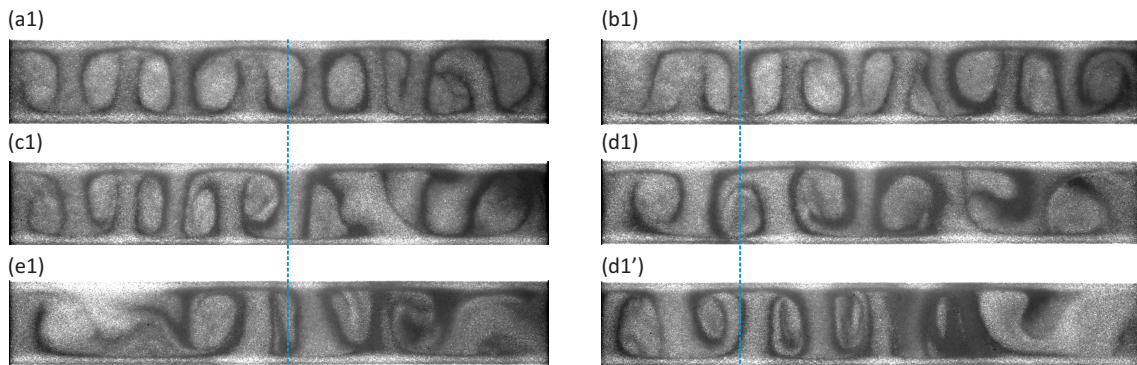


**Figure 3.6:** (a1-d1) Five experiments under same conditions. Same letters belong to same experiments. Brightness reflects particle composition. (a1) Continuation of the experiment in figure 3.3. All pictures are after 18,000 rotations. However (d1') is after 74,000 rotations and belongs to the experiment (d1). The filling fractions can be regarded as identical (a1-c1)  $C = 0.647$ , (d1-e1)  $C = 0.645$ . (a2-e2) Shown are the corresponding developments of the mode amplitudes (relating scales on the right). The strongest modes are selected (red dashed lines) and shown in (a3-c3). The growth rate is determined for the first 6,000 rotations and varies among experiments. Convection at the two blue dashed lines in the upper part is also discussed in section 5.5.

### 3.5 Transition

In the following, the transition between axial segregation and convection is characterized. First it is shown how the flow amplitude changes if one passes from one state to the other. Then it is demonstrated how a modification of the free container volume can easily switch between both states.

The vertical velocity in the central cut is presented in figure 3.7 for different fill ratios. Figure 3.7a is a space-time plot of the flow field at subcritical  $C = 0.581$  for an axially segregated stripe pattern (see figure 3.2a). The global downward flow reflects a small effective difference of the motion at front and rear planes, i.e. an effective vortex in the  $yz$  plane, in the same sense as the cell rotation. Size segregation modulates the flow: in general the regions of higher concentrations of small particles move faster. Figure 3.7(b-e) shows the qualitative change to the convection regime; the convection rolls are manifest in spatially alternating up and down flows. Slightly above  $C_C$ , there is a strong oscillation at the lateral edges of the cell (figure 3.7c), possibly reflecting a competition of rudimentary chute flow with the convection pattern. At higher fill ratios, these oscillations vanish. The velocity amplitude decreases with increasing  $C$ , and the particle motion becomes more and more collective. When  $C$  approaches a value of about 0.66, no motion is observable. No global motion can be observed but individual particles are able to rearrange among their neighbors. Maximum velocities are of the order of  $50 \mu\text{m}/\text{revolution}$ . Thus, a particle needs several thousand cell rotations for a full turn.

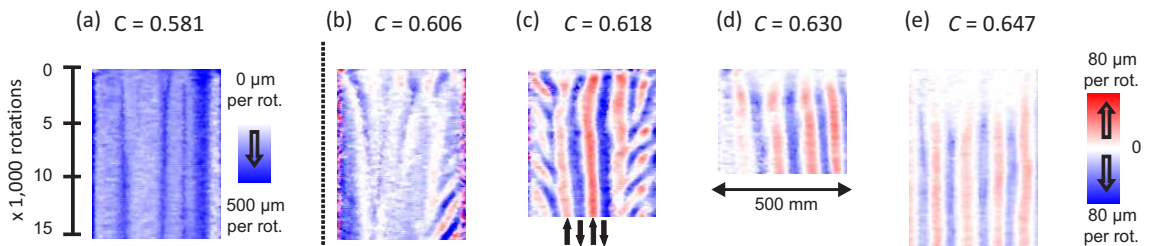


**Figure 3.7:** Time-space plots of the vertical flow field component in the central horizontal axis of the cell. Red indicates upflow, blue marks downflow. (a) Global downward flow at a slightly subcritical  $C$ , reflecting a vortex in sense of rotation. Compare with top right panel in figure 3.2. (b-e) Convective flow in dependence on the fill ratio  $C$ . The flow field is in principle uniform through the cell (in viewing direction). There is a small offset between front and back sides. When the cell is rotated by  $180^\circ$ , up and down stream regions are interchanged. Images of figure 3.3 correspond to the space-time plot (e). Space-time plot (c) will be discussed also in figure 7.6(a-c).

The qualitative differences between both the dynamical regimes, chute flow and convection, can also be shown in a simpler, direct way. A transition between both regimes can be triggered if one changes the container volume during an experiment. First, an axial segregation pattern develops at a low filling state ( $C \approx 0.52 < C_C$ , figure 3.8a). The motion of the beads follows primarily the sense of the container rotation. This pattern is persistent for a period of several thousand rotations. Then, the height of the container is decreased to obtain a relative higher filling ( $C \approx 0.64 > C_C$ ). After reduction of the free volume, the stripe pattern transforms almost instantly (figure 3.8b). The smaller beads (dark region) first migrate towards the outer zones, while later they are drawn into the central region by convective motion (figure 3.8c). It is possible that the undulation of the top edge of the initially axially segregated granulate supports the onset of the convection structure.

### 3 Convection & segregation

However, this idea was not tested further. When the container height is increased again to restore the original low fill level, the system returns to the chute flow regime and axial segregation. This demonstrates clearly how transitions between chute flow and convection can be initiated.

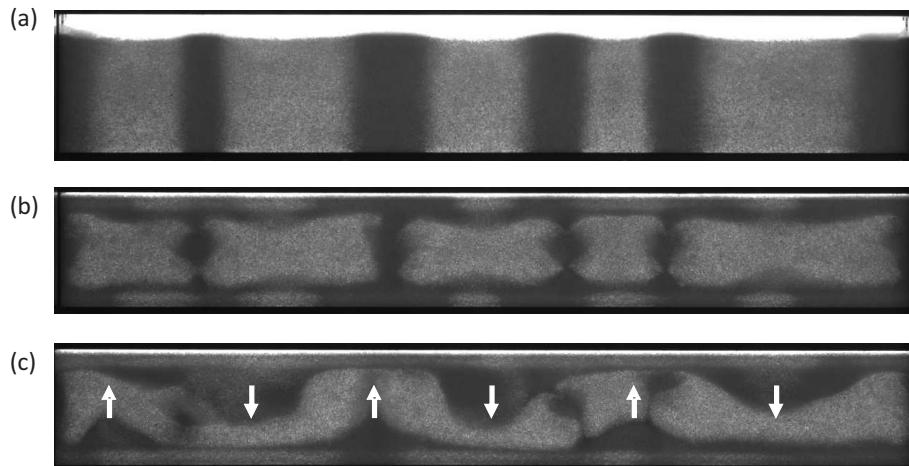


**Figure 3.8:** Demonstration of switching between axial segregation and convection by changing the free container space. (a) Axial segregation pattern after 10,000 rotations in a container with moderate fill level ( $C \approx 0.52$ ). The pattern formed during the first 1,000 rotations and remained stationary afterwards. (b) After further 2,000 rotations with reduced container height,  $C \approx 0.64$ , the material is redistributed. Small beads accumulate at the top and bottom sides and the stripe structure dissolves. (c) A convection structure is clearly established after 5,000 further rotations. Regions enriched with small beads decorate the rolls.

# 4 Influence of driving

The container can be agitated differently. Rotation rate and rotation scheme can be varied. The interstitial medium can also drive the dynamics. Because the majority of granular convection scenarios are observed in vibrated containers and so far never in rotated containers a comparison with shaken systems follows at the end of the chapter.

## 4.1 Rotation speed

All experiments are performed at low *Froude* numbers  $\ll 1$  with a rotation rate of typically 10 or 20 rpm. Slower driving rates down to 1 rpm was tested, this only expands the experimental time and does not influence the qualitative pattern formation. Presumably the driving rate for the convection is not limited from below. For higher rotation rates the case is different as inertial forces have to be accounted for. Convection rolls were still found for driving at 50 rpm. If the *Froude* number is greater than 1, radial segregation inhibits convection and the segregation is partly ‘frozen’ in the top/bottom regions (Fig. 4.1b). Small particles are sieved outwards and accumulate along two horizontal front lines next to the large particles in the center. It might be possible that the fronts of small particles indicate increasing particle density in radial direction. Then small particles are unable to pass if jamming becomes too high. No data are available about temporal development of the front. In the lower and upper thirds the segregation pattern is less affected. For the given system, inertia balances gravity at 189 rpm. Compare to radial segregation in two-dimensional containers (figures 1.6a,b,8.1d,e).

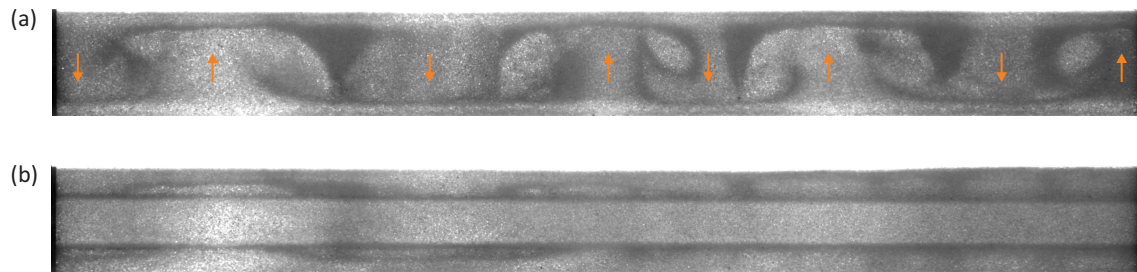


**Figure 4.1:** Influence of inertial effects on the convection pattern. (a) Seven rolls (arrows) have been formed after 44,000 rotations at slow speed (20 rpm,  $Froude = 0.01 \ll 1$ ). (b) After  $\approx 1,500$  further rotations at higher speed (250 rpm,  $Froude = 1.75 > 1$ ) small particles are sieved outwards and form two dark horizontal front lines.  $y = 50$  mm.

## 4.2 Rotation scheme

In standard experiment, the sense of rotation is maintained. This means that the grains slide in a defined direction when one of the cell planes is on the top side. This broken symmetry manifests the details of the segregation texture. Figure 3.4a,b shows circular assemblies of small beads on the front and rear sides. Moreover, one acknowledges narrow dark bands of small beads that are accumulated on the front side of the rotating cell in regions where convective flow is directed upward. At the rear side, these bands are located

## 4 Influence of driving

in regions where flow is downward. After each half rotation of the cell, front and rear sides as well as up and down flows alternate, so that the structures on both sides of the cell are equivalent, but the above mentioned asymmetry prevails.

It is therefore interesting to study the influence of a reversal of the rotation sense. First, it was checked how the flow changes in longer terms when sporadically the sense of rotation of the cell reverses (figure 4.2a,b). Reversal of the rotational sense (arrows) in most cases only slightly disturbs the lateral positions of the convection currents. With the exception of the first reversal in figure 4.2a, the global roll structure and convection velocities are largely preserved after the reversal. The rolls may subsequently drift in the cell, but there appears to be continuity of the convection when the rotation of the cell is reversed sporadically. Locally, details of the the flow profiles may fluctuate and flow amplitude as well as the number of rolls may change, but this is also the case during unidirectional rotation (see figure 4.2a at around 100,000 rotations).

In addition, periodical changes of the directional sense were tested (figure 4.2c,d). The plot in figure 4.2c in the region labeled ‘ $\pm 360^\circ$ ’ was obtained while the sense of rotation of the cell was reversed after each full turn. It is obvious that the convective motion is still present, although the amplitude is low. In the following period, the rotation was reversed every half turn (labeled ‘ $\pm 180^\circ$ ’), and in the last part of figure 4.2c, the cell has been switched back to uniform rotation. The convection pattern remains uninfluenced, but the velocity of flow increases noticeably.

Figure 4.2d demonstrates that a cradle-like  $\pm 180^\circ$  back-and-forth rotation not only preserves an already developed convection scenario as in figure 4.2c, but that it also creates convection in a freshly filled cell. It is noted that in this  $\pm 180^\circ$  experiment, the two cell planes are different. There is only one chute plane and no exchange between the two planes.

The aspect ratio of the cell is 10 in figure 4.2a,b and the number of rolls is on average 8. In figure 4.2c,d, the aspect ratio is 6.25 and the number of rolls is 6 on average.

## 4.3 Interstitial medium

In vibrated systems, it has been demonstrated that air and viscous drag may play a non-negligible roll in the formation of granular convection structures [111, 112]. Even though the velocity of grain motion in the flat cell is much lower, it is interesting to examine the influence of air. So far, all experiments described above have been performed under atmospheric air pressure. In order to qualify the role of the interstitial fluid, the effect of reduced air pressure was tested.

The minimum pressure obtained with the vacuum pump was 3 Pa. At this pressure, the granular convection showed no systematic differences from the dynamics at ambient pressure. The variation of convection velocities between low pressure and atmospheric pressure experiments was within the fluctuations observed for different runs of the experiment at ambient pressure.

The granular dynamics is quantitatively characterized by the vertical flow component of the convection patterns (figure 4.3a). In the vacuum experiment a container of aspect ratio 4 is used and there between 4 and 5 rolls are found. Such a long-term fluctuation of the number of rolls in the convection system is also common in the atmospheric pressure experiments. The results are discussed in relation to vibration experiments (section 4.4).

Also the presence of water did not influence the qualitative findings for the granular dynamics in the rotating flat cell (an exemplary structure has been used to construct figure 2.1a). Moreover, in this test the influence of electrostatic charges on the basic convection mechanism can be ruled out. Again, four to five rolls are formed in a container

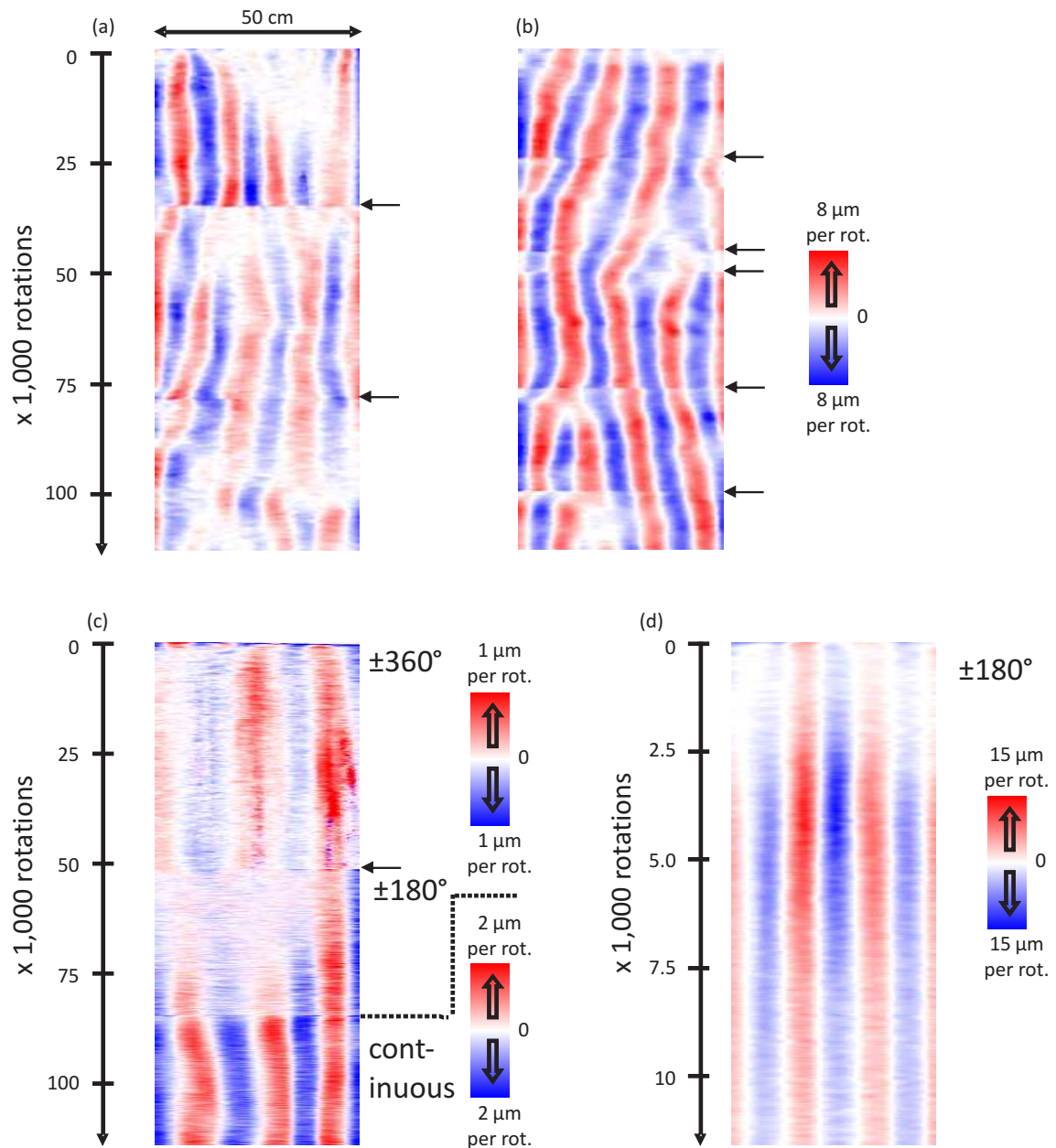


**Figure 4.2:** Time-space plots derived from the vertical flow component in the horizontal cell midplane. (a,b) Sporadic reversals of the sense of rotation (at the positions of the arrows). In most cases, this reversal has only a minor influence on the convection.  $y = 5 \text{ cm}$ ,  $C = 0.646$  (c,d) Periodical reversals of the rotation sense.  $\pm 180^\circ$  indicates a reversal every half rotation,  $\pm 360^\circ$  indicates a reversal every full rotation of the cell. The label ‘continuous’ marks the time period where the cell again unidirectionally rotates. Note the different color scales and different flow magnitudes.  $y = 8 \text{ cm}$ . The magnitudes of the individual experiments cannot be directly compared because of different cell heights and different cell preparations (see section 5.3). (c)  $C = 0.655$  and (d)  $C = 0.645$ .

#### 4 Influence of driving

with aspect ratio 4 (figure 4.3b). Convection flow amplitudes are of the same order of magnitude as in the vacuum experiment.

Additional tests with commercial sunflower oil as interstitial medium were performed. The oil's viscosity is circa 50 times higher than the viscosity of water at room temperature. Rotation rates were chosen between 0.4 rpm and 100 rpm. Slow rotation grants the grains more time to sediment whereas faster rotation increases the inertial forces more on the denser glass beads than on the lighter liquid. Air bubbles could not completely removed. Notwithstanding the given situation convection was found for rotation rates  $< 1$  rpm. The flow is not so pronounced as in situations with lower viscosity and the flow only locates in a part of the cell. For higher rotation rates no clear results are available.

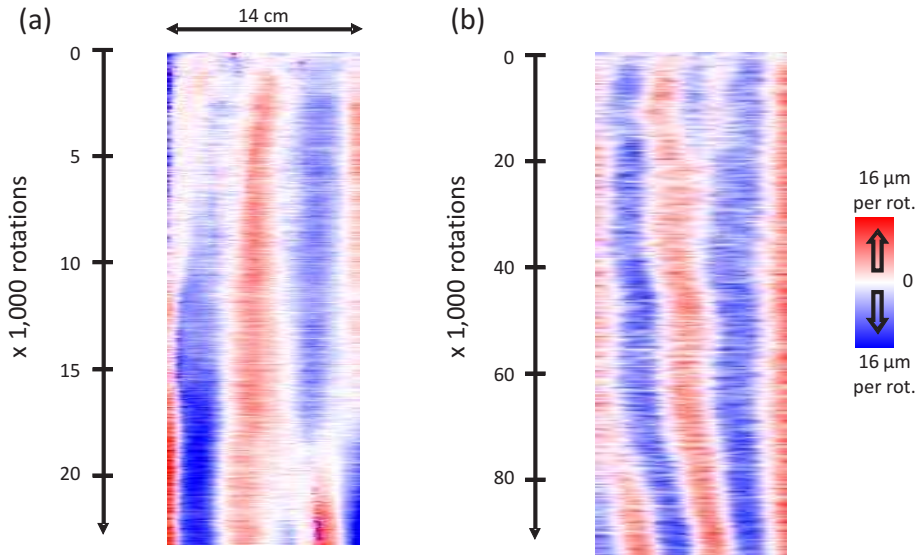


**Figure 4.3:** Time-space plot of granulate in (a) vacuum and (b) water, derived from the vertical flow component in the horizontal cell midplane.  $x = 14$  cm,  $y = 3.5$  cm. (a)  $C = 0.61$  and (b)  $C = 0.60$ .

#### 4.4 Shaking

Convective motion of granular material has also been reported in shaken systems, in avalanches [113], subsurface layers [47] and in a few shear studies [114, 115]. In literature, a long list of papers deals with granulate in shaken containers. It is well known that in these vibrated systems many types of convection structures can form (e.g. [116]). An extensive overview of convection rolls in shaken containers is beyond the scope of this thesis, but some general features of shaken systems are compared with the rotating container experiment. Finally, some shaking experiments with the very sample cells used in the rotation experiment are reported.

**Energy input** In shaken systems, the granulate has to overcome the Earth's gravitational acceleration  $g$ . Typical thresholds reported in literature are  $\approx 1.2g$  and above [30, 117]. The selection of patterns depends on the shaking strength [45, 116]. In contrast, in the rotating cell experiment the effective gravitational acceleration is less than  $g$ . During the phase when the granulate slides, the cell plane forms an angle with the horizontal that is comparable to the angle of repose  $\alpha_{repose} \approx 35^\circ$ , and the effective (in-plane) acceleration

is  $\sin(\alpha_{\text{repose}}) \cdot g \approx 0.6 g$ . Inertia effects are negligible and the observed cell dynamics (measured in units of cell rotations) is independent of the driving angular velocity of the cell in a large parameter range. Similar to the flat cell rotation, convection is suppressed in the vibrated container when the free volume above the granular bed is sufficiently reduced [118].

**Symmetry** Under vertical shaking in the Earth's gravitational field, the up-down symmetry is broken. Forces of the container on the grains can be transmitted only upward. Downward, gravity accelerates the grains. The energy distribution along the container height is different. It can be higher in the bottom region or near the surface. A resulting density inversion can lead to convection [119]. Under horizontal vibration, similar convection rolls are found as under vertical shaking, but gravity influences the particle dynamics as it acts perpendicular to the container forces [120]. In the rotating cell, symmetry of the top and bottom sides of the cell is conserved, because the rotation permanently exchanges top and bottom edges of the container. Asymmetries by a predefined sense of rotation can be balanced by periodical rotation reversals (section 4.2).

**Role of side walls** Side walls may drive convection patterns in vertically shaken containers [104] or can confine the rolls [119]. If convection patterns are driven by friction at the side walls, they always appear pairwise either downwards or upwards at the sides [45, 104] (figure 1.2e). In contrast, it is shown in section 5.3 that side walls are not necessary for convection in the rotation experiment reported here. Any number of rolls (even or odd) can be observed in the cell. The container walls confine the convection structure laterally, but there is not necessarily the same flow direction at opposite side walls in a symmetric cell, up and down flows are equivalent.

**Role of air** Owing to the high particle velocities in shaken containers, air can play an important role in convection structures observed. However, there is no clear trend, as in most experiments the air increases the effect [111, 112], but the opposite has also been found [121]. In shaken shallow layers, convection is found also in absence of air [122]. In section 4.3 it was shown that in the rotating cell interstitial air is irrelevant. Convection still persists at pressures two orders of magnitude lower than the threshold where the mean free path of the air molecules becomes comparable to the particle size. At that pressure (Knudsen regime [111, 112, 123]), friction and viscosity of the air have no major influence.

**Shaking of the flat container** The most straightforward comparison between the dynamics of grains in shaken and rotated cells can be made when the same containers that were used in the rotation experiments are vibrated vertically, at comparable fill levels. In the following, a qualitative, but not exhaustive description of this comparison is given.

A cell as depicted in figures 3.4 and 4.4a was used to test whether vertical shaking instead of slow rotations of the almost filled cell produces comparable results. The energy input during shaking is always considerably larger than in the rotation experiment. The shaken cell is driven with an amplitude of up to  $6 g$ . At  $1 g$ , no collective motion is observable. The strongest convection is found at  $3 g$  and 30 Hz vibration. Irrespective of the fill level of the container, the observed flow structures are qualitatively different from those described in the rotation experiment.

For lower fill heights ( $C < C_C$ ), a single heap develops in the cell (shown in figure 4.4a,b) and a single roll pair emerges, with the direction of flow indicated by arrows in the picture. At high filling level ( $C > C_C$ ), the heaping effect leads to the loss of free volume above the

#### 4 Influence of driving

granulate in the center of the cell. Thus, there is practically no collective transport in the cell center. However, the free volume at the sides of the cell (sketched in figure 4.4c) allows the formation of two rolls acting only at the side walls of the container. In the center, no motion is detectable within the experimental time frame. In both situations, the flow is downward at the cell side walls.

Thus, both structures differ qualitatively from the rotating cell experiment. If the vibration is not exactly orthogonal to the cell orientation, any slight asymmetry moves the peak of the granular bed to one of the lateral sides. In that case, only a single elongated roll forms in the whole cell at lower filling (figure 4.4d), whereas at high fill level (figure 4.4e), a single localized convection roll forms at the side that contains the free volume. At the opposite side of the cell, there is no measurable transport on the time scale of the experiment. Stable segregation patterns were not observed except in the situation of figure 4.4a,b, where a part of the small beads accumulated in the upwards flowing region at the center.

These phenomena are well known from other vibration experiments [117,124,125]. The beads tend to be driven downwards at the side walls, and always move upwards in the inner region towards the peak of the granular surface. It is obvious that the driving mechanism for convection in vibration experiments must be essentially different from that in the rotation experiments, and that the characteristic flow and segregation patterns described in the previous sections cannot be reproduced by vibration techniques. Furthermore, much higher accelerations are needed to drive convection in the vibrating cells. The convection occurs on completely different time scales compared to the rotating cell structures.

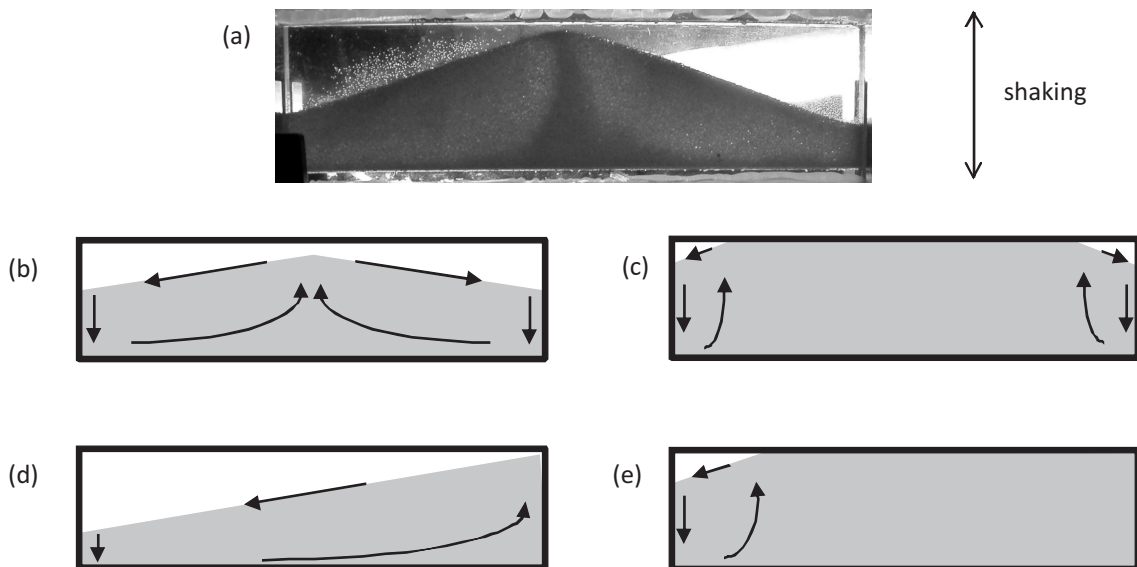


**Figure 4.4:** (a) Photography of a vertically vibrated cell at low filling and schematic sketches of the flow for (b,d) low and (c,e) high filling. A heap forms with either two rolls (a-c) under symmetric driving, or with a single roll (d,e) under slightly asymmetric driving. The lateral expansion of the convection structures depends on the fill level.

# 5 Geometrical influences

There are a large number of parameters that can be varied in the experiment. Concerning geometry of the container, are width, height, thickness, aspect ratio, modulation of container walls, and material of container walls. Related to the granular material, one can differ them by size, shape, relative volume fraction, mono-, bi-, multidispersity, size distribution, surface properties, density, and combinations of them. Furthermore filling fraction (see section 3.5) and initial states can be varied. Most of the listed properties were investigated but a systematic parameter study is still to be done.

## 5.1 Cell aspect ratio

The container aspect ratio is defined by  $x/y$ . Ratios from 0.67 to 15.9 have been tested (for aspect ratios  $\gtrsim 0.67$  see chapter 6 and for aspect ratio 15.9 see figure 7.5). The number of rolls is given roughly by the container aspect ratio. It can adopt even or odd values and may vary slightly during an experiment when individual rolls or roll pairs are formed or extinguished. Even single rolls are possible when the aspect ratio is close to one. The maximum number of rolls is by principle only limited by the aspect ratio of the container. Up to 16 rolls were observed in long cells (figure 7.5). Figure 5.1 shows the influence of the container height on the selected wave number. The dots label runs where the selected mode was constant, while vertical bars indicate that the pattern showed temporal fluctuations of the mode during the experiment. As in typical hydrodynamic convection structures (e.g. Rayleigh–Bénard) the selected wavelength is roughly equal to twice the cell height. The red line shows the relation for circular rolls with diameter  $y$ . The general trend is, in view of the small aspect ratio of the experiment, in reasonable agreement with such an assumption.

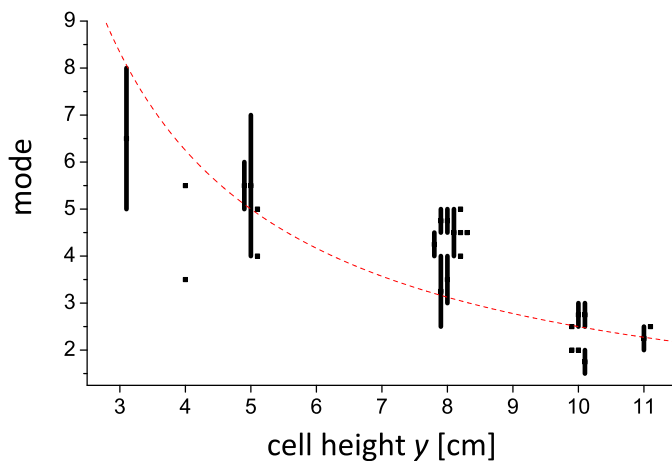


**Figure 5.1:** Range of observed modes in dependence upon the cell height for a constant cell width of  $x = 50$  cm. The data represent 25 individual experiments. The dashed curve symbolizes the relation for circular rolls,  $mode = x / (2 \cdot y)$ . For clarity, individual experiments for the same cell height are slightly displaced on the abscissa. Lines span the mode range during an experiment, a point symbolizes that the mode was stable.

## 5.2 Smallest cell size

The smallest possible container dimension for convection was desired. For a cell of  $x \times y = 6 \text{ cm} \times 3 \text{ cm}$ , a double roll was found as expected by the aspect ratio of 2 (figure 5.2a). For the smaller  $4 \text{ cm} \times 2 \text{ cm}$  box in five experiments, only a single roll or no convection was found (figure 5.2b). One can assume that these dimensions might be the smallest possible size, corresponding to about 100,000 particles in the  $6 \text{ cm} \times 3 \text{ cm}$  cell and about 50,000 particles in the smaller one. Alternatively to shrinking the container geometry one could also increase the particle size or combine both methods. One attempt has been made in two-dimensional experiments (chapter 8). Knowledge of the smallest possible container size gives hints for simulation tests as calculation time increases with number of particles.

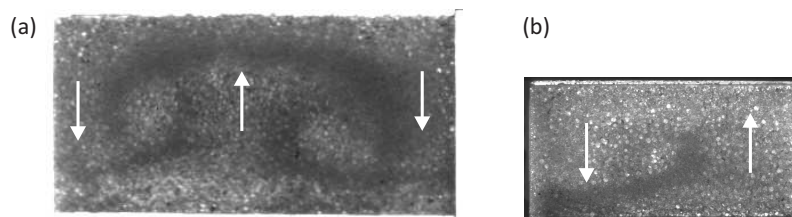


**Figure 5.2:** (a) Smallest tested size where more than one roll was found.  $x \times y = 6 \text{ cm} \times 3 \text{ cm}$ . For the smaller size (b)  $4 \text{ cm} \times 2 \text{ cm}$  only a single roll was found. Notwithstanding the same aspect ratio at least a minimum size must be present to get more than one roll. After (a) 8,000 and after (b) 500,000 rotations.

## 5.3 Left/right walls

Is convection driven by the lateral side walls as in vibrated containers (section 4.4)? Indeed, in most experiments, convection starts from one or both lateral cell ends (see figure 4.2a). But convection can also set in rather uniformly (figure 4.2b). The reason for starting at the side wall might be the filling procedure. The upper edge of the granular bed often has a slightly tilted height profile after filling, i.e. at least at one side the local fill level is somewhat lower than in the central part. Then the convective flow is favored to start at the lower filled sides of the cell as there is more space for fluidization.

One can manipulate the initial local fill level by spinning the box moderately around its central vertical axis before the experiment, so that the material is centrifuged to the lateral cell edges. Then, one obtains a height profile where in the center of the cell there is more free volume on top of the granulate than at the left and right hand sides (figure 5.3a). When subsequently the rotation experiment is started with such an inhomogeneous initial grain distribution, convection tends to start in the central region of the container. Such a preparation was used for the experiment in figure 4.2d. For better visualization, the graph of the vertical convection velocity component in the cell midplane is shown in figure 5.3b. It is evident that the convection flow amplitude is initially highest in the central region (after 1,500 and 4,000 rotations, respectively) and it equalizes later (10,000 rotations) together with the homogeneous redistribution of the granulate. The conclusion is that the side walls may play a certain role for the convection pattern (they fix the wavelength), but they are not necessary for the formation of convection structures. The intrinsic convection pattern would also form in absence of lateral confinement, in an infinitely extended cell. This is a

noticeable aspect when the convection rolls are compared to structures observed in shaken containers (section 4.4).

Vertical side walls can also be avoided by bending the walls outwards (figure 5.3c). Then the effective friction in direction of gravity is reduced. Flow is tilted in the capped regions and some regions (framed by yellow solid lines in figure 5.3c) are not affected during experimental time (31,000 rotations). The fluidized regions (framed by dashed lines in figure 5.3c) extend only along the non-curved borders.

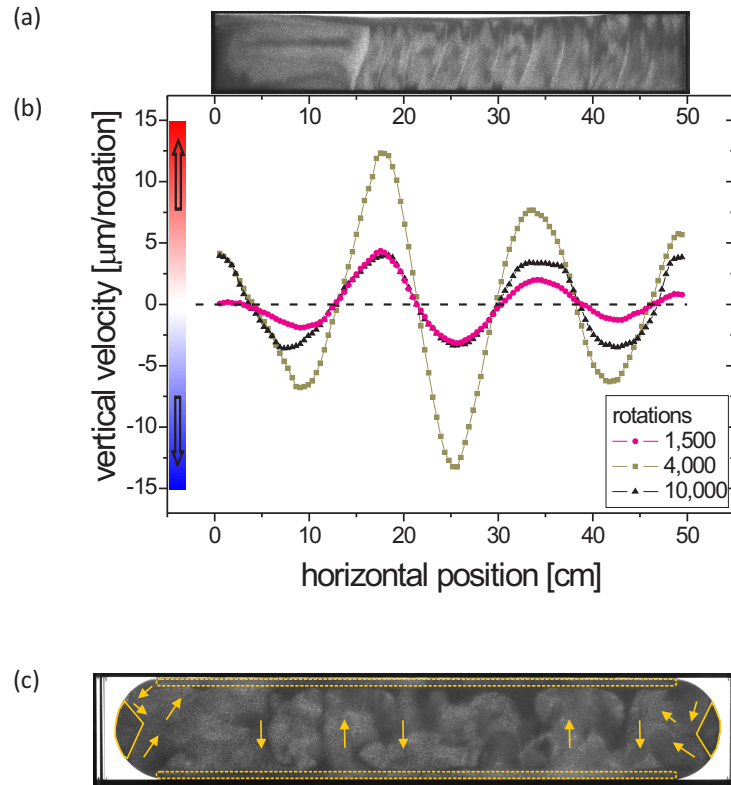


**Figure 5.3:** (a) Initial state of the granular bed prepared for convection onset in the cell middle. Note the locally different fill heights because of the deformed granular surface. (b) Vertical flow velocity in the horizontal cell midplane at 3 instants, extracted from figure 4.2d. Initially, the flow is faster in the central region (1,500 and 4,000 rotations, respectively), but it balances with progressing time. (c) Convection in a box that is lateral capped by half circles (appear white). Arrows show principal flow directions. No flow is observed in segments on the left/right (areas framed by solid lines). Fluidized regions are framed by dashes.  $x = 400 - 480$  mm, after 31,000 rotations.

## 5.4 Top/bottom walls

It is evident from section 5.3 that the locations and dynamics of the rolls can be influenced when the free space above the granulate in the container is modified. A related phenomenon is observed when the upper or lower container edges are modulated. One can control the wave length of the emerging convection pattern within a certain range when a well-defined wave length is imprinted as a variable height pattern at one or both of the horizontal edges. Such a modulation of container edges locks the position of the convection streams (examples are schematically shown in figure 5.4(a-c)).

If the cell edge contains ledges or dimples as in figure 5.4a,b the convection pattern will start at these obstacles. Figure 5.4a,d shows a container with three ledges at the upper container edge located near the center of the cell. These ledges protrude 1 mm into the cell and span the complete cell depth  $z = 5$  mm. Convection sets in first at the ledge positions. This is visible by the dark arches of small particles flowing downwards. At later stages, the convection pattern penetrates the rest of the cell (figure 5.4e). A minor detail is the slightly different segregation pattern in the central structured cell region versus the unstructured lateral regions. At the positions of ledges or dimples, the free space above the granulate adjusts to almost the same level as in other regions of the upper edge. The upper surface of the granular bed roughly follows the modulation of the cell boundary. However, the compensation is incomplete: it seems that the free space at the position of dimples is on average slightly larger, at the level of resolution of the images, than at the ledge positions. Figure 5.4b,f demonstrates that not the modulation of the local cell height but the modulation of the boundary shapes is essential. Here, the ledges of top and bottom edges are staggered such that the local cell height is uninfluenced. As a consequence, the convection structure again follows the modulation of the container boundaries. Small sized particles accumulate below the ledges and the convection current tends to point in the directions away from ledges and towards dimples. Even though there is no simple explanation for this observation, it may help to evaluate the validity of models for the convection mechanism.

In all cases where periodic modulation of the cell boundaries is imposed, there is a competition between the natural and the geometrically imprinted wave lengths. If the difference between these wavelengths is too large, the rolls do not lock to the geometrical constraints.

In particular, this was evident when experiments with very narrow ledges in the top edge were performed. The original idea was to create arbitrary edge shapes by placing small screws equidistantly along the cell edge and to vary the local cell height by adjusting the screw lengths inside. If the natural wave length of the convection is much larger than the screw distance, one might expect that the granulate experiences some local average of the container boundary. However, this concept of an ‘effective’ container wall did not work. Instead, the very character of the convection changed. The rolls did not flow continuously as in the previous experiments, but they exhibited bursts in the convective flow and in the segregation patterns like plumes in a high Rayleigh number thermal convection experiment (e.g. [126]). One typical case is depicted in figure 5.5a. Groups of 3 pins are screwed 3 mm into the container whereas the remaining pins end at the same level with the container border (see figure 5.4c). The volume between the pins is accessible by the granulate as their distances is several time larger than the grain size. The result of this modification is a quite complex interaction of flow processes. The convection is characterized by an intermittent ascent of ‘plumes’ of small particles in the granulate. A plume in the rectangular dashed box in figure 5.5a is studied in detail in figure 5.5d. While small particle material (dark) moves

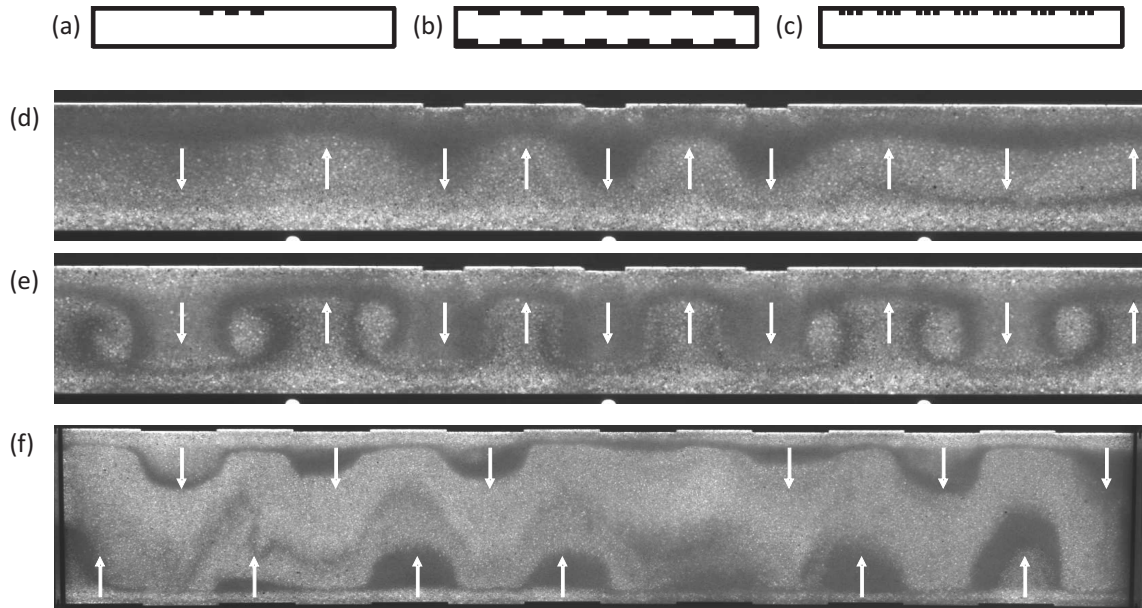


**Figure 5.4:** The cell is modified by different patterns of ledges. (a) Steps on one of the horizontal confining borders, (b) steps on both borders keeping the height constant and (c) assembly of pins on one side. The obstacles' sizes are exaggerated in the sketches. (d) Three steps modulate the cell edge on one side. Steps support the formation of convection streams and lock them at their positions. Arrows indicate the flow direction. Only the central part of the cell is shown, after 1,300 rotations. (e) In the same experiment after 14,300 rotations also the neighboring regions have developed visible convection. The natural wavelength is slightly larger than the step distances. ( $y = 31.5$  mm, step width 10 mm, step height 1 mm, step distance 30 mm). (f) The cell is modified by alternating steps on both sides, keeping the height of the cell constant. Note that convection in this experiment is weak in the center because of the rather high fill level. Image taken after 5,000 rotations (step width and distance 36 mm, height 1 mm).

upwards the granulate accumulates in a circular shape (yellow circle) and dissolves again. This upwards stream opposes the sense of rotation where downwards motion on the front page is expected at least. In general plumes rise at horizontal positions that are between two groups of pins. The downward motion is less pronounced and takes place as continuous flow at the position of the pin groups. Narrow stripes of small particles (dark) form at the top side, apparently influenced by the inward piercing pins. Time-space plots of horizontal cross sections show the segregation (figure 5.5b) and vertical flow field (figure 5.5c). The cross sections were taken along the rotation axis from the transmission profiles of the cell (figure 5.5b) and the calculated vertical flow velocity components (figure 5.5c). Plumes are reflected as short horizontal dark and red stripes in figure 5.5b,c, respectively. Two exemplary plumes are encircled by ellipses in figure 5.5a. Their positions in the space-time diagrams are indicated by arrows. The 'natural' number of rolls in this geometry (cell aspect ratio) would be approximately 6. A frustrated region forms in the center of the cell because of the incompatibility of the wave length imprinted by the pin settings. This is seen particularly in the flow profile of figure 5.5c.

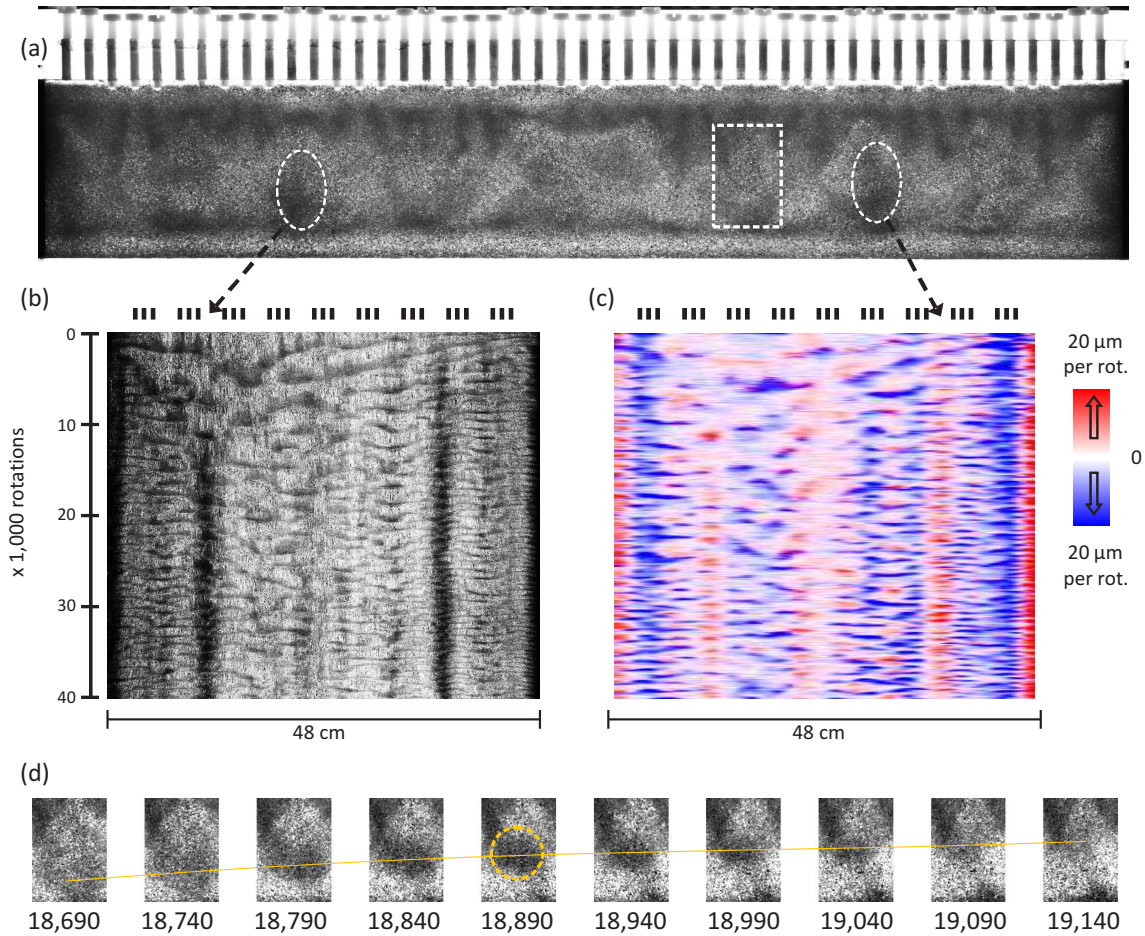


**Figure 5.5:** (a) Segregation pattern after modification of the cell by pins as sketched in figure 5.4c, after 20,000 rotations. Plumes move upwards, two examples are marked by dashed ellipses. Another representation of the same experiment is given as time-space plots of the cell cross sections along the central horizontal axis of (b) the segregation pattern and (c) the vertical velocity. Plumes are represented in a pronounced modulation of the segregation pattern and the flow velocity in time. The position of the pins are indicated above the time-space plots. (d) Temporal sequence of a detail of the pattern (dashed rectangle in (a)). The plume is the dark spot that gradually accumulates small particles. After saturation (yellowly encircled) the plume dissolves. The yellow ascending line connects the center of masses for small particles (estimated by naked eye). The number of rotations is given below the image series. ( $x = 48$  cm, pins are screws of metric size 5 mm). The transparent upper cell edge is not visible in the image, it is at the same height as the screw ends of the upper row of screws.

## 5.5 Cell thickness

One can imagine a situation where insufficient manufacturing conditions lead to slightly different cell thicknesses along the horizontal cell axis. That might imprint a modulation of the flow amplitude on long time scales and enforce convection in some cell parts. To rule out this assumption the flow at the blue dashed lines in figure 3.6 is considered. These five experiments have been performed under same conditions. The cell walls were permanently fixed i.e. they can be considered as made from a single piece. Only the small vertical right side could be opened for filling reasons. Nevertheless, the patterns form at different positions in the cell. Positions that are occupied by a calm roll center (figure 3.6a1,d1) can swap with more active up- or downwards flowing zones later in the same experiment

(figure 3.6d1') or in other experiments (figure 3.6b1,c1,e1). If a small cell thickness variation was a decisive factor, then roll arrays should always form at the same positions. Rather, insufficient mixing during filling instead of the thickness modulations might be responsible for different results (see section 5.7). On the other side, the cell thickness can be artificially modulated to a higher extent so that thickness modulations cannot be neglected anymore. However this idea was not tested except in section 7.1.

In order to answer the question whether the observed structures are unique to a particular cell thickness, experiments with variable thicknesses  $z$  have been performed. In thin cells, down to about  $z = 3$  mm, the convection mechanism continues to exist. Even for monolayers flow and segregation structures are found (chapter 8).

Convection was also found in cells of  $z = 10$  mm. With increasing cell thickness, the convection patterns are more difficult to observe with the transmission technique. Therefore after the experiment, the container is removed from the setup and observed against a stronger light source. In a thick sample cell of  $z = 20$  mm, axial segregation (figure 5.6a) is observed as expected from similar investigations using containers with square profile [76,84]. However at higher fill level the pattern looks different compared to thinner cells (figure 5.6(b-d)). For all cases, smaller particles accumulate at the four borders. For higher filling ratios, a central core of small particles remains (figure 5.6c,d) that is partly diluted by larger beads. The fluidized edges grow with the cell thickness and in the central part of a 80 mm high cell of 20 mm thickness only a narrow core of jammed granular material remains. The fluidized layers also develop a kind of axial segregation structure visible in figure 5.6c. Time development of the structure, cluster motion or typical segregation patterns that decorate convection in thinner cells could not be observed by the technique. There are at least three references that suppose currents in the core of the granular bed in a rotating cylinder at high fill ratio (figure 1.6(e-n)). However, the structure of the currents in that geometry looks different as the central core is mostly occupied by the larger species [80] or is mixed [81].

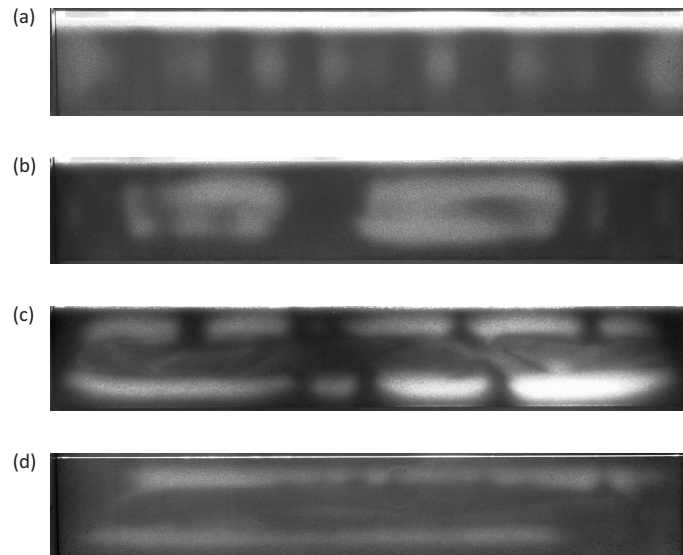


**Figure 5.6:** Patterns in a cell with  $z = 20$  mm. Fill height increases from (a) to (d). Axial segregation can be observed in (a), but the typical convection as in thinner cells is not visible. (a)  $C=0.596$ , after 55,000 rotations, (b)  $C=0.654$  after 114,000 rotations, (c)  $C=0.680$  after 62,000 rotations, (d)  $C=0.693$  after 407,000 rotations. Mixtures seen in transmission by an intensive inhomogeneous light source.

## 5.6 Cylindrical container

In the literature, almost all studies on rotating drum flows were performed in cylindrical geometries (overview in reference [34]). It is therefore at hand to test if besides axial segregation, does convection exists in such geometry. Convection currents were speculated from cuts of the inner drum after rotation at high (70-95%) fill level [80,81]. In order to test this idea, a cylindrical drum was almost completely filled until only a small surface layer was possible. After rotation for some hours optical inspection revealed no special segregation. By means of X-ray tomography the inner structure was visualized (figure 5.7). Three differently composed radial zones can be observed. From the radial axis towards the outer border, the structure is formed by mixed, small and large beads (figure 5.7b). Presumably on the available time scale the inner mixed core was left unchanged and only the outer layers were radially segregated by surface flow. From the segregation pattern along the rotation axis (figure 5.7c), no hints for internal convection could be drawn by this single test. Similar studies [99,102] using MRI have also found radial segregation and concluded convection in order to explain the observations.

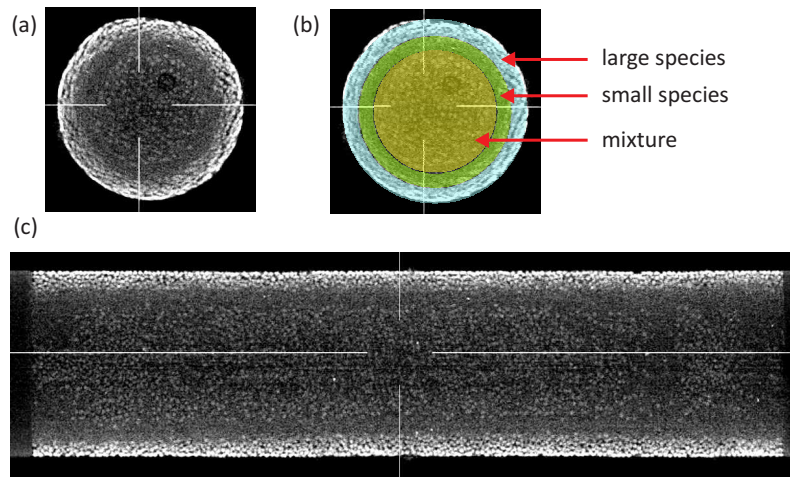


**Figure 5.7:** Computer tomography of an almost completely filled cylinder after one day rotation. (a,b) Radial demixing in the outer shells is colored blue and green in (b). (c) Cut along the rotation axis. The radial cut (a,b) is representative for almost the whole container. Only at the lateral walls higher concentrations of small particles collect in the center. The white straight lines are an artifact of the tomography software. cylinder diameter: 36 mm, length: 140 mm.

An interesting observation was made in a rotating cylinder that was half-filled and rotated continuously back and forth. A change in the sense of rotation after every two full revolutions led to the same type of pattern (figure 5.8a) as continuous rotation. However, after continuation of the run, the rotation angle between reversals becomes low enough, then only a part of the bulk is affected by surface flow (figure 5.8b,c). The segregation pattern is unchanged at the lower bed but forms some irregular lobes on the surface. Decreasing the reversal angle to  $68^\circ$  in the same experiment leads to a shark teeth-like pattern on top (figure 5.8d,e). It is not so pronounced if the last angular setting is repeated from a mixed state (figure 5.8f). Preceding axial segregation facilitates this undulation process. The angle  $68^\circ$  is a little bit larger than twice the angle of repose. This means that after every rotation reversal the granular bed slightly exceeds its angle of repose. The flow is therefore restricted. On the base of the wavy structure and the limited fluidization, one might

## 5.6 Cylindrical container

speculate about relations to the convection rolls in the flat full boxes. A phenomenological similar pattern in a continuously rotated cylinder was observed elsewhere (figure 9 in [127]).

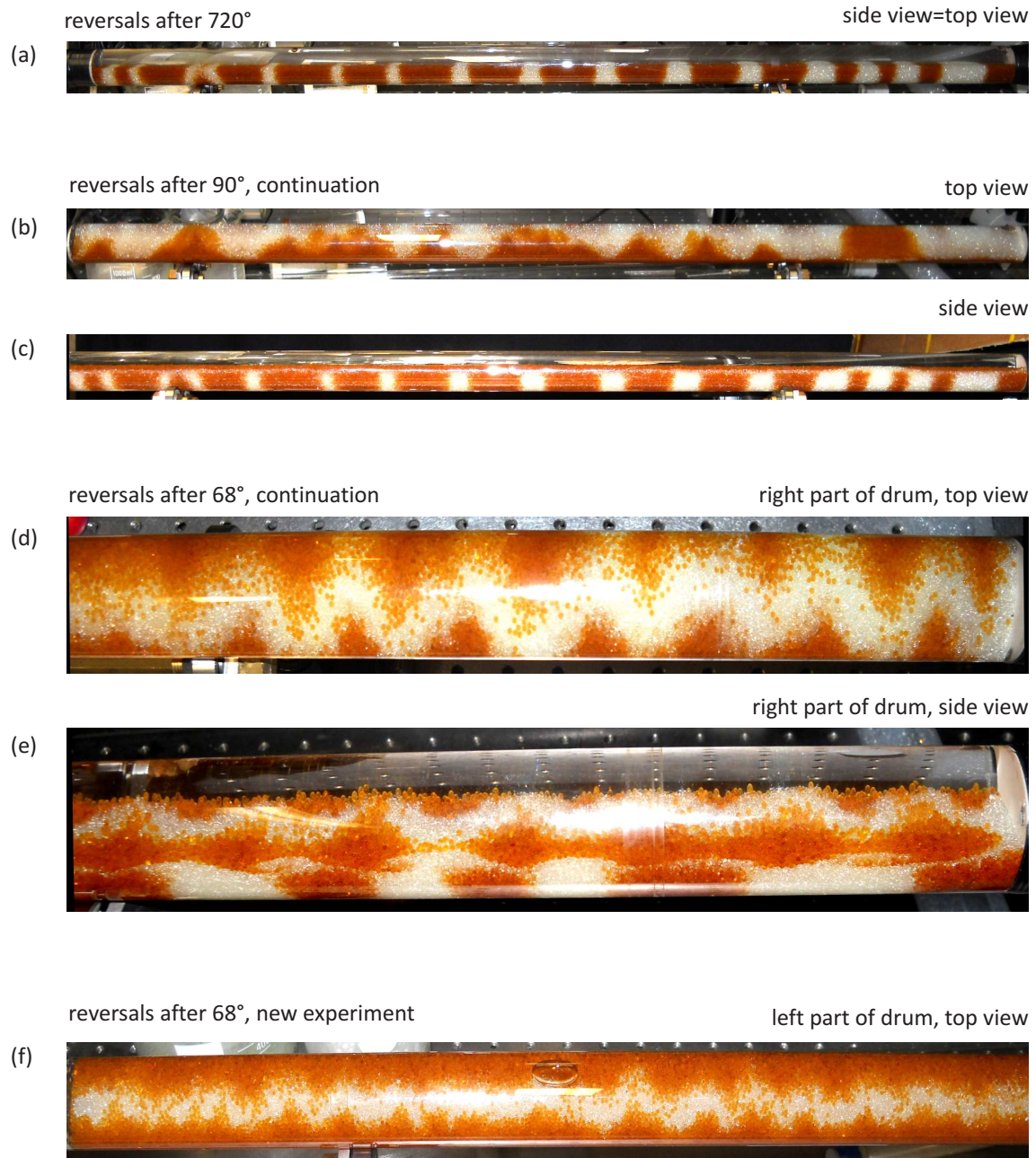


**Figure 5.8:** Patterns that have formed in a half-filled rotated cylinder (slurry, glass beads in water), (a-e) and (f) are separate experiments, respectively. The notes on the left side state the way of agitation and the notes on the right border describe the depicted part of the cylinder. (a) Rotation sense is permanently changed after every 2 rotations. Axial segregation is seen like in the continuously rotated case. (b,c) Continuation by reversals after each  $90^\circ$  leaves the lower granulate bed unaffected. On the surface the stripes dissolve towards an irregular structure. (d,e) Reversals after every  $68^\circ$  form an undulation pattern, even after start from a mixed state (f). tube diameter: 37 mm, length: 100 cm, large orange species:  $(1.5 \pm 0.1)$  mm, small white species:  $(550 \pm 50) \mu\text{m}$ .

## 5.7 Initial preparation

Most techniques of filling container with the premixed beads lead to an unavoidable initial segregation, often similar to stratification patterns in thin cells filled from one side (figure 1.2a). A typical example can be seen in figure 5.3a. These initial inhomogeneities are, however, not essential for the formation of rolls. In order to demonstrate this, a well-defined demixed initial state was prepared where the larger species is stratified below the smaller beads (figure 5.9a). Enough space is left for sufficient fluidization. After 70 rotations, the beads are satisfactorily well mixed (figure 5.9b). If the experiment would continue in this geometry, the beads would start to segregate axially during further rotation. However, the volume is decreased by moving the upper lid inwards (see figure 3.8), to enter the convection regime (figure 5.9c). Thus one can conclude that an insufficiently mixed initial state is not relevant for the onset of convection. The corresponding case with initially axially demixed species on the left and the right cell halves is not suitable. Here, mixing is weak and non-uniform.

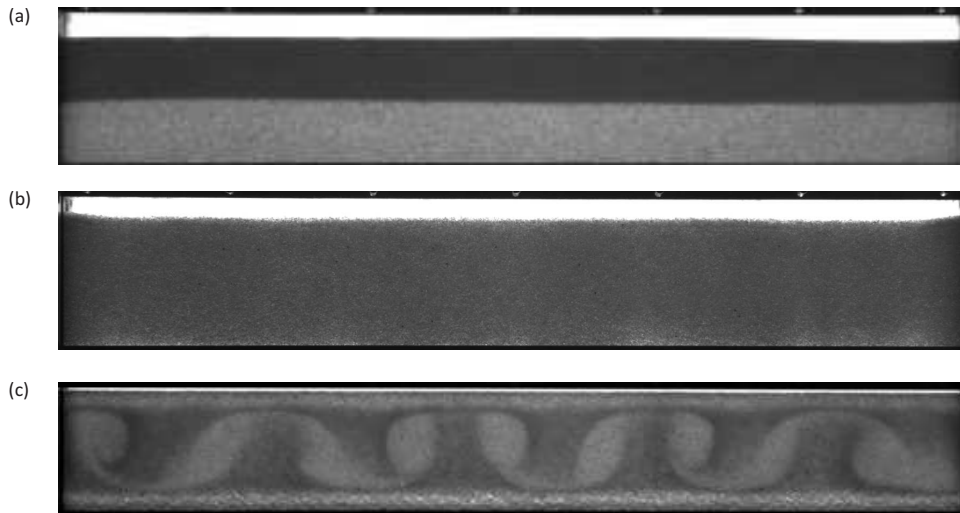


**Figure 5.9:** (a) Demixed initial state to avoid non-uniform filling. Small beads (dark) are stacked above large beads (bright).  $y = 8.2$  cm,  $C = 0.522$ . (b) After 70 rotations the beads are well mixed. (c) After the cell volume was reduced ( $y = 6.7$  cm,  $C = 0.630$ ), a convection pattern forms. The image shows the fully developed pattern after 25,000 rotations.

## 5.8 Variation of granulate

Convection was also found for glass sphere mixtures that contain particles with size combinations 1.5 mm and 2.5 mm or 0.65 mm and 1.5 mm. The following experiments show that the phenomenon is not restricted to the glass bead ensembles. Irrespective of the composition that consists of materials with different size, density and shape, convection sets in. The effect is also robust for sand mixtures containing fine bird grit ( $\sim 100 \mu\text{m}$ ).

Mixtures of crashed stones that are polyhedral shaped produce convection rolls (figure 5.10a) as well as natural products like poppy seeds and mustard seeds or poppy seeds and millet seeds (figure 5.10b,c) or mixtures of glass beads and poppy seeds (figure 5.10d,e). An interesting aspect of the last mentioned mixture is that after approximately 10,000 rotations, the rolls become tilted in the central region. The local direction of the flow is sketched by arrows. The dark areas in figure 5.10(b-e) are enriched with poppy seeds. The fill level is clearly above  $C_C$ , but has not been determined exactly in this experiment. Experiments with mustard and poppy seeds and different kind of sand have been recently reproduced elsewhere [128]. There convection patterns could also be seen. These materials demonstrate that the convection is a quite robust phenomenon as it works also with less well defined grain specifications. But they are not very suitable for experiments because of their opacity. The pattern on the rear side of the cell is generally the same as on the front side.

## 5 Geometrical influences

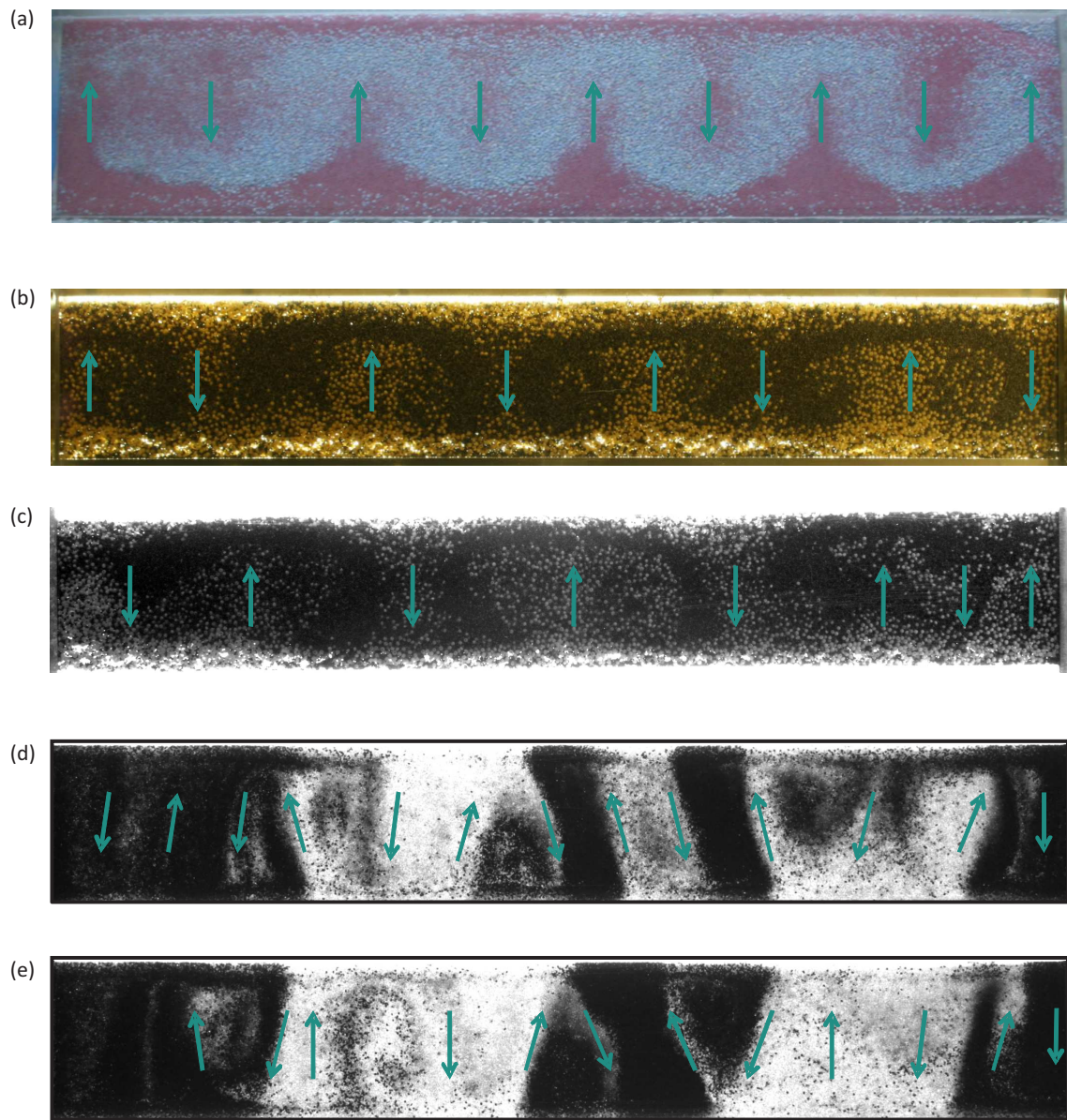


**Figure 5.10:** Flow structures for different material combinations. Direction of flow is indicated by arrows. (a) Stone granulate sold for decoration purposes, (red/dark  $50\text{--}250\ \mu\text{m}$ , blue  $1000\text{--}1400\ \mu\text{m}$ ), after 5,000 rotations. (b) Mustard seeds (yellow,  $\rho \approx 0.75\ \text{g/cm}^3$ , spherical-like size  $\approx 2\text{--}2.5\ \text{mm}$ ) and poppy seeds (dark,  $\rho \approx 0.6\ \text{g/cm}^3$ , size  $\approx 1.0\ \text{mm} \times 0.7\ \text{mm} \times 0.5\ \text{mm}$ ) after 14,000 rotations. (c) Millet seeds (bright,  $\rho \approx 0.6\ \text{g/cm}^3$ , approximately spherical size with  $2\text{--}2.5\ \text{mm}$ ) and poppy seeds (dark) after 19,000 rotations. (d,e) Formation of tilted rolls in a mixture of two grain species of different sizes and densities (glass spheres, bright,  $\rho = 2.50\ \text{g/cm}^3$ ,  $(650 \pm 100)\ \mu\text{m}$ ) and poppy seeds (dark). The peculiarity of these rolls is that flow at the borders of the segregation domains is not vertical but oblique in the cell plane, (d) after 74,000 rotations, (e) after 100,000 rotations. All food densities from [129].

## 5.9 Monodisperse granulate

Finally, tests were carried out whether the convective flow is triggered by the segregation of the granular mixture or whether the segregation of the mixture is a consequence of the convective flow. For that purpose, cells with different types of monodisperse granulate were filled. No convection was detectable for particles that easily crystallize. As there are only a few bead layer in cell depth direction beads nucleate easily at the flat walls. This was the case for the mixtures in figure 5.11(a-c). Locally hexagonal clusters with defects form. Crystallization could be avoided by roughening of side walls.

The large bead fraction from the standard mixture (table 2.1) has  $\approx 10\%$  radius variation but the beads also deviate from the spherical form (see figure 2.2). This inhibits crystallization. It is evident from figure 5.11(d-f) that a convection structure of similar wavelength as in the bidisperse mixture is formed, but with considerably lower flow amplitude (5.11f). In the fluctuation image (5.11e) axial flow modulation along the rotation axis is visible. As expected there is a strong particle activity in the fluidized zones. Segregation could not be determined from single image or by averaging of image series. Obviously the bidispersity of the mixture strongly enforces the convection pattern, and the decoration by the segregation structures facilitates the optical recognition of the pattern. However, the mechanism works in a nearly monodisperse granulate as well, though much less effectively.

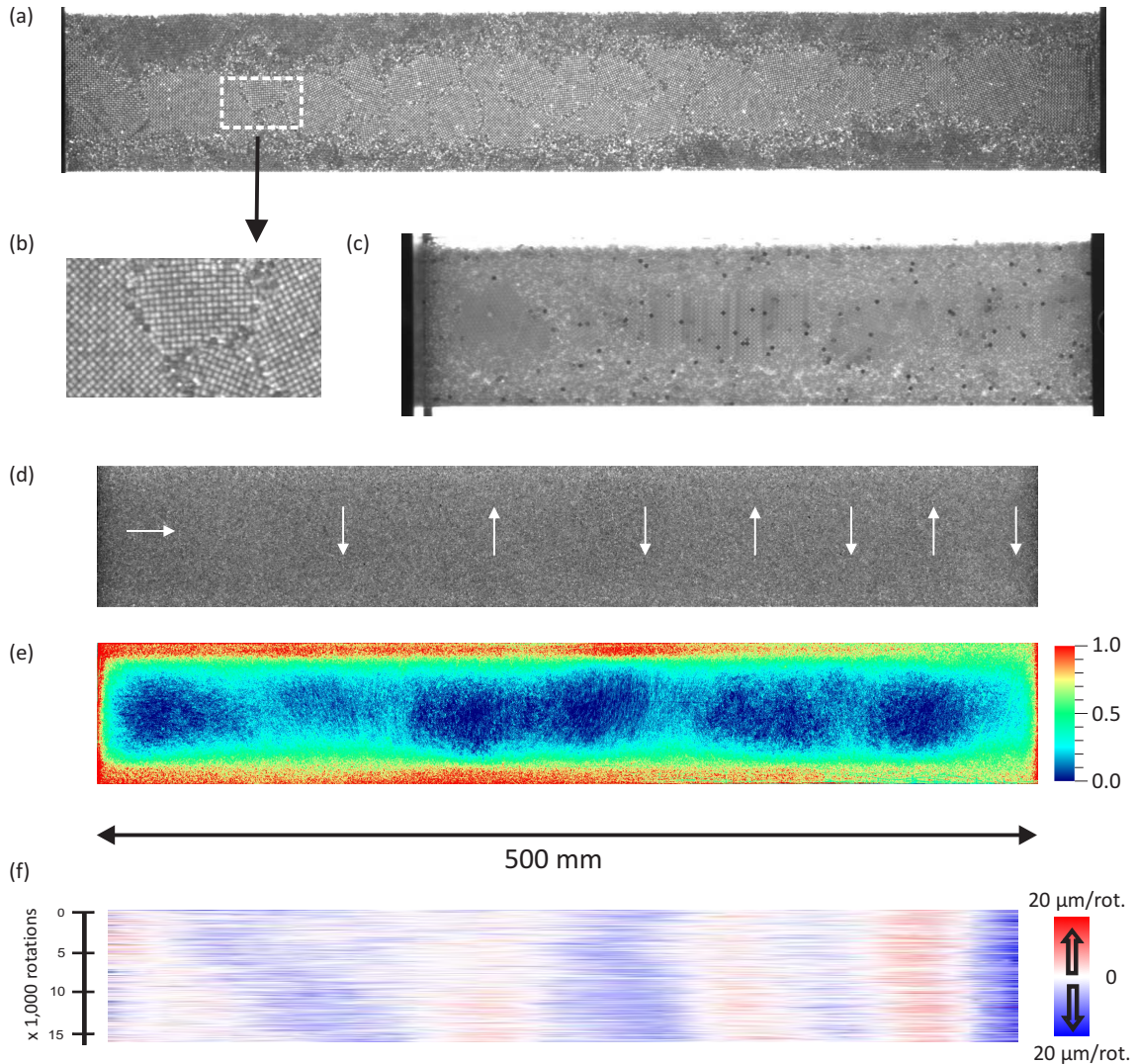


**Figure 5.11:** Behavior of monodisperse granulates. (a) Crystallization but no convection along the central axis for  $(1.5 \pm 0.1)$  mm spheres, after 800 rotations, enlargement in (b). (c) Smaller but more precise beads  $(1.01 \pm 0.01)$  mm crystallize as well without convection. Tracer move downwards on the front page during the whole experiment (experiment durations were 1,000 rotations and 4,000 rotations for the shown cell size and  $>300,000$  rotations for a larger cell (not shown)). Shown is the maximum achieved degree of crystallization (guessed by naked eye) after 150 rotations.  $x = 160$  mm,  $y = 40$  mm. (d) Monomodal mixture of 800-1000  $\mu\text{m}$  beads (from standard mixture) after 20,000 rotations. Arrows show main flow directions. The free volume above the granulate is comparable to that in figure 3.7d. (e) Temporal fluctuations in the pattern of (d) reveal non-uniform dynamics along the axial direction, averaged over 3,000 rotations (150 frames). (f) Vertical flow component along the horizontal axis for (d). The 118 data points along the horizontal axis are stretched for fitting reason.

# 6 Single rolls

## 6.1 General observations

A particularly interesting geometry is the small aspect ratio of a square-shaped cell. If such a container is used, single vortex rolls are observed in the cell plane. They show a more complex behavior than roll arrays in section 3.3, and they differ from other known types of convection rolls in granular media. The circulation of grains produces non-uniform segregation patterns of the mixture that in turn interact with the convective flow. Oscillatory modulations of the convection velocity, cessations and spontaneous reversals of the circulation are observed. All these features are absent in multi-roll granular convection. As known from geophysical systems, the combination of circulation and segregation can have considerable consequences [130].

Boxes of 60 mm×80 mm, 60 mm×90 mm, 80 mm×80 mm, and 83 mm×110 mm (width  $x$ ×height  $y$ ) with fixed depth  $z = 5$  mm (figure 6.1a) are used. The aspect ratios  $x/y$  are thus 0.67, 0.75 and 1.0, respectively. In order to perform multiple experiments simultaneously, a row of square shaped boxes is assembled into a bigger container (figure 6.1b). Images are recorded for periods of 15,000 to 360,000 rotations (corresponding to maximum 2 weeks).

In a container with small aspect ratio the main part of the granular bed performs a collective circulating motion (figure 6.1c). As found in multiroll systems fluidization, i.e. individual grain motion, is limited to narrow zones at the cell top and bottom, alternating after every half rotation of the cell (dashed zones in figure 6.1c). After a few hundred rotations, a roughly circular segregation pattern is visible in the central part of the rotating box. Although the system rotates continuously and has no distinct top-bottom asymmetry, the local net flow does not balance to zero. Instead, stable orbits, indicated by arrows in figure 6.1a,c are found. The term ‘orbit’ is used to describe the grain convection in the cell plane, in order to avoid confusion with the rotation of the box. The granulate orbits about an axis perpendicular to the axis of the driving rotation. During an experimental run, the orbit’s center can shift in the cell.

In some boxes with aspect ratio 1, convection sets in with two counter-propagating rolls. Transitions from single rolls to two rolls and vice versa are observed as well. The preferential spatial periodicity of the convection pattern is obviously slightly smaller than two times the cell height. In quadratic cells, roll pairs may compete with single rolls. When the aspect ratio is 0.75, only single rolls remain.

As a first approximation the flow field is treated as a simple rotation such that the granular dynamics may be described using only the angular velocity  $\omega_{orbit}$ . The angular velocity serves as a quantitative measure for the convection strength. The curl of the in-plane velocity field  $\vec{v}$  is related to  $\omega_{orbit}$  by  $\|\nabla \times \vec{v}\| = 2\omega_{orbit}$ . For data evaluation Stokes’ theorem  $\nabla \times \vec{v} = \lim_{A \rightarrow 0} A^{-1} \oint \vec{v} d\vec{\ell}$  is employed. The mean curl for each grid cell is approximated by the integral of  $\vec{v}$  along the surrounding grid points (path  $d\vec{\ell}$  enclosing area  $A$ , for details see [109, 131]). In order to reduce the effect of outliers in image processing, the median of all local  $\omega_{orbit}$  in the central 40 mm × 40 mm region is taken to characterize the global flow. Positive  $\omega_{orbit}$  corresponds to counterclockwise flow in the reference system (which appears clockwise when viewed from the reverse side of the cell).

Circulation usually starts clockwise or counterclockwise that can change spontaneously on long time scales. Statistically, the circulation sense is preserved for an order of  $10^4$  rotations. Figure 6.2(a-d) shows the long-term dynamics of a few typical runs (time in

## 6 Single rolls

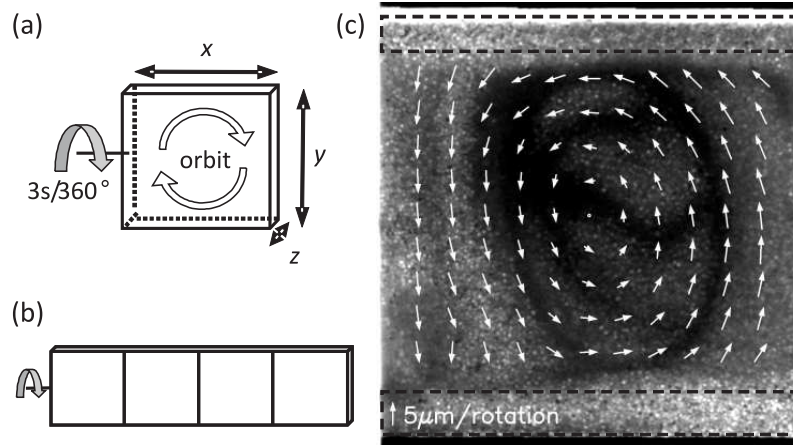


**Figure 6.1:** (a) Sketch of the experimental setup of a box with aspect ratio close to 1. Arrows indicate the sense of the container rotation and one of two possible directions of the granulate orbit. (b) Sketch of the container array for simultaneous experiments. (c) Segregation pattern after 107,000 rotations. The convection roll is reflected in the dark circular segregation pattern in the center. Dashes mark the borders of fluidized regions at the container's bottom and top edges. The white stripe on top is the free volume ( $\approx 2\%$ ) above the granulate (overexposure in the contrast enhanced image makes the cell appear less filled). The overlaid vector field indicates the collective grain motion. In this sample, a full orbit takes  $\approx 40,000$  rotations (average angular velocity  $\omega = 1.6 \cdot 10^{-4}$ /rotation,  $x = y = 8$  cm, fill level  $C = 0.638$ ).

units of cell rotations). One finds stable orbits in one direction, random flow reversals, cessations of the convection, and regular oscillations of the flow, with or without reversal of the circulation. In figure 6.2b, flow ceases for an extended period but starts again after 320,000 rotations. In all experiments, a maximum  $|\omega_{orbit}|$  of the order of  $10^{-3}$ /rotation is found. The air humidity protocol (15-30% rel. humidity, figure 6.2e) shows no correlations with the observed dynamics.

The height of the granular bed and therefore also the free space on top of the granulate varies with the nonstationary segregation process. Therefore it was checked whether the height fluctuations are related to the circulation velocity. In order to achieve this, the height of the free space on top of the granulate was determined at 9,000 intervals for a long-lasting experiment (360,000 rotations). At first 20 consecutive images were averaged and then the resulting picture (figure 6.3a) again averaged along the horizontal coordinate. The values were used to measure the derivative of the gray value (figure 6.3b). Extrema in the derivative yield a reliable measure for the free space on top of the grains. These data points are depicted in relation with the absolute angular velocity in figure 6.3c. There is no systematical relation between the free space at a given moment and the corresponding convection velocity. Fast and slow velocities are possible for the entire range of the granular height. The accumulation of data points close to zero for a free space of  $\approx 1.4$  mm just reflects that in the experiment the granular bed often tended to this gap height. Height differences are  $< 0.5$  mm ( $< 1\%$  of the cell height) and the flow amplitude is in the same range as for the other discussed examples in this chapter.

Asymmetries in the initial preparation of the cells (e.g. partial demixing during filling) might preselect the initial sense of convection flow. In order to avoid this, experiments from an initially demixed preparation (section 5.7) were done. The two stratified, completely demixed grain layers mix completely within a few hundred rotations. After that, the convection starts in a random sense and can later lead to the dynamics described above.

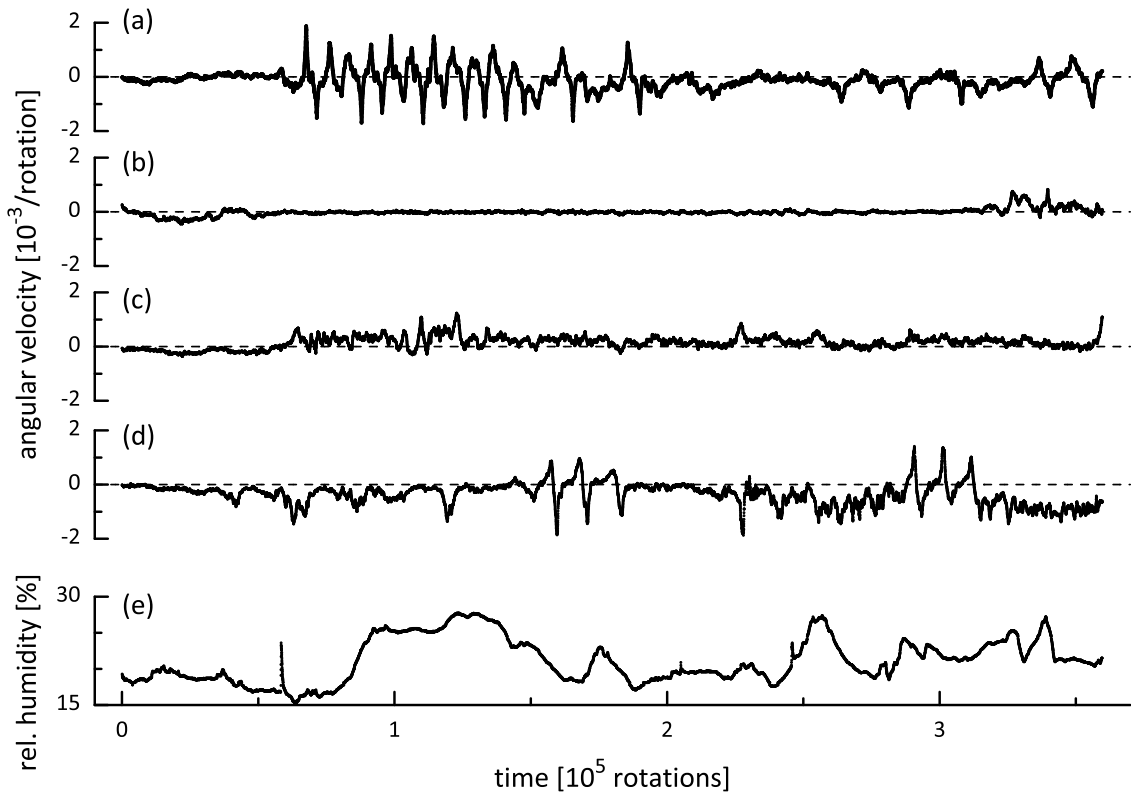


**Figure 6.2:** (a-d) Typical measurement of the average vortex flow velocity with regular circulation, fluctuations, reversals of the vortex sense, cessations and oscillations in four simultaneous experiments. Among the experiments no correlations in the convection dynamics can be found. ( $x \times y = 6 \text{ cm} \times 8 \text{ cm}$ ,  $C = 0.640$ ). Each data point in figures 6.2 to 6.5 is averaged over 200 rotations (10 images). (e) Protocol of the relative humidity in the laboratory.

In the standard experiment, the rotation axis is aligned as closely as possible with the horizontal. But one might expect that the sense of the circulating orbit depends on the inclination of the rotating box. This influence has been tested by tilting the axis. A moderate tilt of the axes ( $\pm 0.5^\circ$ ) has no influence on the convection. Also, the general dynamics is insensitive to axial asymmetries of the container, e.g. if one vertical side of the boxes is covered with sand paper (with granularity of the small bead size). Such a modification does not lead to a preference of one circulation sense. All this is expected since front and rear sides interchange with each half turn of the cell.

## 6.2 Flow oscillations

In addition to spontaneous flow reversals, the self-organized segregation can lead to regular oscillations. In figure 6.4a the angular velocity  $\omega_{orbit}$  of such an oscillating roll is shown as a function of time. For better clearness, time is given in units of cell rotations. It is more instructive to plot the same data as a function of the number of orbits  $\frac{1}{2\pi} \int \omega_{orbit} dt$  of the granulate (figure 6.4b). The flow changes from fast to slow and back with a period of roughly half an orbit. The experiment in figure 6.4a is an example where the global direction of the convection changes its sign spontaneously. The simultaneous onset of oscillations is a coincidence. Details of such oscillation may change in different experiments.

## 6 Single rolls

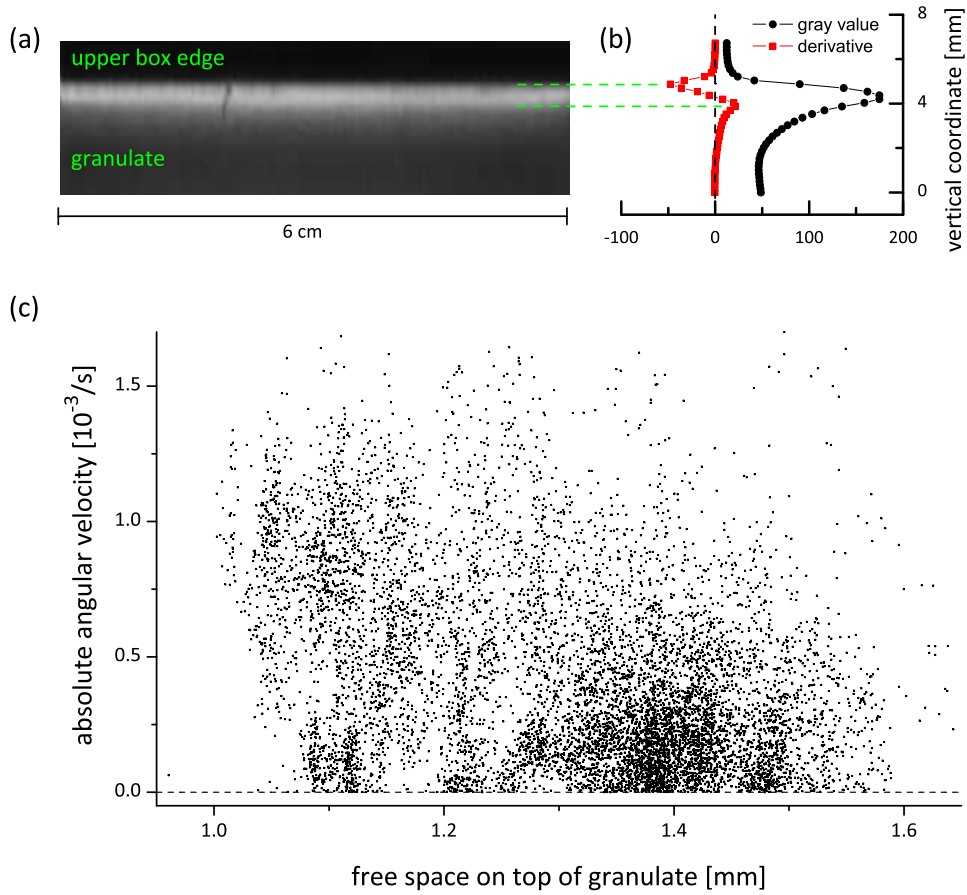


**Figure 6.3:** (a) The bright stripe is the free space between granular bed and the upper box edge (averaged over 20 images, image exaggerated 2 times in vertical direction). (b) The free space is determined by the derivative (red curve) of the gray value (black curve) from images as seen in (a). The distance between extrema in the derivative function is a measure for the free space (green dashed lines). (c) Relation between free space above the granular bed and corresponding absolute angular velocity. High and low velocities are possible for any amount of free space.  $x \times y = 6 \text{ cm} \times 9 \text{ cm}$ , in total 360,000 rotations.

Another experiment is shown in figure 6.4c. After 2.5 clockwise orbits the flow passes over to an oscillatory regime. The direction reverses repeatedly, which is reflected as loops in the figure. Roughly 0.15 counterclockwise orbits are followed by approximately 0.65 clockwise orbits, resulting in a net half orbit in clockwise direction during one oscillation. Even though in this cell the sense of orbital motion changes, the overall convective flow is faster than in the non-oscillating regime (inset in figure 6.4c). Oscillations seem to increase the efficiency of the particle transport, as compared to non-oscillating flows.

In the experiment presented in figure 6.5a, the oscillations were observed over a period of 8.5 days (200,000 rotations). After a short transient ( $\approx 2$  orbits) one can identify periodical oscillations every half orbit. This modulation is overlaid by a period of one orbit. During every orbit, a series of peaks (marked in figure 6.5a by letters A,B,C,D) approximately repeats during every orbit. These modulations are moderately damped in the course of the experiment.

The periodicity observed in all oscillating experiments suggests that the flow modulation is related to the details of the segregation pattern of the granulate, which follows the orbit. This assumption was checked by averaging the cell images for each of the 4 extremal

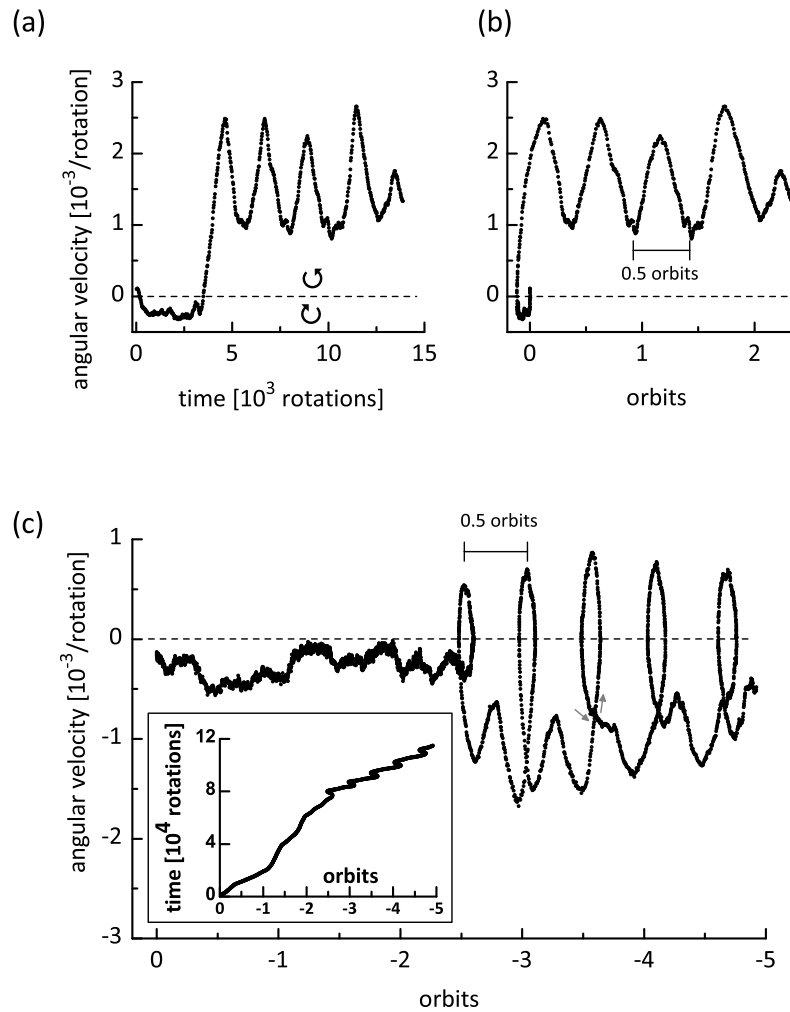


**Figure 6.4:** (a) Angular velocity as a function of time and (b) for the same experiment as a function of the number of orbits. After a slow clockwise motion the direction reverses and the flow amplitude increases. The flow now circulates with a period of a half orbit. ( $x \times y = 8.3 \text{ cm} \times 11 \text{ cm}$ ,  $C \approx 0.63$ ). (c) After fluctuating around a low amplitude the flow in this experiment evolves into an oscillating regime with higher peak velocities that are combined with direction changes ('loops'). The inset shows the time needed for the orbits. ( $x = y = 8 \text{ cm}$ ,  $C = 0.638$ ).

values (A-D in figure 6.5a), to extract typical features of the segregation states. The averaged images are shown in figure 6.5b. Similar patterns are found for the experiments in figure 6.4. Distinct shapes of segregation patterns are recognized from zones enriched with small particles at four different container positions (dark areas, marked with crosses). The segregation patterns orbit with approximately the same velocity as the particle clusters. It is reasonable to conclude that the periodicity of the flow amplitude relates to the position of the small particle enriched clusters in the partially demixed regions during orbiting. Because of the top-bottom symmetry of the cell, one should expect pairwise similar velocities for states A,C and states B,D, respectively. Figure 6.5b demonstrates that the convection is faster when the regions enriched with small particles move out of a fluidized surface zone (states A,C), whereas the velocity is slower when such regions are driven into a fluidized surface zone (states B,D). A difference between states A and C on

## 6 Single rolls

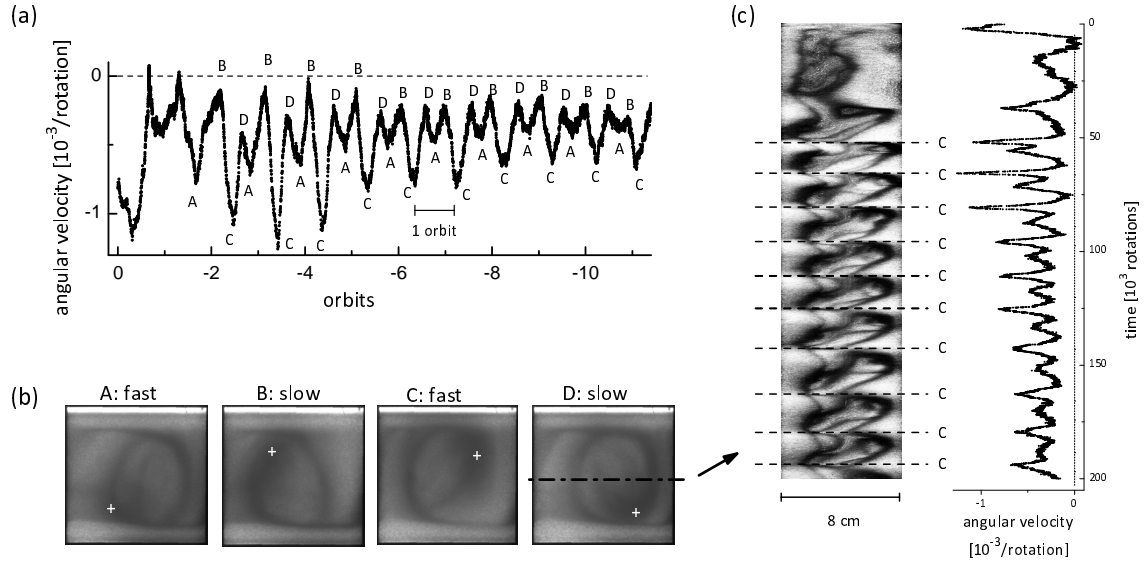


**Figure 6.5:** (a) Angular velocity as a function of the number of orbits. The flow oscillates with a periodicity of half an orbit and shows a superimposed four-fold periodicity (peaks labeled A-D). ( $x = y = 8$  cm,  $C = 0.650$ ) (b) Averaged flow patterns in four phases of the cycle reveal the circulation of the nonuniform segregation cluster (+), clockwise flow. For the dash-dotted line the time-space plot for this experiment is depicted in (c) along with the angular velocity. One phase of the flow (label C and dashed lines) marks the repetition of the segregation structure after every  $\approx 25,000$  rotations.

one hand and states B and D on the other hand can thus be related to a direct interaction of the segregation pattern and local granulate composition with the convection stream.

The meandering of the small beads cluster can also be followed in figure 6.5c. There, the angular velocity is shown in dependence of time for the same experiment. Next to it the corresponding time-space plot along the rotational axis is depicted (marked by a dash-dotted line in figure 6.5b). For orientation, one of the 4 extrema of the fourfold cycle (point C as defined in figure 6.5a,b) is marked by dashed lines. After 50,000 rotations the granular distribution leaves its initial transient and passes to a stable segregation cycle. The repetition of the pattern every 20,000 to 30,000 rotations is obvious. Label C marks the situation after the small beads cluster (dark) has traversed the axis on the left side and before the cluster crosses the rotational axis on the right side of the granular bed, i.e. the small beads accumulate in the upper half and therefore in the upper fluidized layer of the box. This stands in correspondence to the averaged images of point C in figure 6.5b.

The interpretation suggests that the fluidized zones play a significant role in the convection process. Therefore the temporal fluctuations between consecutive images (for a definition see section 2.4) are visualized in figure 6.6. Fluidization, i.e. individual grain motion, is limited to narrow zones at the cell top and bottom, alternating at each half rotation of the cell (dashed zones in figure 6.1c). These zones drive the convection. In the experiments shown in figures 6.4c and 6.5, additional narrow fluidized layers at the left and right sides of the cell (see figure 6.6) are observable. These lateral zones are not developed in the experiments shown in figures 6.1c and 6.4a.

Beads from the convecting central region can enter the more loosely packed fluidized zones, and the net flow is balanced by reentrance of particles towards the central cell area. During transport along the fluidized edges, small beads are ‘sieved out’, which creates and maintains the segregation. It is obvious that a homogeneously mixed state would be an

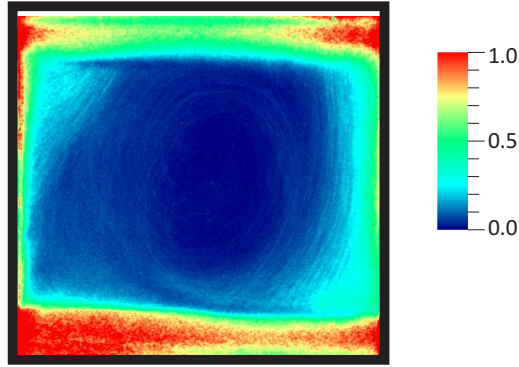


**Figure 6.6:** Fluctuations (normalized) in the brightness distribution averaged over all images taken during the last orbit of figure 6.5a. Highly fluidized zones (red) are observed at the top and bottom, but small stripes also appear at left and right hand sides.

unstable situation. Thus almost all experiments developed clusters enriched with small and large particles, respectively. Therefore the material composition of the fluidized zones varies and might lead to oscillations in the convection velocity. Different segregation in the fluidized regions can be seen in the top layers of states B+C in figure 6.5b. Because of higher mobilization in the fluidized regions the particles can distribute more evenly and can then be sieved out again before they reentrant the convection zone again. Whether the oscillation is periodic or not depends on the spatial distribution and stability of these clusters. In some cases, the granulate develops two opposing clusters enriched with small beads on the orbit and the respective velocities in the maxima and minima practically coincide, as seen in figure 6.4. It is also evident why broader cells with multiple convection rolls (section 3.3) do not develop oscillations. Owing to the exchange of grains between non-synchronized neighboring rolls in a pair or array, oscillations are suppressed, and one observes a uniform convection.

From the experiments, following conclusions on the segregation, convection, flow reversal and oscillation mechanisms can be drawn: Since the stratified preparations led to a mixing of the granulate first, an initial segregation is not considered for the onset of convection. Rather, the subsequent segregation in the vortex center accompanies the convective motion. This segregation is not uniform: at long time scales the granulate often develops one or two clusters that orbit the vortex center. During this orbiting motion, the position of these clusters relative to the fluidized layers modulates the convection velocity.

In contrast to rotated containers, there is a large variety of convection scenarios in strongly vibrated granular systems (see also section 4.4). Single rolls in simulations of shaken systems have been explained by gradients in granular temperature [132,133], or they appear at special driving conditions [134–137]. They are found also in experiments with vertical [117,125,138–142] and horizontal [142,143] shaking. Vertical shaken containers are connected to Faraday heaping. This effect vanishes at reduced air pressure [112] and when the acceleration is less than 1.2 times the gravity. Compared to the Faraday instability, the flat cell system is not influenced by air and the effective gravitational acceleration (during sliding of the grains) is lower than  $g$ .

Single roll convection has been also extensively studied in Rayleigh-Bénard convection under very high Rayleigh numbers ( $Ra > 10^8$ ) in cylindrical [126,144–146] or (quasi-) two-dimensional rectangular containers [147,148] of aspect ratio 1. Single large scale convection rolls perform diffusional azimuthal motion and occasional flow reversal after cessation of the vortex flow. Irrespective of the very different materials and driving mechanisms, there are

## 6 *Single rolls*

some formal similarities to granular convection rolls, for example the ‘grainy’ structure of vortices (as opposed to laminar fluid flow), the existence of boundary layers at the top and bottom plates, and the strong local density fluctuations in the convecting material. The beads in the quasi two-dimensional system do not allow azimuthal fluctuations, it behaves more like flow in a cuboid geometry [147, 148] rather than in a cylinder [126, 144–146].

# 7 Traveling waves

Traveling waves are considered one of the intriguing and still unexplained phenomena in pattern formation in granular media [34]. One of the remarkable observations in the rotating flat cells is the existence of such axially moving structures. At a subcritical fill level, within the chute flow regime, traveling bands of segregated beads were observed. They can travel in either direction along the cell axis. Their motion may be very regular and periodic. At supercritical cell fill levels, i.e. in the convection regime, traveling convection rolls can be found. As the effects are quite unique compared with other known phenomena a literature review (section 7.3) will close this chapter.

## 7.1 Traveling stripes

The common observation in rotating drums at long time scales are bands that are either stable or merge slowly [75, 76, 79, 149–151]. Here, it is demonstrated that, in flat cells, bands do not reach stationary states at reasonable experimental time scales. The observed dynamics shows a pronounced spatio-temporally periodic drift of segregated patterns. In the course of long experiment durations, the system switches between different states that appear to be stable oscillatory solutions over many periods. In the long term limit, the system does not tend towards a stationary state and scenarios with multiple marginally stable states may have been overseen in experiments by other researchers. Instead of a complex internal convection roll scenario like in another study [81], the underlying primary particle dynamics reduces to chute flow in the cell plane. This may facilitate the modeling of the system considerably. Examples for the band dynamics are depicted in figure 7.1b,c. The cell width is either 17 cm or 50 cm. Typical experiments are performed for 1 to 2 weeks (several hundred thousand rotations). Fill heights are alternatively 50% or 80%.

For convenience, only the dynamics of the small particle bands are described. By this definition, two basic processes can be distinguished: band depletion and band enrichment. More complex scenarios during progression of the stripe evolution can always be considered as combination of them. The composition of the granulate in a given region varies in time, material exchanges axially. In figure 7.1b, five zones are initially enriched with small particles. During continuous cell rotation, the central three zones mix with the surrounding granulate in directions marked by arrows. The material reappears to form new segregation bands in areas that were previously dominated by large particles. Figure 7.1c shows that some small-particle bands dilute (i.e. incorporate more large particles) by expansion, while others enrich (i.e. lose large particles) by shrinking. Local depletion of small particles leads to the formation of regions with predominantly large particles. The visual impression are bands of large particles which move permanently sideways.

On both alternative upper horizontal cell edges, a well-segregated  $\approx 5$  mm high zone of predominantly large beads forms above a layer of small particles each. The explanation is that smaller particles are sieved out of zones of high particle mobility. A closer view shows that the top surface of the granulate is not flat. Above regions that are enriched with small particles in the bulk zone, the upper boundary extends approximately 1 mm higher than in the large particle bands (the height differences seem to appear larger in figure 7.2 because of overexposure of the top surface).

The primary motion of the granular material is chute flow twice during each full cell revolution ( $360^\circ$ ). During sliding, a small shear between front and back sides leads to

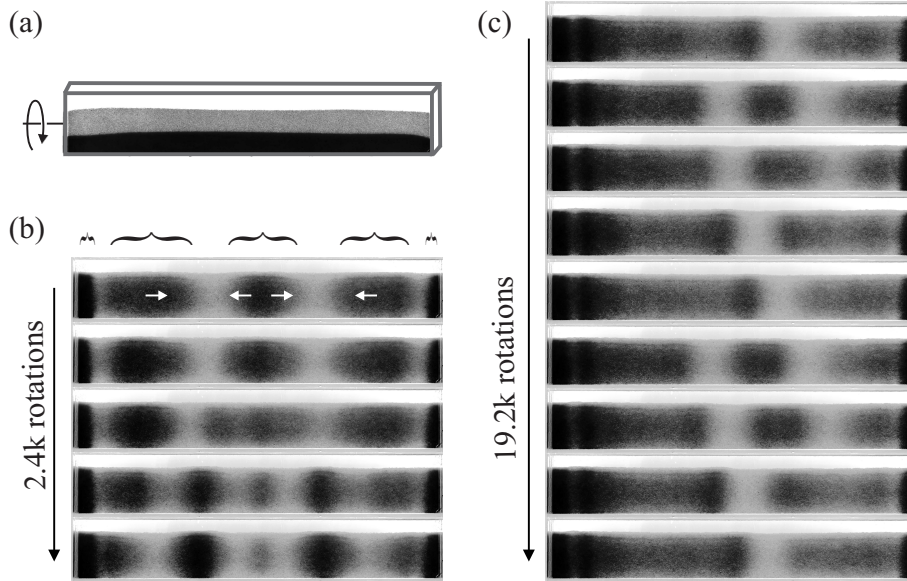


**Figure 7.1:** (a) Schematic sketch of the rotating flat mixer. Overlaid is the initial pre-segregated state, small particles (dark) are below large particles (bright) at 80% fill level. (b) Five bands enriched with small particles (marked by brackets) dissolve in the direction of the arrows and enter areas initially enriched with large particle. (c) Traveling waves of large particles are made possible by partial depletion of the small particle bands. (b) and (c) correspond to points I and IV in figure 7.3a.

a slow net circulation of the material around the rotating axis. Tracers of the cell with the higher fill level are manually tracked in images taken after every full turn (figure 7.2). The temporal order of the particles is color-coded (see color scale). Tracers on the front side move in the sense of the selected standard cell rotation sense (table 2.1). As tracers can vanish into the granulate and later reappear only particles are shown that could be surely tracked after  $360^\circ$  cell rotation. Some possible larger particle jumps can therefore be overseen by this technique. Vertical motion dominates and a horizontal drift cannot be derived by the data at hand. From the tracking of tracers one can conclude that the tracers move, on average, with velocities of the order of 5 mm/rotation. A complete orbit takes therefore approximately 30 rotations. The axial band dynamics is one to two orders of magnitude slower than the circulation velocity and cannot be measured on single particle level, because tracers only can be tracked for a few rotations.

For better visualization the complex band dynamics is reduced. Considering the simple quasi-1D spatial structures, from each picture, a horizontal line (averaged over a height of 8 mm) around the vertical center of the granular bed is extracted. They are stacked in two-dimensional time-space plots. The initial stages of four different experiments are depicted in figure 7.3. For the dashed regions in figure 7.3, zoomed details are shown in figure 7.4.

The following description lists scenarios that are observed in long term experiments. All start from the same demixed configuration (large species on top of small species, figure 7.1a). The mixers generally develop phases with different types of regular periodic dynamics that are characterized by sudden transitions, even when all experimental parameters are kept constant.

Figures 7.3a and 7.4a<sub>1</sub> show during the first 30,000 rotations interpenetrating waves with a periodicity of  $\approx 5k$  rotations. This is an order of magnitude slower than similar waves in reference [82]. Subsequently, outwards moving bands emerge and the period increases. In

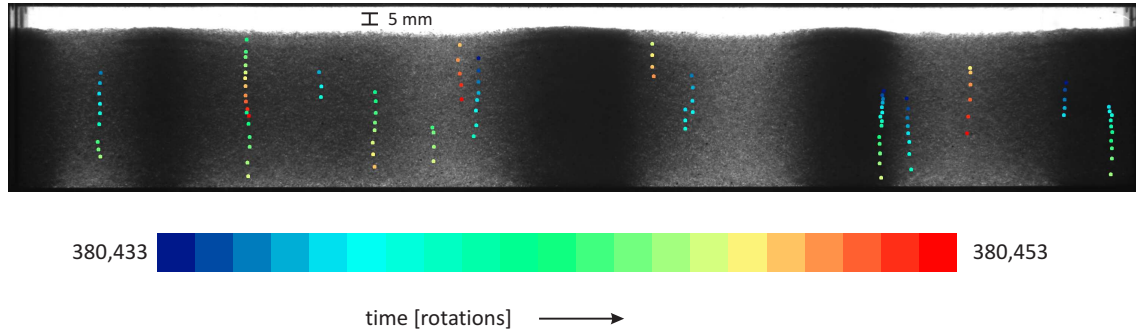


**Figure 7.2:** Tracers (large particles species) during wave traveling that could be tracked after consecutive cell turns during a period of 20 rotations, beginning after 380,433 rotations. In the presented case individual tracers could be followed between 3 to 15 rotations before they were lost. They move  $\approx 5$  mm per rotation. The coloring of the beads corresponds to time in number of rotations (color scale). After the investigated 20 rotations the segregated bands in principle have not changed their positions. Shown is the pattern after 380,443 rotations, corresponding to green tracer color.

order to test whether the dynamics is sensible to the segregation pattern, the pattern was destroyed by random shaking of the cell at points II and III. Obviously, the composition of the segregation bands and their dynamics changed quantitatively, but not qualitatively after the rotations resumed. Periodical traveling waves were still found. They appeared particularly regular after the second shaking (III). The cell rotation paused for 56 hours at point V. The pause had no influence. This indicates that a possible accumulation of electrostatic charges during rotation can be ruled out as an essential part of the driving mechanism.

The experiment in figures 7.3b and 7.4b<sub>1</sub> shows band traveling only at the very beginning, followed by a long phase of a slightly segregated stationary state. After 100,000 rotations, superimposed waves were formed on the right hand side of the cell. At the same time, in the left half of the cell, the drift of individual bands is accompanied by sporadic discontinuous displacements of bands. Similar processes affect the whole cell after about 150,000 rotations (figure 7.4b<sub>1</sub>).

In figures 7.3c, 7.4c<sub>1,2</sub> coarsening is followed by local periodic band drift. An image series (inset figure 7.4c<sub>3</sub>, 280 rotations between individual images) for the dashed region in figure 7.4c<sub>1</sub> reveals that the dynamics can be described by dilution and enrichment of bands similar to figure 7.1b. At about 150,000 rotations the pattern changes spontaneously. A drift that is initially restricted to a limited axial range transforms into waves traveling across the entire cell, similar to the traversing bright band in the center of figure 7.4c<sub>2</sub>. The direction of wave propagation can spontaneously change, as seen in figure 7.4c<sub>2</sub>.

The experiment depicted in figures 7.3d and 7.4d<sub>1</sub> was carried out in a smaller cell and it shows coarsening at the beginning, followed by regular waves. At 120,000 rotations, the wave speed decreases and bands enriched with large particles (bright) are formed alternating at each of the side walls (figure 7.4d<sub>1</sub>). Before they reach the opposite cell side they dissolve and a new wave starts opposite to the previous wave. This process is observed 13 times. After that ( $\approx 170,000$  rotations), faster waves emerge. They look very similar to those that occurred after the initial coarsening period in the same experiment (after  $\approx 60,000$  rotations). This recurrence indicates that the variation of patterns is not a consequence of aging of the system (e.g. irreversible abrasion of beads or container).

As described above, the material exchange in axial direction leads to a large variety of dynamics and the pattern evolution appears to be quite unpredictable. Note that, to

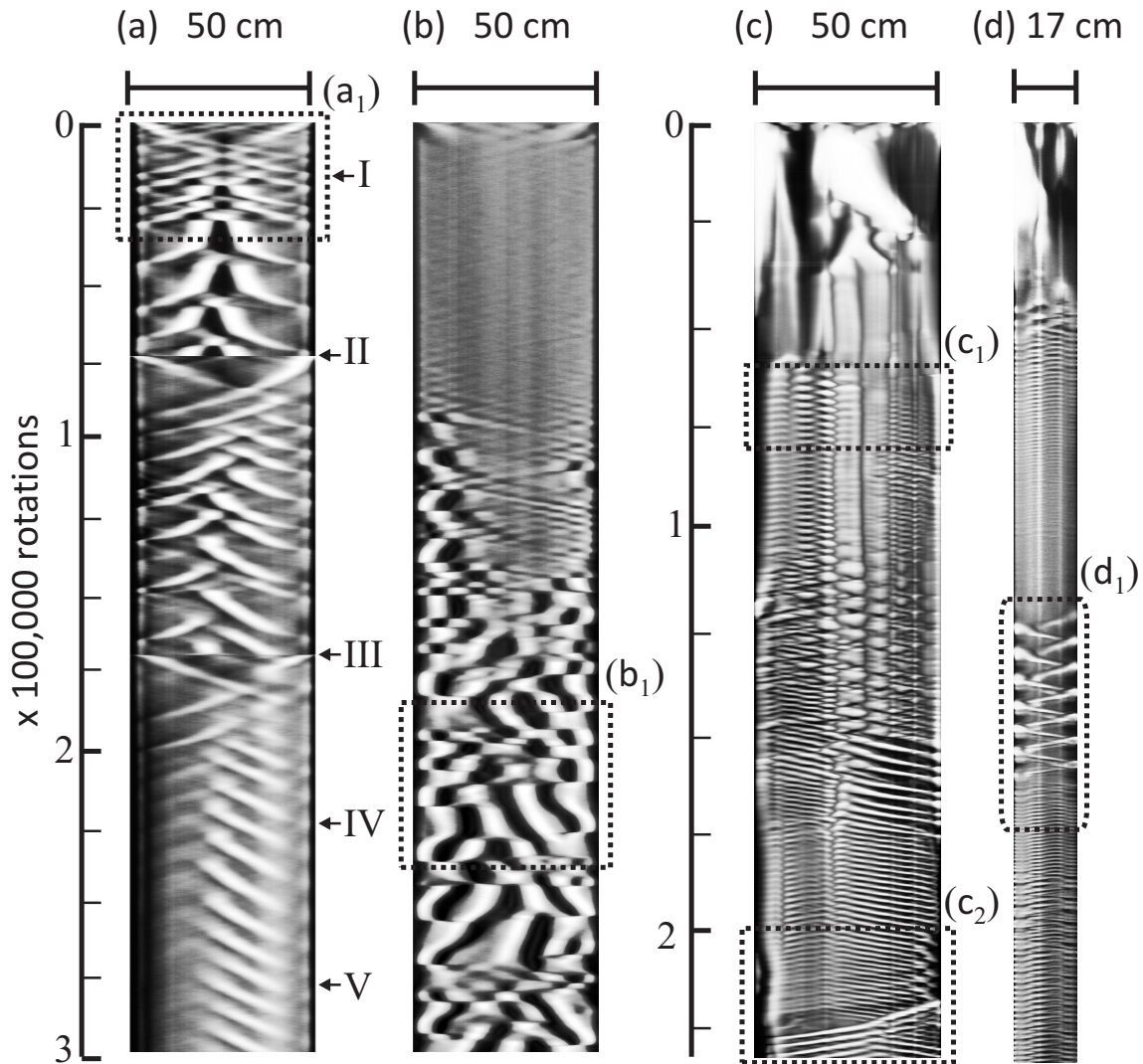


**Figure 7.3:** (a-d) Time-space plots of traveling waves for four different experiments. Enlarged parts for dashed regions (subscript labels) are shown on the next page (figure 7.4). (a) Interpenetrating waves that are drifting outwards from the center. After the pattern was destroyed by shaking the cell (points II and III) the character of the waves changed. A simple long pause of the rotation (point V) does not influence the pattern when rotation continues. For points I and IV see figure 7.1b,c. (b) Axial drift goes along with spontaneous displacement of bands. (c) After coarsening, local periodic waves are formed that pass the whole cell width afterwards. (d) Regularly moving waves crossing the whole cell width are observed. Filling heights are (a,b) 80% and (c,d) 50%. Plots (a,b) are also corrected for temporal and spatial inhomogeneities in illumination intensities, (c,d) are not corrected.

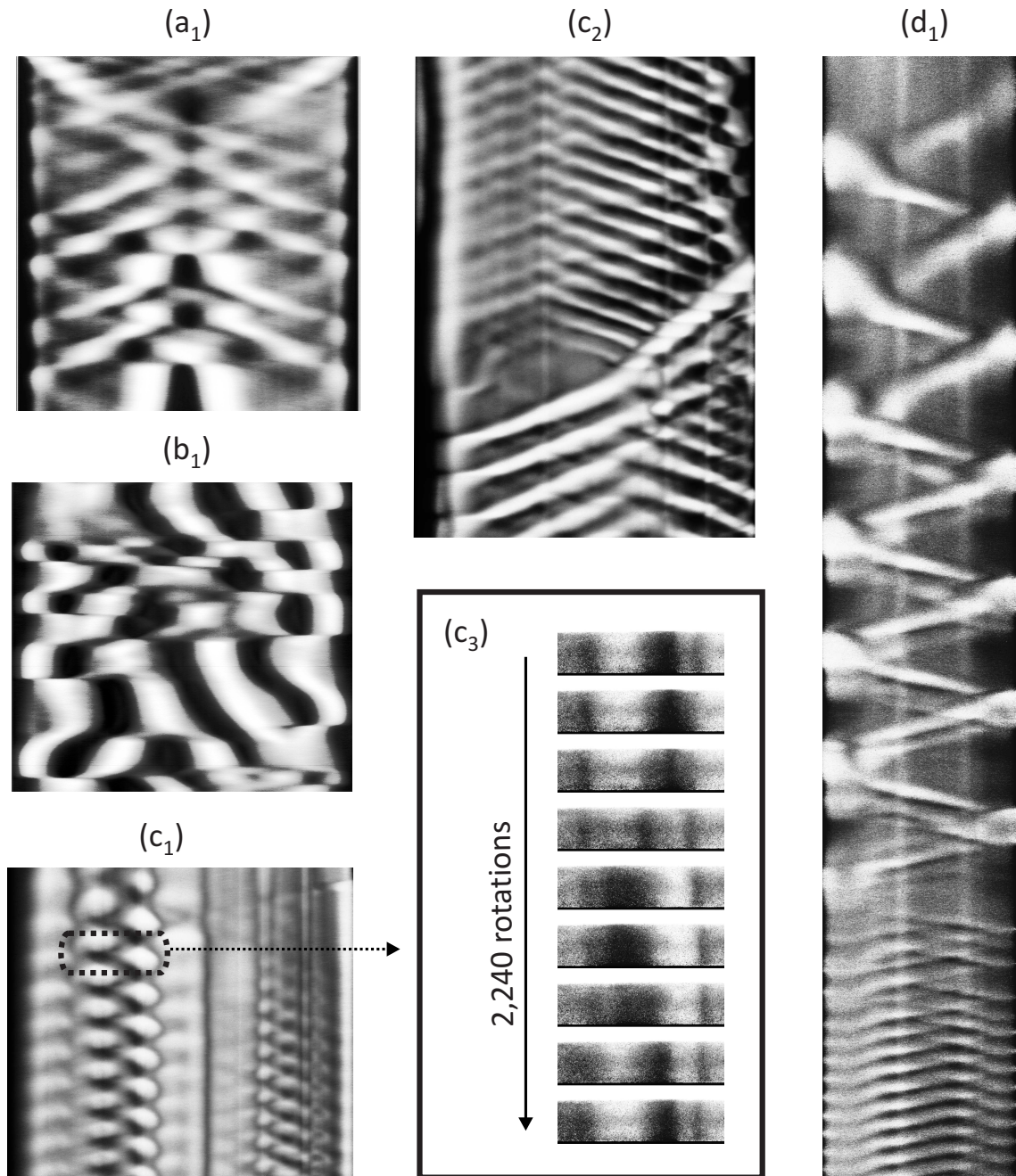


**Figure 7.4:** Enlarged details of the time-space-plots on the left page (figure 7.3). The zoom scale varies for different extracts. See figure 7.3 for description. Inset ( $c_3$ ): Image series for the dashed region in ( $c_1$ ).

## 7 Traveling waves

a certain extent, this applies to the evolution of segregation bands during coarsening in classical cylindrical mixers as well. There, only the time-dependence of the number of stripes is reproduced, on a statistical level, in repeated experiments [75, 76, 79, 149–151] or simulations [152, 153].

The observed maximum velocity of band propagation is about  $10 \mu\text{m}/\text{rotation}$  in containers with higher fill levels (80%, figure 7.3a,b) and about  $60 \mu\text{m}/\text{rotation}$  in less filled containers (50%, figure 7.3c,d). In some cases, the oscillations of the patterns show considerable persistence. The temporal period can be 10,000 rotations (figure 7.3a after point III) or 1,500 to 2,000 rotations (figure 7.4c<sub>1,2</sub>). Large variations can occur within an individual experiment. A change from 6,500 rotations/period to 1,000 rotations/period is seen in figure 7.4d<sub>1</sub>. From the observed space-time plots, a dispersion relation between the stripe widths and their velocities at constant fill level was constructed. It turns out that there is no significant correlation between both quantities.

In general, the lateral ends of the cell are occupied by the small species (figures 7.1b,c and 7.4a<sub>1,b1</sub>). Occasionally, exceptions are observed (right border in figure 7.4c<sub>1</sub> and alternating borders in figure 7.4d<sub>1</sub>). No material or geometrical parameter was identified that changed in the course of the experiment.

The robustness of the patterns was tested by changing several external parameters. Influence of the initial preparation can be ruled out. Traveling waves are both observed when the beads are previously mixed before filling, and when a pre-segregated stratification (figure 7.1a) is prepared. An initial prepared pattern of axially alternating stripes of large and small particles quickly dissolves to leave a mixed state, from which any of the described traveling solutions can form. A potential tilt of the rotation axis can be ruled out as the cause of the band motion, since the waves can move simultaneously in opposite directions (figure 7.4a<sub>1,c2</sub>). As described above, the effects were observed for different fill heights and different aspect ratios, and after manual distortions of the pattern and long pauses of the experiment. Relative humidity was measured and varied between 30% and 60%, but no correlations with the dynamics of the time-space pattern could be found. Baking the beads for 1 hour at  $100^\circ\text{C}$  before the experiment did not inhibit wave formation immediately after start of the experiment. Therefore cohesion by liquid bridges can be ruled out as a driving mechanism. Small variations of the cell thickness may be relevant for details of the resulting patterns. Construction-conditioned, the side planes of the cell used in the experiment of figure 7.3a were bent outwards, and the cell gap was about 15% thicker in the central part than at the lateral ends. It is evident that, throughout the run of the experiment, the waves start in the thicker part of that cell (the center) and move outwards.

In a broader context one can interpret the results as multiple manifestations of marginally stable states. The dynamics are quasi-stable on short time scales, but small fluctuations over large time scales lead to transitions between alternating attractors. The very observation of nearly periodic temporal behavior is astonishing, but the observed multistability is a feature that is otherwise observed only in systems with large numbers of degrees of freedom (e.g. climate cycles [154] or brain activity [155]). The simplicity of the granular mixer experiment is a certain advantage with respect to other dynamic systems with multiple attractors. It may open the opportunity for a simple model description or straightforward numerical simulations. The quantitative characterization of these structures and the extraction of the parameter ranges necessary for their formation require more experiments to be done.

## 7.2 Traveling rolls

Besides stripes at lower fill level there are also traveling wave scenarios in the convection regime. In cells with a higher aspect ratio of 15.9 traveling rolls were found. One can think of them as convective motion (section 3.3) with an overlaid axial drift. The development of the pattern in such an experiment is depicted in figure 7.5a. In figure 7.5b the corresponding time-space plot along the rotation axis is given. Arrows direct to the position of the images in the time-space plot. At the beginning, 16 rolls emerge as it is expected by the aspect ratio of 15.9. A slight drift to the right side is observed and at  $\approx 50,000$  rotations the global character switches to leftwards motion. The uniformity in the direction of the rolls is lost during their development from  $\approx 80,000$  to 150,000 rotations. At 150,000 rotations (marked by the green line) the sense of rotation direction is changed. This modification yielded for the rest of the run a direction change of the waves. The rolls look initially circular (until 40,000 rotations). Their shapes stretch horizontally as soon as they move in the axial direction. Nevertheless the convection is maintained as seen in the time-space of plot of the vertical flow velocity in figure 7.5c. Only the flow amplitude decreases slightly. The mode number decreases from 8 to 5 as the flow has to reorganize itself if waves move apart (between 80,000 to 120,000 rotations). It shall be noted that the horizontal flow component can be neglected in comparison to the vertical flow as axial drift takes place on very long time scales. Small particles (dark) arrange preferred between vertical streams where the velocity is smaller as expected from stable rolls (section 3.3).

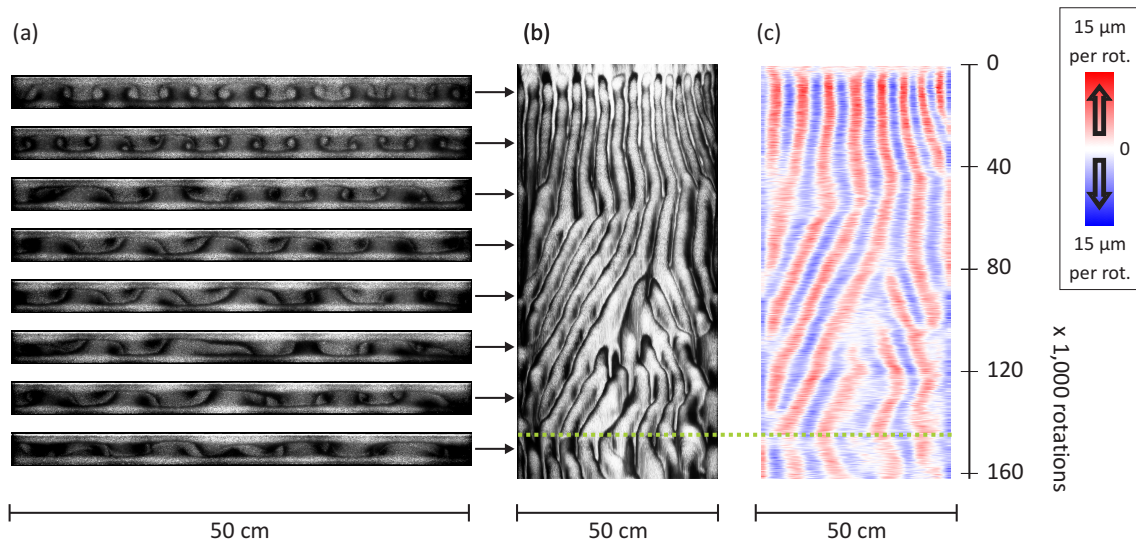


**Figure 7.5:** (a) Time series of mostly outwardly moving rolls in a container with high aspect ratio of 15.9. The arrows indicate the positions in the time-space plot (b). Manifestation of the rolls is visible in the time-space plot of the vertical velocity (c). Above the green line the rotation sense of the container is opposite to the default sense and below the line the default sense was selected (for definition see figure 2.1b).  $y=31.5$  mm

**Inwardly traveling rolls** Another type, traveling waves that always travel inwardly can be found. They can be limited to a local part of the cell if the fill ratio is near its critical value  $C \approx C_C = 0.6$ . In the transition regime, in cells with mediate aspect ratios, edge oscillations are found. Figure 7.6a,b depicts the time-space plot of segregation and vertical

## 7 Traveling waves

flow amplitude of such an experiment. A roll shifts inwardly and at its previous place a roll emerges with opposite direction. That can be readily seen in the outer regions of figure 7.6b. In figure 7.6c the upwards and downwards moving regions have been marked by red and blue rectangles, respectively. The yellow dashed border serves as guide to the eye and corresponds to the black framed area in figure 7.6b. Far from the lateral borders the rolls are stable. Inwardly moving rolls can also be seen in figure 7.6d,e. Here, the fill level is higher and also the flow amplitude is lower. However the cell was higher, i.e. the two experiments should not be compared relating to their fill levels. The rolls extend the whole cell width and stop meandering when they collide with waves from opposite directions. In these experiments the axial drift is a magnitude faster than in the case at high aspect ratio (figure 7.5).

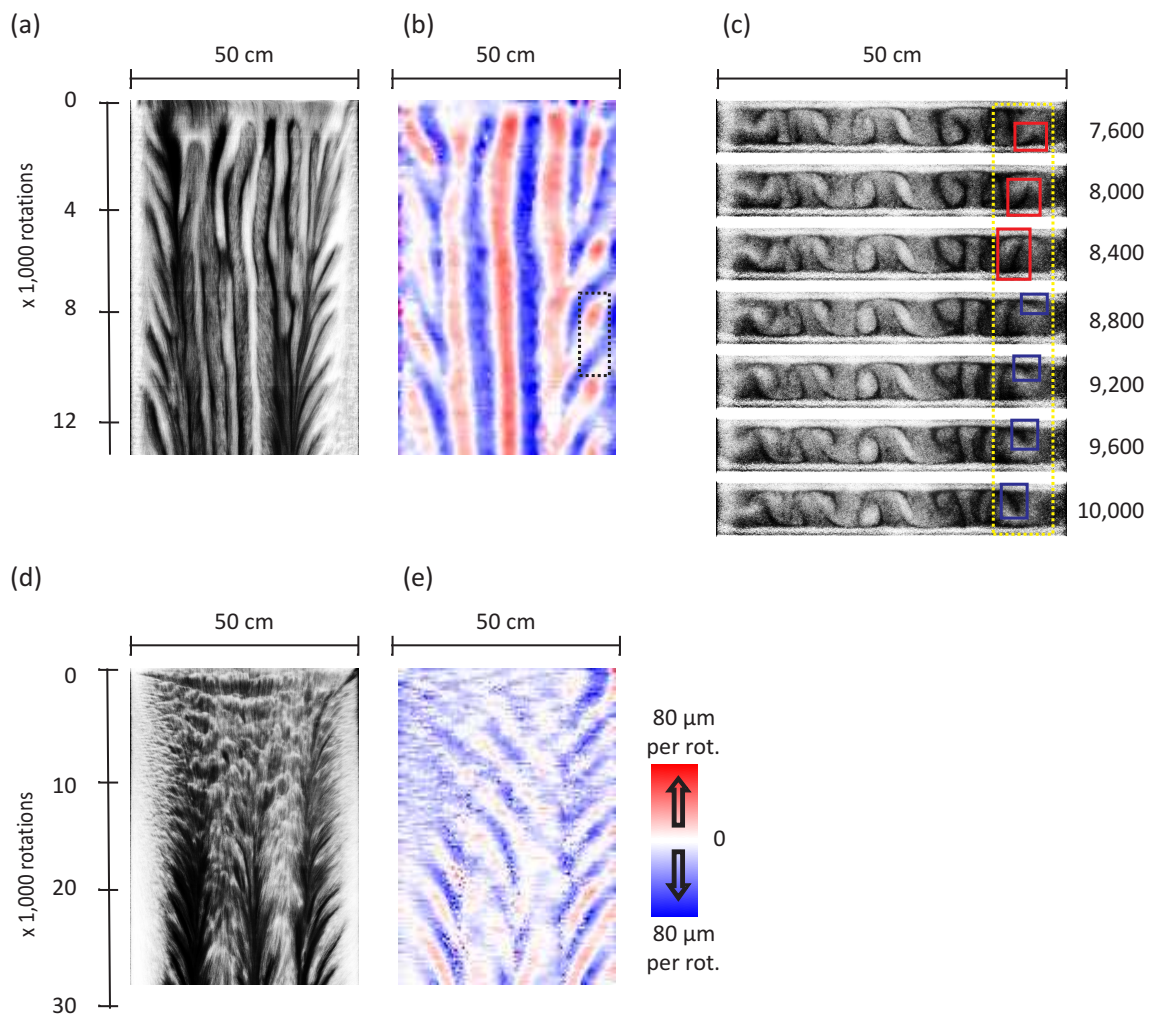


**Figure 7.6:** Inwardly moving traveling rolls. For the same experiment time-space plots of (a) segregation and (b) vertical velocity and (c) some snapshots of the whole container are shown. The number of rotations are given at the right. The yellow frame in (c) corresponds to the black frame in (b). Blue/red boxes in (c) mark downwards and upwards rotating rolls.  $C=0.618$ ,  $y=8$  cm (the run is also depicted in figure 3.7c)). (d,e) Example for rolls that are not limited to the edges but penetrate the whole cell.  $C=0.647$ ,  $y=10$  cm. The velocity scale is valid for both plots.

### 7.3 Comparison with literature

Traveling convection rolls in granular media (section 7.2) are so far found only in the experiment presented here. Traveling stripes (section 7.1) are also found on a lower level of complexity in rotating drums in three independent studies [76, 81, 82]. They are now compared with observations in the flat container.

An optimal condition for waves in previous experiments [82] was an initially pre-segregated stripe arrangement, with a spatial period below a certain threshold wavelength (figure 7.7a). When the prepared wavelength was too large, the bands were found to be stationary [83]. An initially mixed state led to less pronounced waves [82] (figure 7.7b). Similar observations were made in another study [76] (figure 7.7c). Axial particle separation was also the initial state in reference [81] (figures 7.7d, 1.6(j-h)). In contrast, the granulate in the flat rotating container does not require such preparation, the initial local composition can be arbitrary. In literature, traveling waves in cylindrical mixers were observed from the first 3,000 rotations [76, 82] up to 200,000 rotations [81]. In some cases [82], it was found that waves vanished after the bands had mixed and had lost purity. Persistence of traveling wave patterns up to at least 400,000 rotations (2.5 weeks) were observed in the flat box, whereas most drum experiments in the literature, with some exceptions (e.g. [75, 79, 81, 149, 156, 157]), run over much shorter time intervals (for example 2,500 rotations [76]). One might think that some interesting phenomena may have escaped the attention of other researchers that were interested mainly in the formation of patterns, but not in their long-term dynamics.

Traveling waves observed by Choo *et al.* [82] were discussed by the authors and were tried to explain by existing models [69] and previous observations. However, the new phenomenon was not comparable to older results. In order to close the gap a continuum model has been developed [71, 72]. But this model disagrees with experimental results [77] that were performed to verify the outcomes of the model. Therefore one of the authors concludes: ‘the principle is unclear to everybody: we have no good explanation for the segregation, or the waves’ [158].

Waves were also observed in an almost completely filled drum [81] where the effect of the fluidized layer is limited. Therefore the generally favored idea that segregation is driven by surface flow was questioned [81]. Instead, slow bulk motion may be significant at longer time scales. Based on this assumption, a global convection roll with backflow in the core of the granulate bed was proposed [81]. A simple model was developed which reproduces phenomenologically the experimental studies, but adds no new insights to the physical driving mechanism. In contrast to that experiment, backflow of particles in the bulk is hardly conceivable in the flat cell geometry. Because the experiments are not comparable, another mechanism must be sought.

Besides regular traveling wave observations, there are also reports about other unstable but less regular phenomena in granular media. These are: oscillating sideward motions of bands in a ternary mixture ([159, 160], figure 7.7e), fuzzy propagating band edges ([149, 151, 156, 161], figure 7.7(f-h)), irregularly meandering bands ([75], figure 7.7i), and drifting bands as precursor of ensuing coarsening [160, 161]. A single observation of a band that emits waves in opposite directions has been described. For the so called ‘fountain band’ [83] see figure 7.7j. Vanishing and reappearing bands were also mentioned without giving more details in reference [157]. Simulations reproduced similar effects, for example unstable band motion [159, 162, 163]. Though the theoretical results might resemble the experimental data, they are very much simplified and an explanation on the particle level is still missing.

## 7 *Traveling waves*

In hydrodynamic systems of rotating suspension flows [34], one can find phenomenological analogies to pure granular experiments, such as oscillating bands [164] and traveling waves [165]. In particle-laden rimming flows, the most diverse band motions in a rotating drum have been found thus far [166,167]. Although these systems can partly be described by hydrodynamic laws, they cannot contribute to a better understanding of purely granular systems.

As the literature review reveals, there is only a weak theoretical basis of unstable or periodical segregation phenomena in cylindrical geometries. Periodical effects in stripe motion, if observable at all, are limited to a few cycles in previous studies. Here, more diversified dynamics observed in a flat rotating container were added. These dynamics combine some previous results, but apparently on a higher level of complexity. The instabilities of segregated bands remain one of the interesting and unsolved phenomena in agitated granular media. In a recent review article it is stated: ‘various models have been successful in reproducing axial segregation in binary granular mixtures [...]. However, the related phenomenon of traveling waves in granular mixtures has to date not been adequately explained’ [34]. The results presented here complement and extend previous observations in cylindrical geometries, and represent a challenge for modeling and theoretical description.

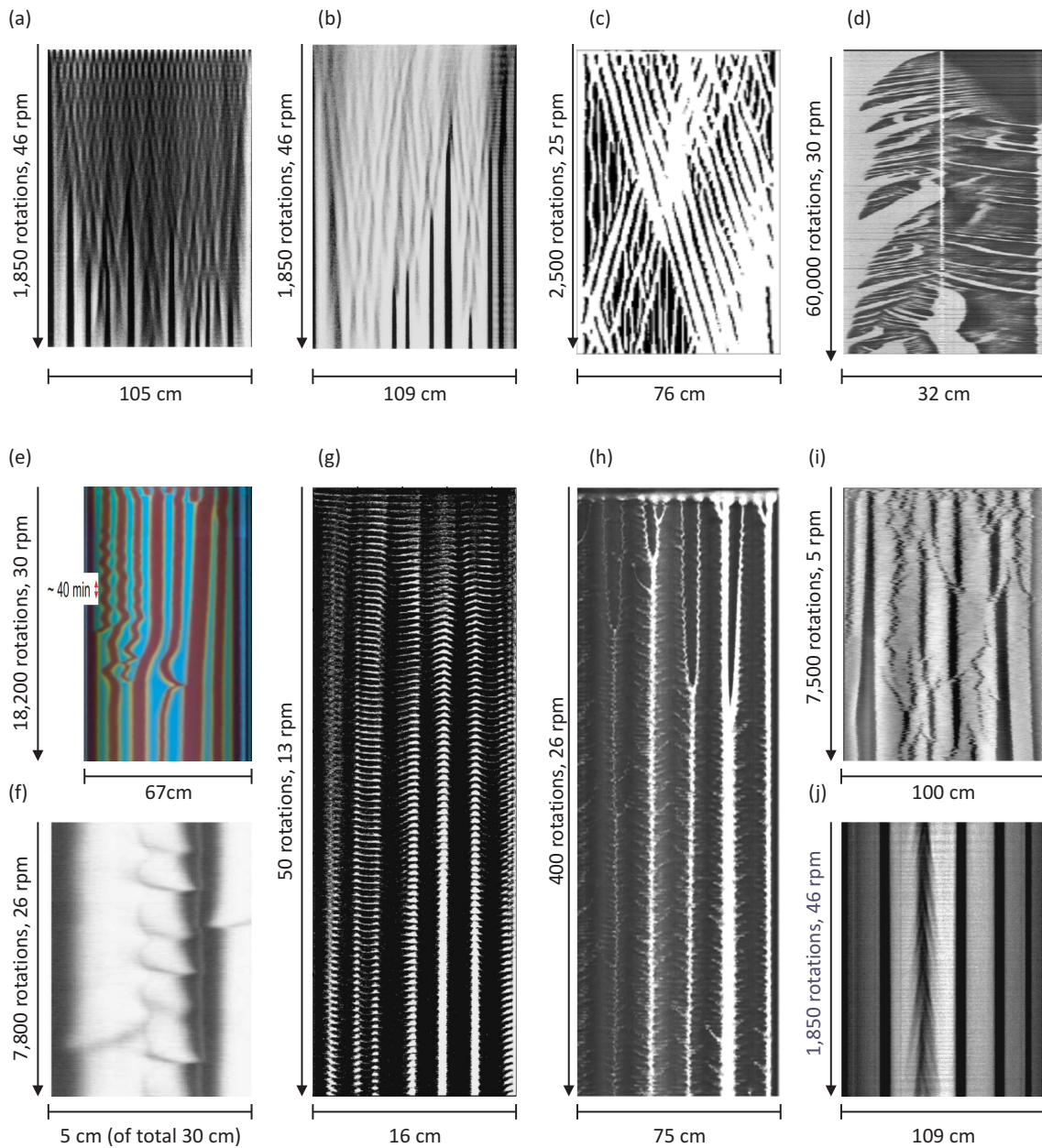


**Figure 7.7:** The compilation depicts time-space plots of all principal observations of (a-d) traveling waves and (e-j) instable band motion found in granular rotating drum flow till date. (a) First observation of traveling waves from a preseggregated state and from a (b) mixed state [82]. A similar experiment is shown in (c) [76]. (d) An axially preseggregated state (initially on the left/right sides are large/small species) led to irregular traveling waves (adapted from [81], the white vertical stripe in the center is due to construction of the drum). (e) Periodical band motion [160], (f-h) fuzzy periodical band edges ((f) [156], (g) [149], (h) [151]), (i) chaotic band motion [75]. In (j) the band that is slightly to the left of the center emits waves [83]. Axial drum lengths, rotation rates and number of rotations are given next to the subgraphs. Always roughly half-filled cylinders were used, except in (d) where the drum was almost fully filled. Gray scale images consist of bidisperse mixtures and the smaller/larger species are dark/bright. In the case for the ternary mixture (e) the colors for small/middle/large species are blue/yellow/red.



# 8 Two-dimensional systems

It is an interesting question if a three-dimensional system is a condition for convection or if it also occurs in two dimensions. There are so far no experiments in the literature with two-dimensional rotating granulates except for the simulation by Awazu [1]. Convection studies with large food grains (figure 5.10b,c) can already be considered as quasi two-dimensional. This stimulated a study of real two-dimensional systems with spheres and discs. Box profiles for the already discussed three-dimensional geometry and for the now introduced two-dimensional systems are sketched in figure 8.1(a-c). The experiments resulted in more or less robust convection scenarios. They could also be repeated in follow-up experiments.

In most experiments presented, tracer particles could be used. Particle positions were detected manually or automatically depending on the image quality. Therefore post-processing differs for the experiments between Eulerian and Lagrangian description. All experiments start from a mixed state. Typical size segregation patterns were found only for systems with spheres but study of segregation was not the aim of the experiments. The main topic was to characterize convection at high fill level. Lower fill levels were not checked.

## 8.1 Spheres

In the beginning, a suitable fill level had to be found. At 95% fill height, particles fluctuate only around their positions, as it was too full. All experiments were performed at  $\approx 92\%$  with sufficient fluidization and observed either in transmission or reflection if one wall is opaque. Monodisperse sphere packings crystallize along the borders and crystal defects move along the cell. There is no convective motion thus this type of experiment is disregarded. The following experiments deal only with bidisperse packings. They were all performed in the same way. Most experiments exhibited segregation and in some rare cases convection under absence of segregation took place.

Experiments are done with uncoated and coated glass spheres. Coated spheres are easier distinguishable but also abrade which might lead to unwanted effects. However all main effects are also observed with untreated beads. Another problem is the charging, which presumably occurs as the cell gap is almost as narrow as the bead size (see hanging beads at top edge in figure 8.1h). Gluing ITO foil on the cell inside has removed this effect but inhomogeneous glue distribution led to rough walls. A better test would be using a transparent conducting coating.

The different segregation types are summarized in figure 8.1(d-k). Radial segregation is displayed in figure 8.1d,e. At low speed (20 rpm) small particles (bright) collect along the rotation axis (figure 8.1d) and at faster speed (180 rpm) collect outwards (figure 8.1e). One might explain this analogous to figure 1.6a,b. The phase inversion velocity is 150 rpm. A close inspection shows that the segregation has a wavy-like structure in figure 8.1e. Another case of segregation shows figure 8.1f. Here, small and large particles sort on top of each other. In general segregation must not be stable. For the same experiment a segregated state can completely mix and then demix again.

Observation of axial segregation demonstrates figure 8.1(g-k). Demixing is clearly visible after 1,000 rotations (figure 8.1i). For the rest of the run (in total 17,600 rotations) the purity of stripes increased but coarsening did not take place. Small particles have a higher surface profile than larger ones. This is analogous to three-dimensional variants of the

experiment (compare to figure 3.8a and [69, 77, 78]). In the rotating cylinder a higher surface profile is related to a higher repose angle. The angle of repose refers to an angle that forms in a continuously flowing granulate. This condition is not fulfilled in the flat drum and the meaning of an angle of repose is debatable.

It is not clear how different segregation patterns are triggered and when convection or segregation sets in. Therefore more experiments are needed. If spacially segregation takes place then no convection is observed. Tracer were added to detect any flow during segregation. However, they agglomerated in one or a few zones. This happened for manually painted spheres and different types of manufactured coated spheres. The manufacturer states that there are no additional attractive forces and that they do not distinguish from other uncoated spheres [168]. Notwithstanding, there must be small differences that lead to tracer accumulation.

If statistical physics can be applied then segregation might be explained by attractive depletion forces [169–171]. Stripes occur also in horizontal shaken quasi monolayers of bidisperse mixtures (figure 8.11,m, from [172]). However there the stripes align orthogonal

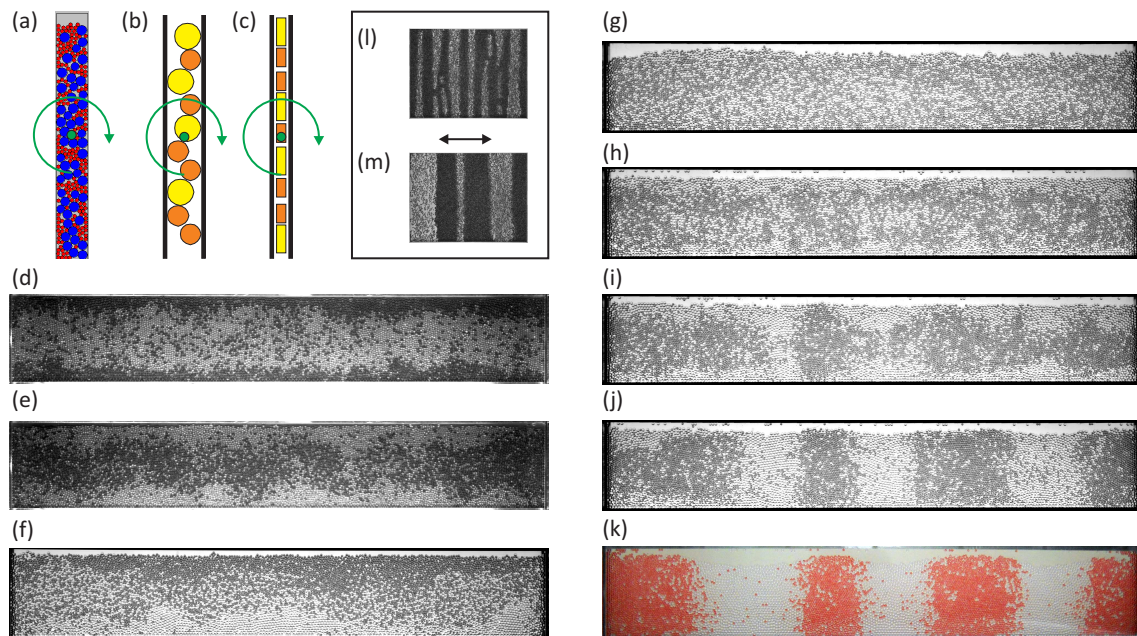


**Figure 8.1:** (a-c) Schematic profiles of cells. (a) Three-dimensional system with about 15 bead layers in the short direction. Two-dimensionality is achieved by using (b) spheres or (c) discs. (d-k) Different types of segregation in two-dimensional experiments with spheres analogous to (b). (d,e) Radial segregation can be triggered by the driving rate. (d) Small particles (bright) at low rotation speed (after 1,600 rotations at 20 rpm,  $Froude = 0.018 \ll 1$ ) and large particles (dark) at higher rotation rates (after 3,000 rotations at 180 rpm,  $Froude = 1.45 > 1$ ) accumulate in the center, seen in reflection. (e) In another experiment small (dark) particles stratify above large particles (bright) after 17,900 rotations. (g-k) Development of axial segregation. (g) Before start of the experiment, after (h) 500 rotations, (i) 1,000 rotations, (j) 1,500 rotations, (k) 17,600 rotations (color camera). The degree of segregation increases however no coarsening takes place in experimental time. In all experiments small spheres ( $2 \pm 0.2$ ) mm and large spheres ( $2.5 \pm 0.2$ ) mm are taken from Sigmund Lindner (type M) and rotated at 20 rpm, except (e).  $z=3$  mm. (l,m) Comparison with a double layer of copper beads (bright) and poppy seeds (dark) at horizontal acceleration of  $1.32g$  after (l) 30 min and coarsening after (m) 6 h (taken from [172]). From an initially mixed state, stripes form orthogonal to the driving direction (arrow).

to the vibration direction whereas in the rotating container the stripes are parallel to the direction of gravity.

An experiment that exhibits convection is displayed in figure 8.2a. For the same picture spheres were manually detected and reconstructed with different colors in figure 8.2b. Orange/yellow are small/large discs. Automatic detection were also possible and qualitatively correct if one accepts a high error rate. During the whole experiment (in total 82,000 rotations) no segregation took place and is seen in the reconstruction image where only at a few spots demixed zones exist. After 30,000 rotations, convection gradually set in starting at the right wall (time-space plot in figure 8.2d). But in general, convection can also start in the whole cell from the beginning. Figure 8.2c shows tracer positions after convection has evolved to a great extend. Time is visualized by color. Starting/ending points are blue/red. Clearly vortex-like motion is visible. There is erratic motion on the particle size level if positions are compared after single rotations. After  $\sim 10$  rotations uniform motion dominates. Figure 8.3b depicts tracers for fully developed rolls. 8 rolls are formed, slightly higher than the container's aspect ratio of 6.25. Streams can also be derived from brightness fluctuations (green vertical zones in figure 8.3a). There is an asymmetry between top and bottom layer. The bottom layer is higher fluidized. This cannot easily be explained and is independent if cell stopping occurs after 1 or after 10 rotations. A similar asymmetry was already observed for a multilayer-system (figure 3.3e).

It is interesting that the dynamics is stable against external disturbances. The closed cell was substantial shaken. The strength of the disturbance is characterized by different tracer positions before and after shaking (figure 8.3d). After shaking, convection continued with almost no influences (see tracers in figure 8.3c and horizontal arrow in figure 8.2d). For a limited experimental time, a better resolved time-space plot is available (figure 8.2e). Convection spans the whole axis and rolls drift like in multilayer studies.

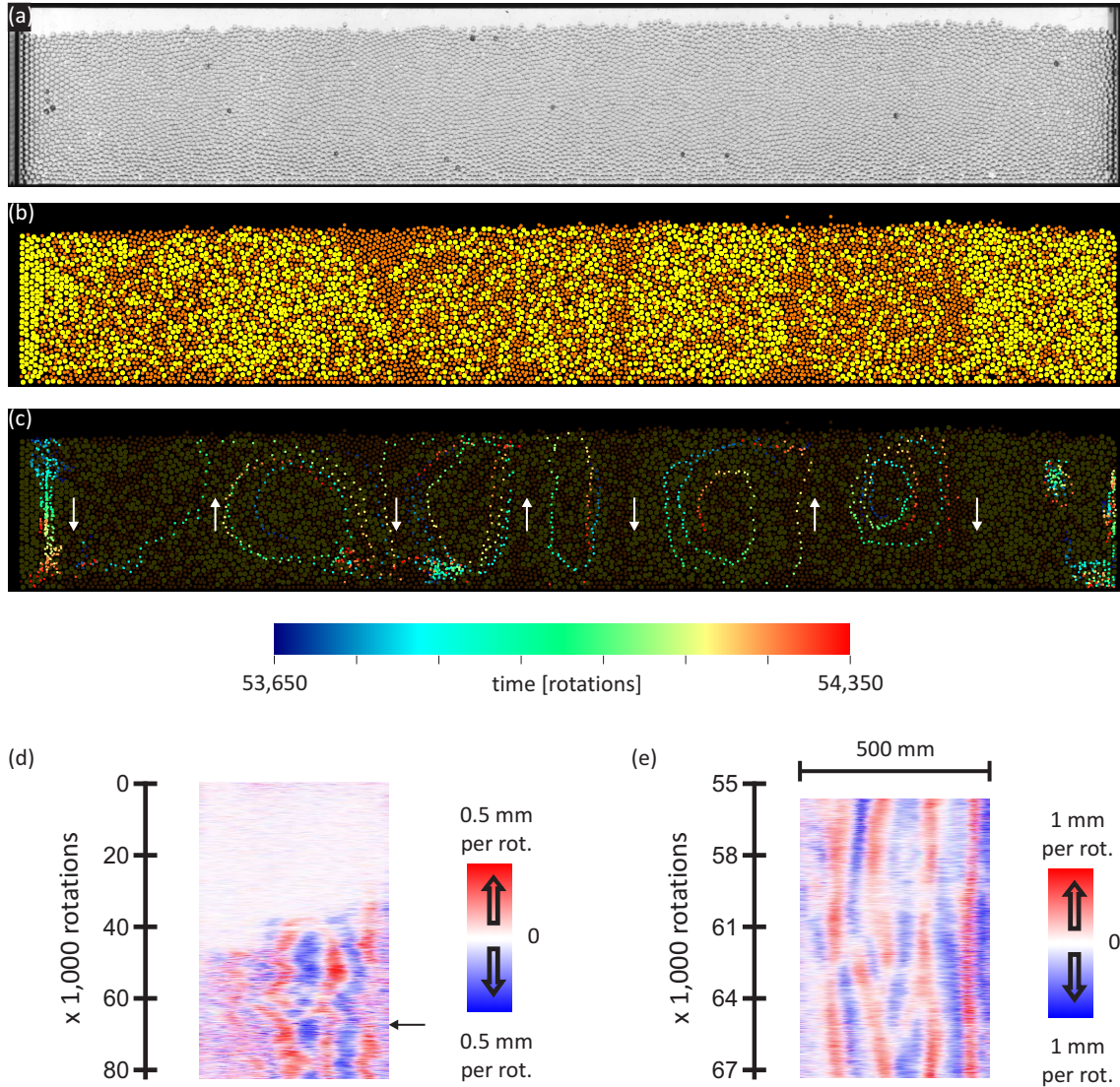


**Figure 8.2:** (a) Snapshot of a two-dimensional cell filled with a monolayer of bidisperse spheres after 54,000 rotations. (b) Reconstruction after manual detection of small (orange,  $(2\pm 0.2)$  mm, quantity 4,769, cell area occupation 37.5%) and large (yellow,  $(2.5\pm 0.2)$  mm, quantity 2,878, cell area filling 35.3%) species. The dark spots in (a) are 10 small and 10 large tracers. (c) Paths of tracers for 700 rotations (71 images, around the moment of (a)) overlaid over (b) after onset of convection. Time is coded by color (scale). Arrows show main convective currents. (d) Time-space plots of the vertical velocity component along the rotational axis. The horizontal arrow marks shaking of the cell (see figure 8.3d). The data is based on pictures after every 10 rotations. (e) For a part of the experiment, images after every rotation are available. They allow better conclusions on the convection. The flow is faster and expands over the whole cell.

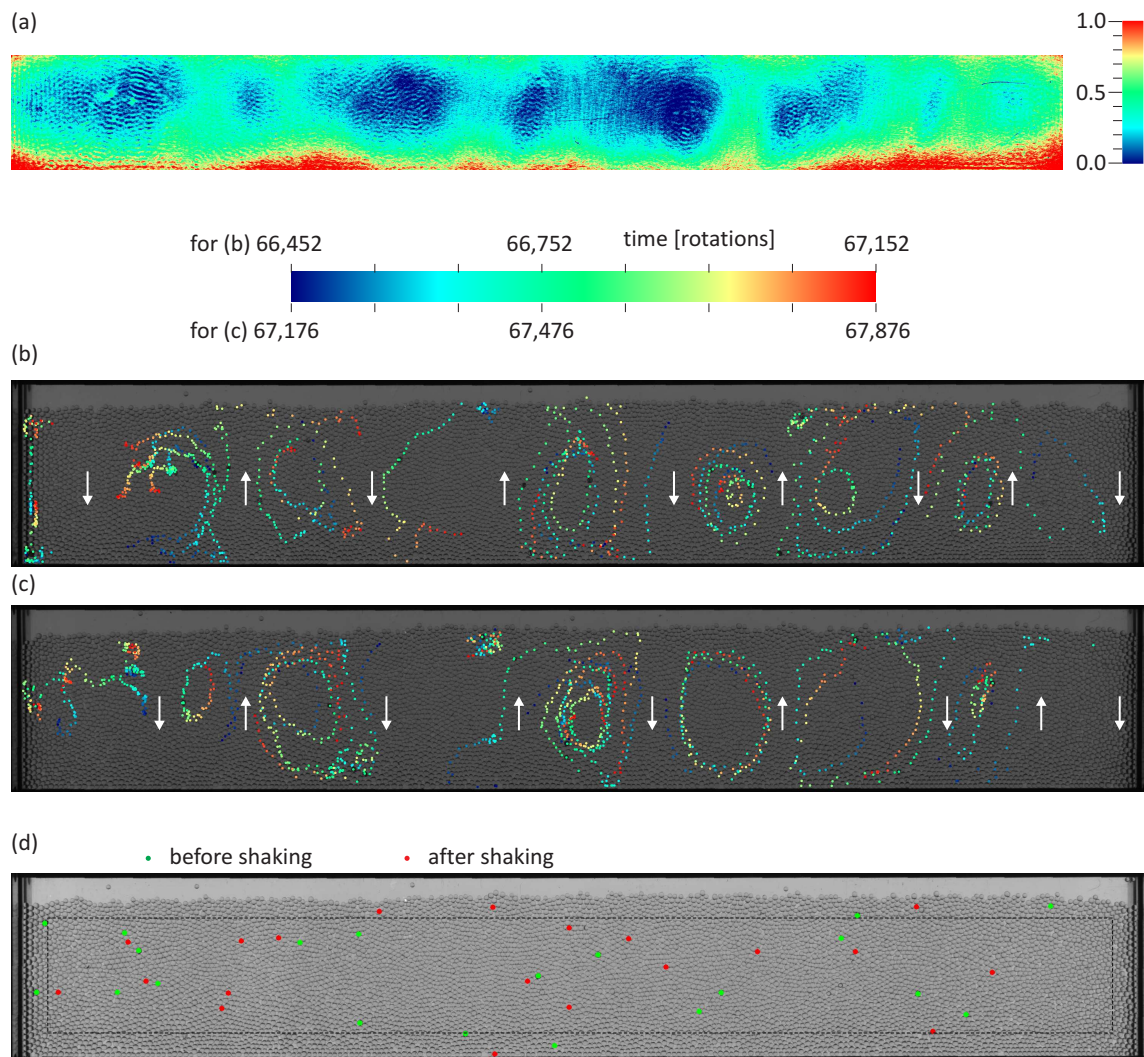


**Figure 8.3:** (a) Brightness fluctuations (normalized, for a definition see section 2.4) averaged over 700 rotations (701 images) for the dashed region in (d). (b) Corresponding tracer paths after full development of rolls for the same experiment as in figure 8.2. Low fluctuations are found in vertex centers. (c) The convection is undisturbed after container shaking (horizontal arrow in figure 8.2d). In order to characterize the degree of particle displacements by shaking the tracer positions directly before (green) and 10 rotations after shaking (red) are shown in (d). Tracers after shaking cannot be identified from their original positions (tracer motion during the 10 rotations after shaking can be neglected).

## 8.2 Discs

Another and presumably more intuitive way to realize two-dimensionality is the usage of a monolayer of discs instead of spheres. Discs in the requested dimensions are not easily commercially available. For example the aspect ratio for washers is too large. Thin washers are hard to handle and if they are thick enough then they are quite large in diameter. This would request a huge experimental setup. Suitable materials that were found are hollow plastic cylinders and purportedly manufactured aluminum discs.

**Nylon discs** Nylon spacer (Micro Plastics, Inc., Flippin, AR) with height  $0.125'' \pm 0.005''$  ( $3.2 \text{ mm} \pm 0.13 \text{ mm}$ ) and two diameters  $0.187'' \pm 0.015''$  ( $4.8 \text{ mm} \pm 0.4 \text{ mm}$ ), type 13SP001 and  $0.25'' \pm 0.015''$  ( $6.4 \text{ mm} \pm 0.4 \text{ mm}$ ), type 13SP031 were used. The given tolerances are derived from the data sheet and are smaller in real life. They have a hole with diameter  $0.091''$  ( $2.3 \text{ mm}$ ), but this is indifferent for the aim of the experiments (see figure 8.4a). The hollow shape increases only the effort in post processing during disc detection as disc holes resemble gaps that are formed by three triangular contacting discs. Discs can be detected by digital convolution with a structure element that resembles the real discs. More than 99% of the particles are correctly detected. Pictures are taken after 20 rotations. After this period more than 95% of the particles have moved less than their radius which allows mostly reliable detection of the displacements. The paths of the discs can be tracked almost completely, but sometimes their positions are lost.

Segregation was not found, except in some limited areas with maximum 100 small particles or 20 large particles. In segregated zones convection is inhibited. No tracers were used and sometimes particles are lost during tracking. Therefore the long-time dynamics are derived from short-term behavior. On short time scales, erratic fluctuating disc motion is observed. However on longer time-scales, convection can be found. This fact is not surprising as the number of particles is several orders lower than in multilayer studies. The increase in particles can attribute towards the increase in robust self-organizing structures. There is also a second reason for the erratic motion. The cross-correlation technique that is used for multilayer systems (section 2.4) includes averaging over many particles. Here, information on a single particle scale is accessible and therefore averaging must be done additionally by considering longer terms i.e. including a larger number of particles over time.

Figure 8.4(b-e) shows short term behavior. The images are reconstructed from the automatically detected discs. In all cases, they are colored concerning their displacements after 20 rotations (2 consecutive images in the run). Whereas in figure 8.4(b,c) they are colored relating their directions of the displacements (circular scale) they are colored in figure 8.4(d,e) relating their distances of displacements (linear scale). Information about the motion after every single rotation is not available for this experiment but the quantity distance/(20 rotations) would be a measure for the average disc speed per rotation. Both representations allow separate conclusions about direction and magnitude of flow. Figure (c) is the next taken image after (b) and panels (b,c) belong to (d,e), respectively. Although the particles have moved only a fraction of particle size, large fluctuations can be seen from (b) to (c) and (d) to (e). From such description no global motion can be derived. Therefore the data for the two moments shown in figure 8.4 are averaged with additional data that totally span 2,000 rotations. For any pixel that is occupied by a disc the corresponding displacement vector is stored and finally the mean angle and mean distance are calculated for every pixel. The result is depicted in figure 8.5a,c. Now regular downward and upward flow is seen but not as regular as for three-dimensional systems or for two-dimensional

experiments with spheres. In the left part, two rolls can be distinguished (figure 8.5c). The higher the value of the mean displacement, the more and faster particles have passed the region. One can understand this measure also as a kind of particle flux. The preferred direction of the flux is seen in figure 8.5a. In order to get insights into the paths of small and large single discs, the trajectories for the discussed averaged images are separately shown in figure 8.6a,b. The coloring corresponds again to the direction of the connecting paths between a disc from two consecutive pictures. Paths resemble partly vortex flow that is overlaid by fluctuations.

For the same experiment but at another moment, the averaged flow is displayed in figure 8.5b,d. Obviously the regularity of the convection is lost. Also the mean displacement length is lower. Irrespective of the meaning of convection in this system, one can say that there can be more ordered and less ordered phases. A simple measure for the robustness of convection streams is given. For the framed region in figure 8.5b the local contrast between neighboring pixels is measured by edge detection (Sobel filter [173]). The mean value of the edge detected image serves as a quantity for the fluctuations in the image. The convection homogeneity is the reciprocal of this value and shown in figure 8.6c. Any point is averaged over 2,000 rotations. The two examples in figure 8.5 correspond to highest and lowest homogeneity, respectively.

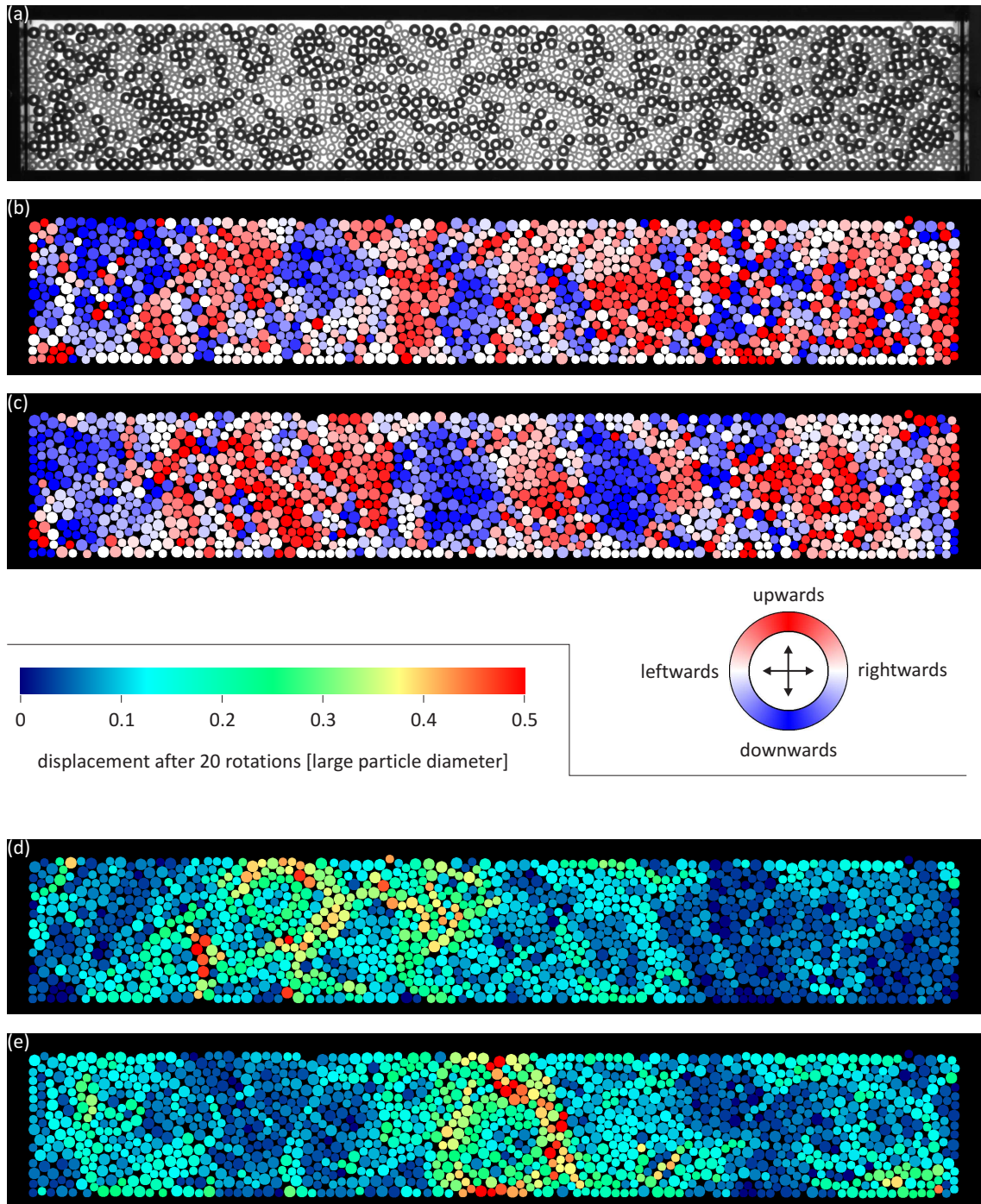


**Figure 8.4:** (a) Picture of the cell filled with 495 large (dark, 39.2% cell area filling) and 889 small (bright, 39.6% cell area filling) hollow plastic discs after 9,080 rotations. No segregation is visible. Discs are detected and tracked and artificial images are reconstructed in (b-e) and figures 8.5,8.6. (b) The beads from (a) are colored concerning their direction of displacements between rotations 9,080 and 9,100. Blue/red indicates downwards/upwards motion and white horizontal motion (circular scale). (c) Directions of disc displacements between 9,100 and 9,120 rotations. (d,e) Magnitude of displacement for (b) and (c), respectively (linear scale). Discs move less than their radius but exhibit strong fluctuations on a short time-scale. Convection can be seen only on larger time-scales (figures 8.5,8.6).

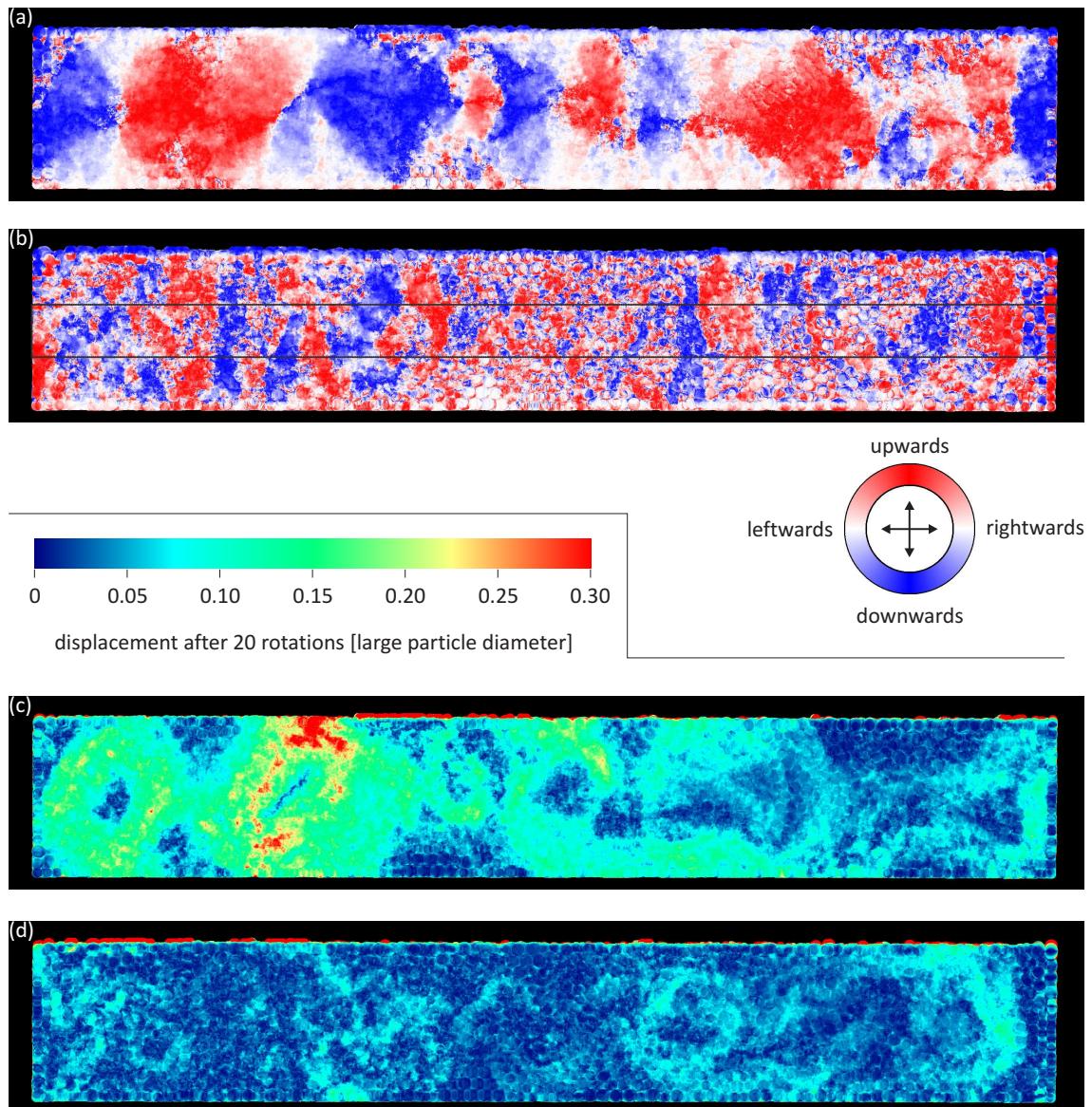


**Figure 8.5:** (a) The same run as in figure 8.4 but the coloring of the direction is averaged from rotations 9,000 to 11,000 (101 images, see circular scale). To a large extent alternating upwards and downwards streams can be recognized. (b) The situation for the same experiment averaged between 31,500 and 33,500 rotations (101 images). The convection field has lost its regularity. (c) Corresponding averaged distances for the disc displacements in (a). High mean displacements i.e. high particle flux is clearly manifested in two rolls on the left side whereas the convection strength diminishes towards the right cell side. (d) The mean flux is low and irregular as expected for the corresponding direction field in (b). The uniformity of the convection is measured along the horizontal central area in (b) and shown in figure 8.6c).

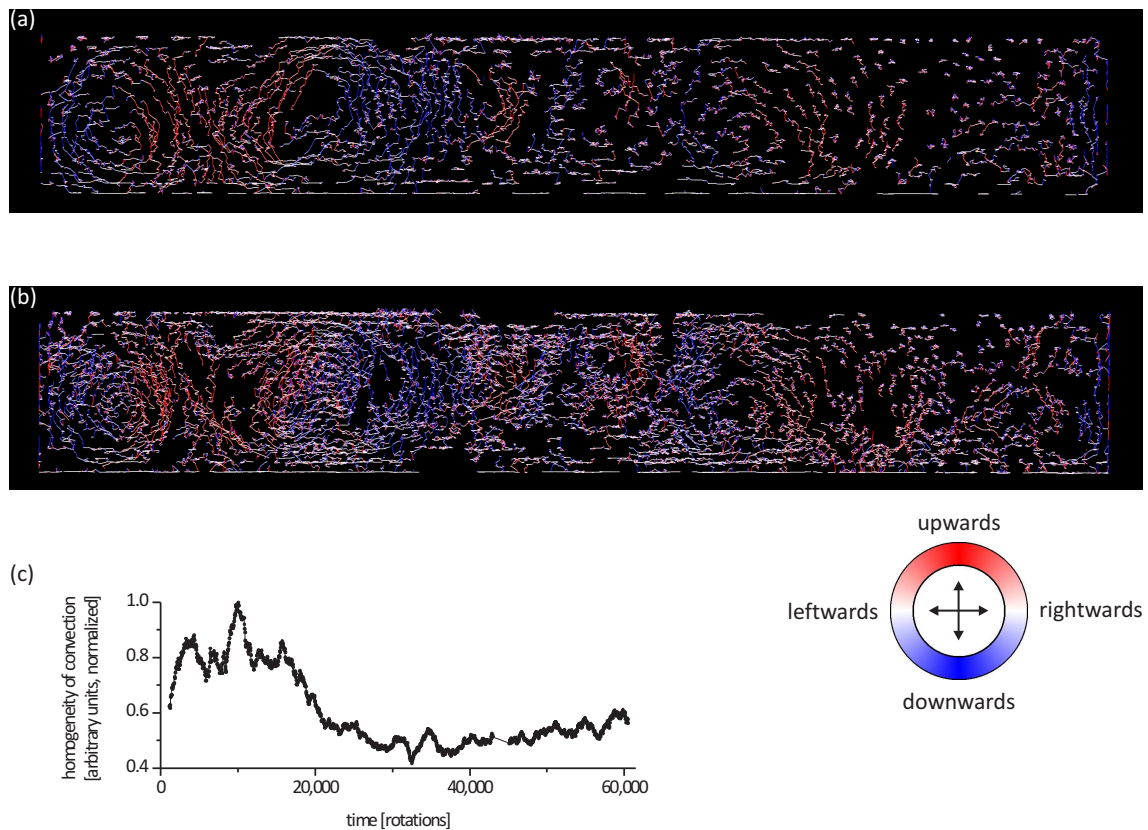


**Figure 8.6:** Trajectories for all discs from the experiment in figures 8.4,8.5 tracked for the time from 9,600 to 10,400 rotations (41 images). For clarity the particles are shown separately, the large ones in (a) and the small particles in (b). Both species behave similar. Trajectories are colored relating their momentary direction (circular scale). Regions with preferred upward and downward flow are recognizable. There are interruptions in the disc paths as they cannot always be detected reliably. (c) Homogeneity of convection derived from averaged direction fields like figure 8.5a,b. The homogeneity is measured only for the dashed region in figure 8.5b and can fluctuate in a single experiment, i.e. the convection is stable only on limited time scales. The two panels in figure 8.5a,b correspond to the highest and lowest homogeneity of the whole experiment after 10,000 and 32,000 rotations, respectively. For a definition of the convection homogeneity see text.

**Aluminum discs** Experiments with aluminum discs are currently done by Robert Prusas. They differ from the described experiment previously in two respects, namely more particles are used and the driving method is different. One particular experiment is described now. More details can be found in the student thesis [174].

Aluminum discs were punched by a metal processing company (Karl Behrens GmbH, Berlin). Side effects of the punching process are differently formed caps of the discs. One side is flat and the other slightly curved (see figure 8.7d). Due to differences in friction, beads slip faster on their curved sides and smaller beads slip faster on their flat sides than the larger species on their flat sides. Demixing because of different slip behavior on front and back sides of the container dominates over size segregation. This effect is diminished by two modifications. Firstly, all discs are filled in the box in the same orientation, i.e. all flat disc sides direct towards the same cell wall. Secondly, continuous rotation is replaced by back and forth motion of  $\pm 60^\circ$  around the horizontal cell orientation (similar to experiments in section 4.2). The cell is oriented in a manner that all particles slide on their curved side. One back and forth cycle lasts for 40 s. Because of slow driving, a few bead layers at the lower front chute earlier than the remaining particles. At one of the two end positions, pictures are taken by a digital camera (Nikon E4500,  $2272 \times 1704$  pixel) after every cycle.

A first experiment where convection-like motion was found is shown in figures 8.7, 8.8. The net discs' space is 74.7% of the container area with roughly equal area fractions among the two species. Including the interstitial gaps the occupied disc area is  $\approx 95\%$ . The free space of 5% is larger but comparable to the free space on top of the granulate in the experiments with multiple bead layers.<sup>1</sup>

Convective motion sets in instantly after the start of the experiment. Only the first 7,692 cycles are considered here. A picture of the disc distribution after 3,820 cycles shows figure 8.7a and a manual reconstruction of the discs was made in figure 8.7b. Segregation is seen only in some limited areas. In order to visualize the particles' motion, the fluctuations of the brightness intensities of images around figure 8.7a are depicted in figure 8.7c. High fluctuations, i.e. high fluidizations are localized at the bottom and top zones. This is expected as here particles can move freely. Three convection rolls can be distinguished. This is close to the container's aspect ratio of 3.7. High degree of fluidization is interconnected with positions where discs drift up- and downwards.

Information on a single-particle level gives figure 8.8. In figure 8.8(a-d) the paths of 10 tracers (differently colored discs in figure 8.7a) are shown and distributed for better visualization in 4 panels. In the fluidized zones the discs drift mostly horizontally whereas in the central region vertical motion dominates. To a great extent the discs move in circular orbits if they stay in the central area. White arrows indicate tracers at the moment shown in figure 8.7. The tracers follow in general the averaged motion recognizable in figure 8.7c. The rolls are not stable. In the course of the run, they change their positions. This can be seen in figure 8.8e. Here, all tracer paths are colored regarding their direction (see circular scale). In regions where upwards flow is observed later can be downwards flow and vice versa.

Currently the setup is improved in areas concerning long-term stability and image quality to allow automated post-processing of the images. Determination of local packing density, order parameters etc. is at hand. It is refrained doing this for the available coordinates. This task is reserved for the outcomes of the new setup.

---

<sup>1</sup>The diameter ratio of small to large disc is 0.65. It shall be noted that for a similar size ratio of 0.638 the densest infinite packing with however equal population of small and large discs is 91.1% [175, 176]. The density is slightly higher than the densest arrangement of a single species (90.7%, hexagonal packing). Only for nine distinct diameter ratios  $\leq 0.638$  exist densest compact bidisperse disc packings [177].

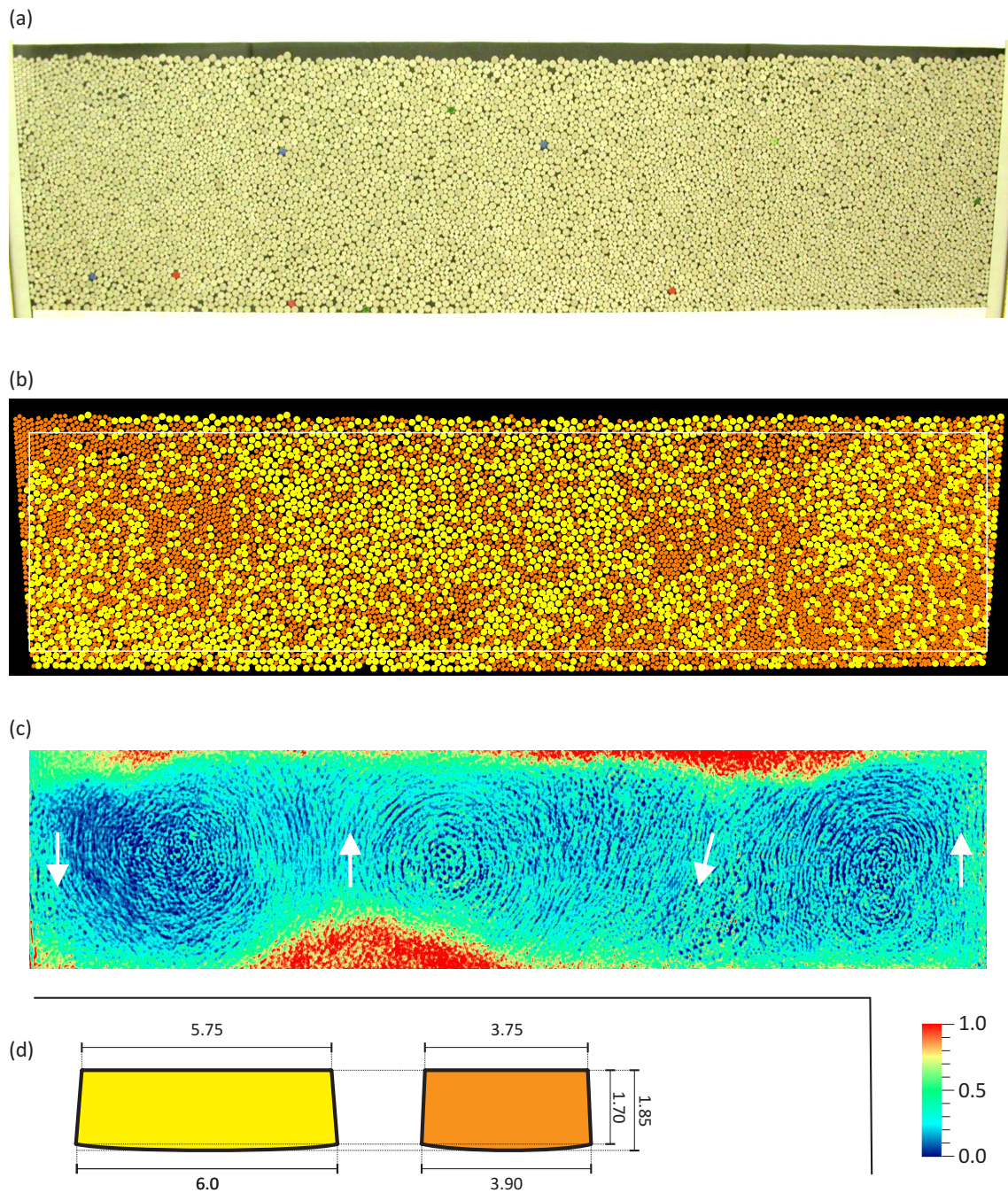


**Figure 8.7:** (a) Picture of the rocking container filled with aluminum discs after 3,820 cycles. Colored discs are tracers. (b) Manual detection of larger (yellow, diameter 6 mm, quantity 2,648, cell area filling: 39.3%) and smaller (orange, diameter 3.9 mm, quantity 5,635, cell area filling: 35.4%) discs. There are mostly nonsegregated areas. (c) Fluctuations (normalized) in the brightness distribution for the white framed area in (b) reveal main disc displacements (averaged between 3,628th and 4,012nd cycle, 385 images). Three vortex centers can be distinguished by circular lines (resembling streak lines). In the lower and upper parts high fluidization is seen. The main directions are indicated by arrows. (d) Approximative profiles of the discs (units in mm). Tolerances  $< 0.05$  mm. Discs slide on their curved surfaces (lower surface in the sketch).  $x = 835$  mm,  $y = 228$  mm,  $z = 2$  mm.

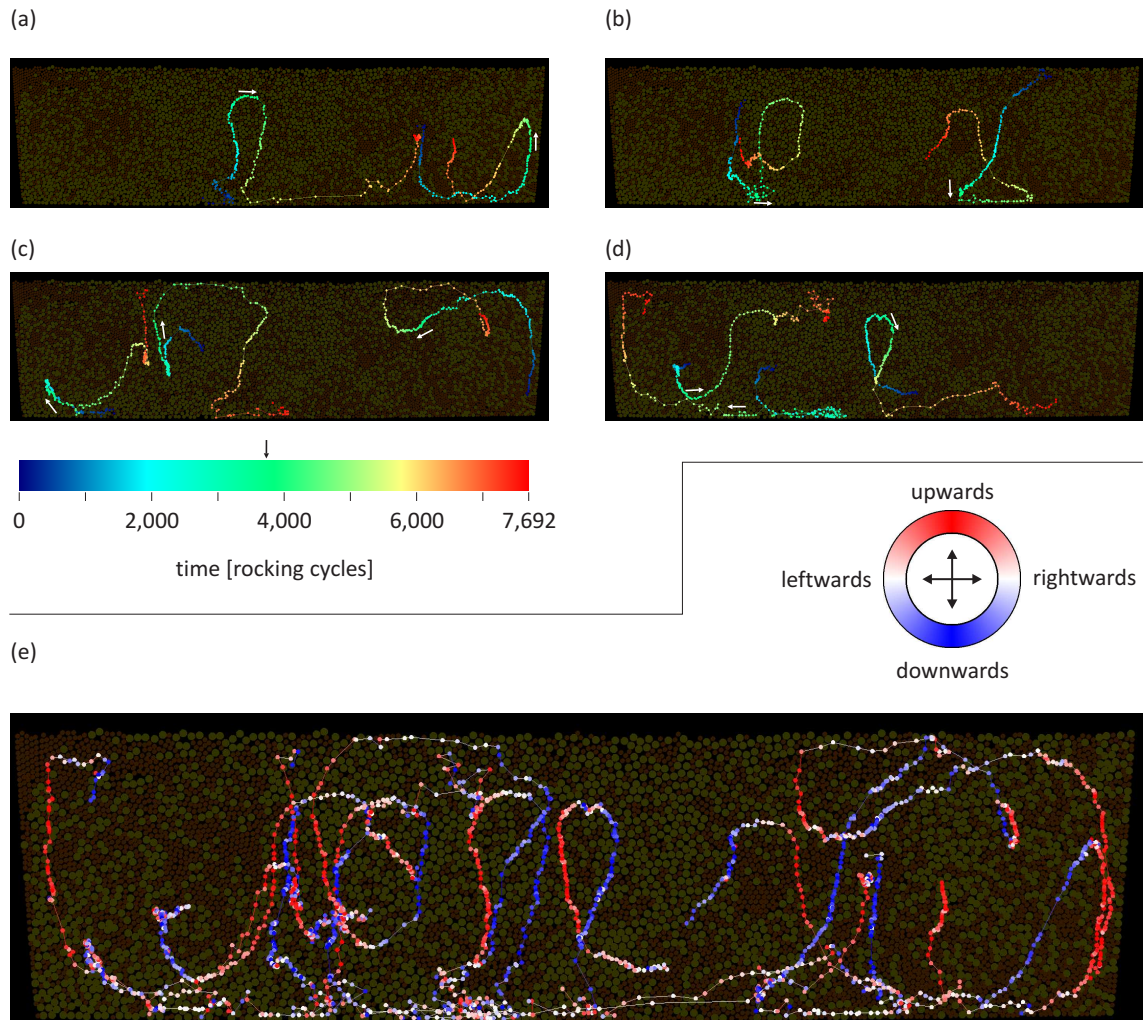


**Figure 8.8:** (a-d) Paths of total 10 large tracer discs overlaid on the segregation pattern (figure 8.7b). Their temporal positions are colored (see scale). Tracers are shown at the start of the experiment (blue) and they end after 7,692 cycles (red). White arrows mark the tracer direction for the moment shown in figure 8.7(a-c), i.e. after 3,820 cycles (green, black vertical arrow at scale). Vertical motion dominates in the center but erratic horizontal motion in the upper and lower zones. The positions are shown every 32 cycles. (For a few cycles the coordinates are missing due to camera failure. This leads to larger steps in the tracer positions without changing the general character. Missing are cycles 961 to 1,291, 4,013 to 4,171, 4,301 to 4,371, and 5,685 to 5,931.) (e) All tracers from (a-d) are combined in a single image. Colors now indicate directions (circular scale). Convective motion in a given area can change its direction in time. Rolls are not stable.

## 8 Two-dimensional systems

Segregation and convection have been found in two-dimensional systems. At least for discs the convection is not as robust as for the multiple layer system. The reason might be the smaller number of particles. Whereas there are  $< 10,000$  particles in the two-dimensional experiments there are at least 100,000 particles in multilayer studies (section 5.2). Boxes with standard dimensions in which most experiments are done occupy several million particles. Characteristics of convection systems are summarized in table 8.1. It is unclear how two-dimensional and three-dimensional experiments are related and how two-dimensional experiments with spheres and discs can be compared. Obviously the particle motion during fluidization differentiates in two-dimensional and three-dimensional systems. Even within two-dimensional studies there are differences. The slow driven discs slide gradually whereas the faster rotated spheres chute at once for the naked eye (see also discussion related to figure 10.1).

particles	figures	total number of particles	size ratio small:large	total area filling [%]	effective convection speed [large diameter per rotation]
spheres	8.2,8.3	7,647	0.80	72.8	$\approx 0.2$
nylon discs	8.4-8.6	1,384	0.75	78.8	$\approx 0.01$
aluminum discs	8.7,8.8	8,283	0.65	74.7	$\approx 0.03$

**Table 8.1:** Summary of observed convection in two-dimensional experiments. (In the last column the unit for aluminum discs is [large diameter per rocking cycle].)

# 9 Convection mechanisms

From experimental observations presented in the previous chapters, general conditions can be derived that any model must fulfill to explain multilayer convection cells (i.e. observations that are described in chapters 3-5).

The first, and probably most important experimental observation is that if the cell is halted at any moment during the rotation, the convection resumes unchanged after such an interruption. The flow and segregation patterns are the same as in a continuously rotating cell. The crucial point here is that when the cell is at rest, all information on the state of the convection roll structure must be coded in the static distribution of the grains, i.e. a ‘memory’ of the effective flow field pattern exists in the packing structure. When the cell rotation continues, for example after a stop in upright orientation, the local vortex motion is resumed. This is independent of whether the container rotation is in the same sense as before the stop or in opposite direction.

The second important feature of the convection pattern is that the direction of cell rotation is of minor importance. A continuous rotation with uniform sense produces similar flow patterns as a periodic change of the sense of cell rotation after each full turn or each half turn. This has been demonstrated in section 4.2. Thus one can conclude that small differences between front and rear sides of the cell (as seen in figure 3.4) are not relevant for the convection mechanism.

Finally, it is emphasized that in the search for the physical origin of the pattern, one has to look for a subtle mechanism: The convection velocity is in orders of magnitude slower than the excitation dynamics (container rotation), and even moderate chute flow in the container at lower filling ratios will eliminate the convection mechanism.

The key for the elucidation of the mechanism is the understanding that the convection pattern structure must be encoded in the packing of the grains. The vertical transport during the slide phase must be slightly modulated in axial direction, and this modulation must change its sign after each half turn of the cell.

Two options are suggested to explain this: the vortex direction is either encoded in height differences of the granular bed (model 1) or encoded in the packing density (model 2). In both models, the fluidized edges play a major role. They were so far not considered in detail and are described now.

## 9.1 Fluidized zones

The fluidized zones confine the convection streams and are located at the top and bottom granular surfaces. There, the particle velocity is at least two orders of magnitude larger than the convection roll speed. Their height is 5 to 6 mm each, of the same order as the cell thickness, but decreases with decreasing free volume above the granulate.

Figure 9.1 sketches the direction of particle circulation observed in a cross section of the cell perpendicular to the rotation axis. Figure 9.1a defines the frame of reference with respect to the cell rotation. At subcritical fill levels (figure 9.1b), there is a global circulation of the granular material with the rotation of the cell rotation. This is the consequence of the sliding during the chute flow being somewhat faster at the current top side of the cell than at the bottom side [74]. The velocity of this motion has been found to be of the order of several hundred micrometers per cell rotation, so that a number of cell rotations necessary for a full orbit of the granulate will be of the order of 1000. The

situation changes at supercritical fill levels where this global convection breaks down. Two fluidized regions remain at the upper and lower edges of the granular bed. Figure 9.1c sketches a global circulation stream in each of these fluidized layers. The velocity of motion is roughly of the same order of magnitude as in the global circulation at subcritical cell filling. Tracers at both cell edges are observed to track the sense of direction in the fluidized zones. In the standard experiment with uniform sense of cell rotation, the two fluidized edges develop circulation with the same sense as the cell rotation.

Interestingly, the situation changes when the cell is rotated  $\pm 180^\circ$  back and forth. For the  $\pm 180^\circ$  rocking motion, it started always from a cell in upright position with the rotation sense depicted in figure 9.1a and then reversed. In that experiment, the sense of circulation of one of the two fluidized zones reverses. Front and back sides of the cell can now be clearly distinguished because one of the cell planes is always above the other during the half circle. The granular dynamics in the fluidized zones reorganizes such that at the side that is always below, flow in these zones is toward the center of the cell, while at the upper side, the fluidized material flows away from the center (see figure 9.1d).

If the sense of rotation is reversed every full turn ( $360^\circ$ ), the flow in the two fluidized regions is not as pronounced as in the other experiments. However, a continuous flow of the grains at the cell plates toward the outer cell edges is observable from tracer motion (figure 9.1e). Because of mass conservation, it is assumed that there must be an oppositely directed flow in the central cell plane (marked by ‘?’ in figure 9.1e), forming a roll pair that cannot be monitored with the optical observation technique.

In any case, it is obvious that the sense of rotation in the fluidized regions plays no role for the general appearance of the convection patterns in the cell plane. The in-plane convection patterns in the central, jammed region of the granulate cell develops irrespective of the circulation dynamics of the outer fluidized zones.

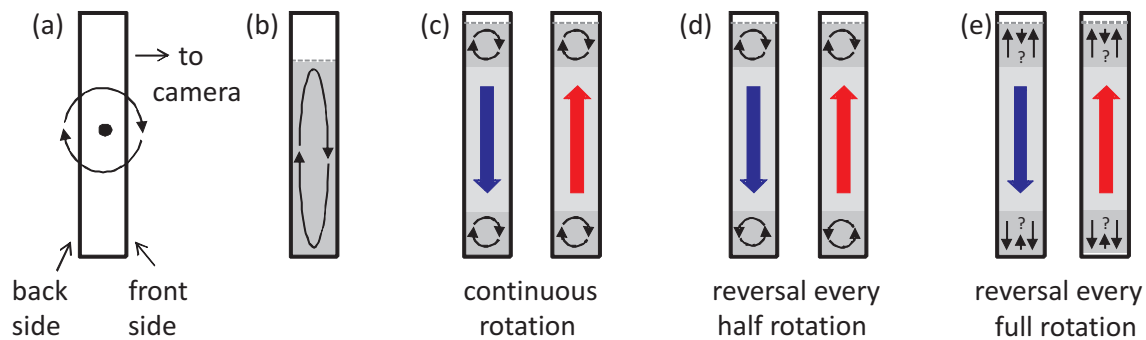


**Figure 9.1:** General circulation schemes in the rotating flat cell, seen from the side. (a) Cross-section of the flat rotating container. The reference system is given by the sense of rotation and the definition of the front view. (b) At lower fill level the whole granular bulk circulates. (c) At higher fill level ( $C > C_C$ ) and continuous cell rotation, only shallow fluidized regions rotate. In the central parts, one has essentially up and down net flows in the cell plane within the convection rolls. This is symbolized by two cross-sections in the respective upward and downward convection roll segments. (d) At periodical reversal after every half rotation, the two fluidized regions rotate in opposite directions. (e) At periodic reversal after every full cell rotation, the observable motion is ‘outward’ on both cell planes. Dark and light shaded regions in (b) to (e) mark the fluidized zones and convection regions, respectively. White areas indicate the free space above the granulate.

## 9.2 Model 1: height differences

The first model is based on the assumption that the fluidized zones are comparable to a rotating granulate like in common half-filled cylinders.

In figure 9.2a,c time-space plots of the upper and lower fluidized zones are shown. They are constructed analogous to time-space plots in chapter 7 and are strongly contrast enhanced. Segregation is weaker than in the convection zone i.e. the concentration differences between large and small particle bands in the fluidized layer is smaller. Also coarsening during the first 3,000 rotations can be registered before the bands are stable. Segregated bands of small and large beads oppose each other in the cell. After a half rotation, when the lower edge reaches the top, the segregation is the same, but the pattern is shifted axially by one convection roll width. This creates an unexplained synchronization effect between the two axial segregation bands. The segregation extends through the whole cell depth. There is a clear relation between segregation and convection. The wave length of the flow corresponds exactly to the axial band periodicity. Regions where the convective flow is directed towards the fluidized zone are always enriched with smaller beads (arrows in figure 9.2b).

Systematic height differences of the upper edge of the granular bed, if there are any, are much smaller than in the case of pure axial segregation at lower fill ratios where small particles have a higher surface (figure 3.8a and [69, 77, 78]). When one analyzes the averaged top edge from a series of images, height modulations with the wave length of the convection pattern would be below experimental resolution ( $< 20 \mu\text{m}$ ). However there is indirect evidence to assume that fluidized zones are comparable to axial segregation. One could accept similarities like flow circulation (section 9.1), segregation and coarsening (figure 9.2a,c) as satisfactory proof to equal fluidized zones with axial segregation in cylinders and endow them with a height modulation. Height differences might be quite small as segregation is not as strong as in lower filled rotating cylinders or flat cells (figure 3.2).

Because the segregation bands shift by half a wave length after every  $180^\circ$  rotation, the height modulation must shift by the same value also. Exaggerated height variances along the upper fluidized zone are depicted in figure 9.2d. If mixed material enters the fluidized layer at zones enriched with small particles the beads drift axially along the slopes. During particle migration the smaller species is partially ‘sieved’ out and enters the central core again, whereas the larger species remains to a greater extend in the fluidized zone. The sieved small particles are transported away at positions where convection is directed from the fluidized zone toward the core. Therefore the fluidized zone is somewhat richer with smaller beads in the regions where the convection roll moves toward the fluidized layer. The ring-shaped segregation pattern in the convection roll is a consequence of this sieving. After  $360^\circ$  rotation the fluidized zone is replenished with small and large particles. Due to axial drift and subsequent sieving their concentration is decreased. This forms a cycle shown in figure 9.2f.

Finally, material conservation leads to convection. Particles flow in depressions that are accumulated by large particles (green arrows in figure 9.2d). Material is added at this position (labeled ‘+’) and after  $180^\circ$  rotation at the same position balanced by material removal by the second fluidized zone (red arrows and label ‘-’ in figure 9.2e). Inflow into a depression zone for one fluidized layer is conserved by the same amount of outflow along the slope after  $180^\circ$  in the other fluidized zone. The alternating height modulation between the two fluidized layers makes sure that defluent particles are replaced by other particles at the same axial position on the vertically opposite cell side. After  $360^\circ$  rotation there is a constant net flow with imprinted wave length defined by the height modulation.

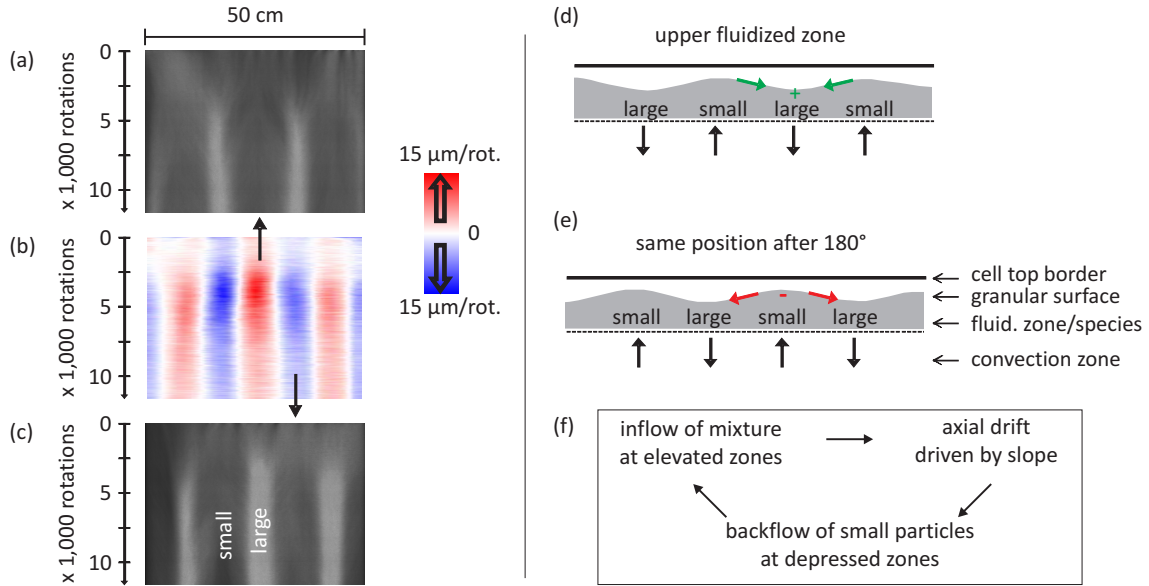


**Figure 9.2:** Model 1: Driving of convection by local height differences of the granular bed. (a-c) Three time-space plots for one experiment with cradle-like agitation ( $\pm 180^\circ$ ). (a) Time-space plot of the segregation in the upper fluidized layer, (b) vertical flow component in the horizontal midplane, (c) segregation in the lower fluidized layer. Dark/bright are enrichments of small/large particles in the fluidized edges (contrast enhanced). Small and large particle segregation at the top and bottom edges oppose each other. Flow is directed towards small particle enrichments (arrows). The experiment is identical with figure 4.2d but now the other cell side is seen. (d) Sketch of the fluidized region (shaded). Only the upper surface of the granulate is shown. The modulation of the height profile related to partial segregation and convection is greatly exaggerated here. (e) Same cell position after a half cell rotation. The modulation shifts by half a pattern wave length. Arrows indicate assumed slope driven flow and labels '+'/'-' show positions where particle material is added/removed. (f) Suggested feedback cycle for small particles that drives convection (see text).

### 9.3 Model 2: density differences

Figure 9.3 sketches the basic dynamic processes that are considered in the second model. The material moves exclusively during a short slide phase in each half turn of the cell. The essential motion is normal to the rotation axis, in the cell plane (vertical arrows in figure 9.3a,b). This sliding motion is modulated along the horizontal axis, as indicated in the figure schematically by the difference of the arrow lengths. After two opposite slides during a full turn of the cell, only a small residual net displacement of the beads in the center of the container remains, cf. figure 9.3c.

A vortex with clockwise sense of the local convection as shown in figure 9.3c is considered and it is presumed that the packing is more loose in the bottom right corner (3) than in the bottom left corner (4). Figure 9.3a sketches the situation immediately before the critical angle for sliding is reached. As a consequence, the grains slide down more efficiently on the right (edge 2-3). In the fluidized top zone of the granulate, a sideward flux from (1) towards (2) balances this difference by transporting beads towards the right hand side, diluting the corner (1). Very small density modulations are sufficient to explain the experimental observations. During the next half turn, edge (1-2) becomes the bottom edge and the material slides back as indicated in figure 9.3b. Since corner (1) is packed less densely than corner (2), grains slide down earlier and faster on the left hand side (edge 1-4). Corners (1) and (3) change their roles. This is balanced by a horizontal transport from (3) to (4) in

the upper fluidized zone. This mechanism maintains the packing density modulation. The observed convection (figure 9.3c) results from the small net difference between two large displacements, i.e. the slide from (1) to (4) in one half cycle (a) and the slide from (4) to (1) in the second half cycle (b).

In order to get a realistic impression of these processes and the orders of magnitude of the involved parameters, one has to recollect that during each half turn the beads shift by roughly the height of the free volume above the granulate. This height ranges from a few hundred micrometers at high  $C$  to a few millimeters near the critical  $C_C$ . The average convection velocity, i.e. the difference between the downward flows shown in figure 9.3a,b, is of the order of  $10\text{-}50\ \mu\text{m}$  per cell rotation, i.e. two orders of magnitude smaller. In order to achieve such a net difference between the two slides, the packing densities of opposite corners (e.g. (1) and (2)) need to differ by about one percent. The net axial transport in the fluidized zones is two orders of magnitude smaller than the downward slide. It is also much slower than the dynamics of individual beads in the fluidized zones (see section 9.1).

As the experiments show, the material in the central zone of the cell is characterized by slow collective dynamics. Thus it is reasonable to assume that the relevant packing density modulations are those in the fluidized edges. If these ideas are correct, then there is some indication that the local composition of the mixture and local packing densities are interrelated: In the regions where the rolls transport grains into the fluidized zone (the region with lower packing density), accumulation of smaller beads is observed, whereas in the regions where the rolls transport material out of the fluidized zone (higher packing fraction), this zone contains a more balanced mixture of grains (cf. section 9.1).

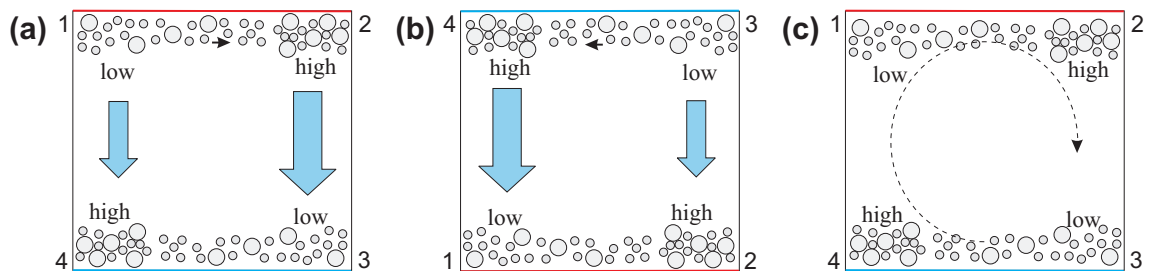


**Figure 9.3:** Model 2: Driving of convection by local packing density differences. (a,b) Downsiding of grains in the cell in two half-cycles of the container rotation, and (c) the net convection as the effective particle motion averaged over a complete cell rotation cycle. Local packing density inhomogeneities in the fluidized zones are sketched. For clarity, the inhomogeneities are unrealistically exaggerated.

**Synopsis** The models explain a number of features of the observed convection pattern, like the independence of convection of the cell rotation sense. They are also in accordance with the observation that a modification of the cell edge geometry (section 5.4) imposes a defined flow pattern: below ledges, the granular surface is slightly depressed, and a small net drift in the fluidized zone transports material there (model 1), increasing the packing density marginally (model 2). Model 1 also explains why convection only for almost full containers takes place. Only then localized rotating fluidized zone are possible. If the fill height is lower then there is sufficient space to form a global roll during particle sliding. The observations that the same patterns are observed in vacuum, in air and under water are compatible with the proposed mechanism as well. Also, the robustness of the convection rolls with respect to the composition of the granulate is explainable.

## 9 Convection mechanisms

Small initial packing density or inhomogeneous distribution of small and large species will always be present in a broad wavelength range. From this spectrum, the wavelength of the convection pattern is selected in a similar way as in hydrodynamic systems where the container geometry plays the dominant role. Too broad convection rolls are damped because the lateral transport efficiency is too large, and for short wavelengths, the gradient in vertical transport is too large. Thus, the most efficient coupling of flow and packing structures is found for rolls of nearly circular geometry.

The question is how the proposed models could be tested. Since height and packing differences are probably very small, their confirmation requires highest precision measurements. Concerning packing fractions the differences inside the fluidized zone were too small to be detected with transmission X-ray images (figure 3.5, so a direct test could not be achieved.

# 10 Conclusions

## 10.1 Roadmap to the future

Of course, after such a long series of experimental work there are more open questions than at the beginning. Usefulness of tests becomes clear only afterwards. There are already some prepared experiments that could not be finished during the doctoral thesis. These and other open questions are outlined in the following roadmap.

**General experimental setup** First at all, one should perform multiple experiments simultaneously to reduce experimental time. That was done only for single rolls (chapter 6). Construction effort increases for larger containers at higher aspect ratio that contain multiple experiments. Independent experiments in several boxes must be synchronized if a single camera is used. On the other side, it came to light in the thesis that large containers of width 50 cm are not obligatory as many effects were also observed in smaller geometries. Concerning the wall material of the rotating box, other materials with different frictional properties should be tested. So far all cell walls consisted of acrylic glass. ITO or TCO coatings can be used to avoid electrostatic charging. Experiments under water (section 4.3) have shown that electrostatic effects are not the primary cause for convection, however they might play a role in effects that are beyond convection. It would be desirable if the humidity can be controlled in the laboratory because at some days did not permit experiments due to low humidity. Systematic tests with different bead densities or different relative quantities of small and large species are so far not made. Coated beads should be avoided as they abrade. Better are spheres that are colored in the bulk during the glass melting process. It would be also interesting to know how a slight cell thickness modulation along the rotation axis modifies the patterns.

**Fluidization** How the particles flow at all? Which species rolls earlier and faster? This can be answered by continuation of experiments with a co-moving camera (figure 2.5e). Also one might limit the rotation angle in the cradle-like rotation scheme (section 4.2) in order to reduce fluidization. So far angles not smaller than  $\pm 90^\circ$  were tested. What is the minimum amount of chute flow that is necessary for the emergence of convection? One can also imagine a situation where the vertical standing cell is quickly flipped by  $180^\circ$ . Then chute flow is absent and particles will just fall down in alternating vertical directions. Are there any relations between a rotating box that is filled with a granular mixture and a box that is filled with a density matched non-miscible binary liquid?

**Three-dimensional insights** Adequacy of a computer tomography study was already positively confirmed (see figure 2.5(b-d)). Now real measurements must follow. After virtual reconstruction of the packing, local densities are accessible. ‘Positron Emission Particle Tracking’ (PEPT) that is only available in Birmingham, UK would be a method to measure three-dimensional tracer coordinates for maximum 90 minutes. For thicker cells and cylinders (sections 5.5 and 5.6) index matching would be a method to get deeper insights. By using bead species of different optical indices one can match the liquid to one species and then better observe the inner structure [178]. The flow - if there is any - should be observable by this technique.

**Single rolls** How can spontaneous segregation and flow modulations be avoided in cells with aspect ratio near one (chapter 6)? Is the periodicity of the circulating segregation a suitable measure, for example to determine the degree of segregation?

**Traveling waves** Explanation of traveling band periodicity (chapter 7) is a difficult task. One might probe the system externally by modulations of the rotation rate. Does this imprint a periodicity on the stripe motion? Can box tilting enforce a wave direction? Another question concerns the motion of individual particles. Is there a constant axial drift or erratic bead exchange?

**Two-dimensional systems** In these ongoing experiments (chapter 8) in principle phenomenological similar pattern formation was observed. One might now reason that three-dimensional systems can be reduced to two-dimensional containers. However as long as there is no suitable theory this cannot be concluded. This type of experiment permits easier experimental access and theoretical modeling.

**Simulation** So far no simulation or numerical study exists for the flat rotating container. There are some trials at the ‘Institute for Multiscale Simulation’, University Erlangen-Nürnberg (group of Thorsten Pöschel) and at the ‘Institute of Energy Technology’, ETH Zurich (group of Christoph Müller) but to date presentable results are missing. Two-dimensional systems which were so far not popularized in the community should be easy to simulate at low computational costs.

### *Last but not least*

**Speculation** Convection was found under quite different circumstances: in boxes filled with glass beads and with undefinable food particles, in monolayers and multilayers, in rotated or rocked cells and with different chuting scenarios. One might now conclude that a combination of fortune or impure circumstances have led to similar observations. Such a high degree of coincidence has a low probability. It is also conceivable that all structures are governed by an inherent basic principle. In the following, reduction of the complexity and extraction of the essential characteristics have been attempted. Figure 10.1 shows a configuration that is reduced concerning agitation and physical effects. Two connected mobile walls confine the packing to an area slightly larger than its occupied disc area. They shift the bidisperse discs on a horizontal surface periodically back and forth. Wall motion is slow in order to reduce inertial effects and momentum transfer between particles. Then physical laws are suppressed in favor of geometrical restrictions. Rearranging of particles to overcome jamming is the only fluidization. Of course, instead of horizontal agitation, the discs can also be fluidized by cradle-like or rotational motion. Then already tested experiments would be approached. It is speculated that in these cases always multiple convection rolls emerge.

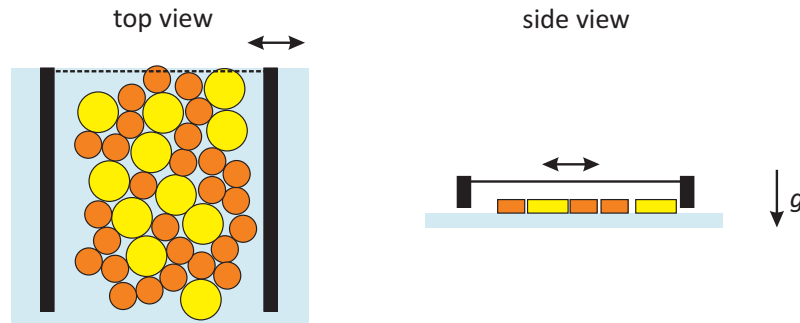


**Figure 10.1:** Suggestion of an experiment that might produce convection rolls under pure geometrical conditions. The side walls (black) shift periodically the bidisperse disc packing (orange/yellow) in a back and forth motion on a plane surface (blue). The agitation process is slow and there are no inertial forces. Only a detail of the experiment is shown. More particles are needed than shown.

## 10.2 Summary

Granular materials are ubiquitous in industry and daily life. Their handling is not easy as they tend to segregate under external energy input. However, optimal mixing plays an important role, e.g. in the processing of food and particulate chemicals.

The continuously rotated horizontal drum filled with different kinds of particles serves as one of the standard systems in granular matter physics to study segregation. Since the pioneering work of Ôyama in 1939, a variety of studies have dealt with the formation of axially segregated bands in long mixers.

In the thesis it was demonstrated that convective flow can be found in almost completely filled rotated thin cells under various parameter conditions. This type of pattern formation was so far overseen by previous studies and might be relevant for situations where fluidization is restricted (e.g. in subsurface processes). Its mechanism is still not completely resolved, but it is obvious that a different explanation than for vibrated granular mixtures has to be found.

Some features of the convection structures have been clearly identified. They appear for a limited range of fill levels of the cell, but they are otherwise not very sensitive to the composition of the granular material as long as crystallization is avoided. The patterns form under atmospheric pressure in air, but they are also present under low pressure down to a few Pascal, and they are equally present when the complete experiment is submersed in water. The role of the initial preparation of the mixture for the formation of the convection rolls is not relevant. A uniformly mixed or a completely segregated initial preparation, led to qualitatively similar convection patterns.

There are several opportunities to manipulate the pattern wavelength and appearance. For example, a special structuring of one or both of the cell edges can be used to imprint a certain pattern wave length. When the initial fill height of the cell is locally modulated, the convection pattern can be forced to start in predetermined regions of the cell.

Another interesting property of the rolls is that sporadic or continuous reversals of the rotation sense do not reverse the convective flows, but rather leave the convection structure unchanged. This means that the local flow structure of the convection pattern must be encoded in the particular arrangement of the grains in different parts of the cell, irrespective of the direction of cell rotation.

In cells with aspect ratio close to one, single rolls were found. Their dynamics are completely different from multi-roll arrays. An interaction of segregation and circulation leads to self-organized modulations of the flow velocity. Spontaneous reversals and cessations of the flow and oscillations of its amplitude are observed.

Traveling wave segregation can be observed in half-filled containers. Their dynamics show a pronounced spatio-temporally periodic drift of segregated patterns. In the course of long experiment durations, the system switches between different oscillatory states that are stable over many periods. The observed periodicity in the dynamics resists so far any theoretical explanation.

Besides in three-dimensional studies also in two-dimensional monolayers segregation and convection scenarios were found. Because of the easier experimental access at comparable pattern complexity a two-dimensional system seems to be a favorable candidate for future studies.

Two mechanisms were suggested for the convection. They assume that either small height differences or packing density fluctuations couple to the global vortex flow. However the models could not be tested from the available data.

Summarizing, even though the behavior of beads in a rotating flat cell was characterized in different aspects, many details are not yet fully understood. The role of the fluidized zones and the partial segregation of mixtures during the convection process should be studied in more detail. Elaborated tomography and tracking studies should be performed to achieve information on single particle level.

### 10.3 Deutsche Zusammenfassung

Konvektion und Entmischung von Kügelchen in einem flachen rotierenden Behälter

Körnige Materialien sind allgegenwärtig in der Industrie und im täglichen Leben. Deren Handhabung ist nicht einfach, da sie unter externer Energiezufuhr zur Entmischung neigen. Eine optimale Durchmischung spielt jedoch eine wichtige Rolle, z.B. bei der Verarbeitung von Lebensmitteln und partikelförmigen Chemikalien.

Die kontinuierlich gedrehte horizontale Trommel, die mit verschiedenen Arten von Partikeln gefüllt ist, dient als eines der Standard-Systeme um die Segregation granularer Materie zu studieren. Seit den wegweisenden Arbeiten von Ôyama im Jahre 1939, hat eine Vielzahl von Studien die Bildung von axial getrennten Bändern in langen Trommeln behandelt.

In der Dissertation wurde gezeigt, dass unter verschiedenen Bedingungen konvektive Strömungen in fast vollständig gefüllten rotierenden dünnen Behältern gefunden werden können. Diese Art von Musterbildung wurde bisher bei früheren Studien übersehen und könnte relevant sein für Situationen, in denen die Partikelbewegung beschränkt ist (z.B. bei unterirdischen Prozessen). Der Mechanismus ist noch nicht vollständig geklärt, aber es ist offensichtlich, dass eine andere Erklärung als für vibrierte granulare Mischungen gefunden werden muss.

Einige Merkmale der Konvektionsstrukturen wurden eindeutig identifiziert. Sie treten in einem begrenzten Füllstandsbereich der Zelle auf, aber sie sind anderweitig nicht sehr empfindlich gegenüber der Zusammensetzung des Granulats, solange Kristallisation vermieden wird. Die Muster bilden sich unter atmosphärischem Luftdruck, aber auch bei niedrigem Druck von wenigen Pascal. Sie sind ebenso präsent, wenn das gesamte Experiment unter Wasser durchgeführt wird. Der anfängliche Zustand der Granulatmischung ist für

die Bildung der Konvektionswalzen nicht relevant. Gleichmäßig gemischte oder vollständig segregierte Ausgangszustände führen zu qualitativ ähnlichen Konvektionsmustern.

Es gibt mehrere Möglichkeiten, um die Wellenlänge des Musters und deren Aussehen zu manipulieren. Zum Beispiel kann eine spezielle Höhenstrukturierung für eine oder beide Zellränder verwendet werden, um eine bestimmte Wellenlänge des Musters zu erreichen. Wenn die anfängliche Höhe des Granulats lokal moduliert ist, kann erzwungen werden, dass die Konvektion in bestimmten Regionen der Zelle startet.

Eine weitere interessante Eigenschaft der Rollen ist, dass sporadische oder kontinuierliche Drehrichtungsumkehrungen des Behälters, die konvektiven Strömungen nicht umkehren, sondern die Konvektionsstruktur unverändert lassen. Dies bedeutet, dass unabhängig von der Drehrichtung der Zelle, die lokale Strömung des Konvektionsmusters in gewissen Modifikationen der Packungsstruktur entlang der Zelle kodiert sein muss.

In Zellen mit Seitenverhältnis nahe eins, wurden Einzelrollen gefunden. Deren Dynamik ist ganz anders als bei Multirollen. Das Zusammenspiel aus Segregation und Zirkulation der Kügelchen führt zu selbstorganisierten Modulationen der Strömungsgeschwindigkeit. Spontane Umkehrungen und Unterbrechungen des Flusses sowie Schwingungen der Strömungsamplitude wurden beobachtet.

Segregierende Wanderwellen können in halb gefüllten Behältern beobachtet werden. Die segregierten Bänder zeigen eine deutliche periodische raum-zeitliche Dynamik. Im Laufe der langen Laufzeit des Experiments, schaltet das System zwischen verschiedenen oszillatorischen Zuständen, die über viele Perioden stabil sind. Die beobachtete Periodizität in der Dynamik widersteht bislang jeder theoretischen Erklärung.

Neben dreidimensionalen Untersuchungen wurden auch in zweidimensionalen Monolagen Segregation und Konvektions-Szenarien gefunden. Wegen des leichteren experimentellen Zugangs bei vergleichbarer Komplexität der Muster bietet sich ein zweidimensionales System als Kandidat für zukünftige Studien an.

Zwei Mechanismen wurden für die Konvektion vorgeschlagen. Sie gehen davon aus, dass entweder kleine Höhenunterschiede oder Schwankungen in der Packungsdichte mit der globalen Strömung koppeln. Allerdings konnten die Modelle nicht mit den verfügbaren Daten getestet werden.

Zusammenfassend gesagt, wurde das Verhalten von Kügelchen in einer rotierenden flachen Zelle unter verschiedenen Aspekten charakterisiert. Viele Details sind noch nicht vollständig verstanden. Die Rolle der fluidisierten Zonen und die teilweise Trennung der Mischung bei der Konvektion sollte näher untersucht werden. Ausgeklügelte Tomographie- und Tracking-Messungen sollten durchgeführt werden, um Informationen über Einzelteilchen zu erhalten.



# Appendices



# A Public outreach

## A.1 Rotating box

### Publications

- Frank Rietz, Ralf Stannarius: On the brink of jamming: Granular convection in densely filled containers, *Physical Review Letters* 100, 078002 (2008).<sup>1</sup>
- Frank Rietz, Ralf Stannarius: Convection and segregation in a flat rotating sandbox, *New Journal of Physics* 14, 015001 (2012).
- Frank Rietz, Ralf Stannarius: Oscillations, cessations and circulation reversals of granular convection in a densely filled rotating container, *Physical Review Letters* 108, 118001 (2012).
- Frank Rietz, Ralf Stannarius: Transitions between multiple attractors in a granular experiment, *Physical Review E* 85, 040302(R) (2012).

### Talks

- Harzseminar, Strukturbildung in Chemie und Biologie, Hahnenklee, February 12, 2007
- DPG Spring Meeting, Regensburg, March 30, 2007
- 396<sup>th</sup> Wilhelm and Else Heraeus Seminar, Nonlinear Dynamics, University Bayreuth, October 10, 2007
- Center for Nonlinear Dynamics, University of Texas at Austin, February 6, 2008
- DPG Spring Meeting, Berlin, February 28, 2008 (presented by Ralf Stannarius)
- IMA Conference on Dense Granular Flows, Cambridge, January 9, 2009  
videotaping: <http://sms.cam.ac.uk/media/526872>
- Max-Planck-Institute for Dynamics and Self-Organization, Goettingen, March 6, 2009
- DPG Spring Meeting, Dresden, March 27, 2009
- Powders & Grains, Golden, CO, July 17, 2009
- European Dynamics Days, Bristol, September 6, 2010
- Dept. of Computational Physics for Engineering Materials, ETH Zurich, November 17, 2010
- DPG Spring Meeting, Dresden, March 14, 2011 (presented by Ralf Stannarius)
- DPG Spring Meeting, Dresden, March 16, 2011
- Institute for Multiscale Simulation, University Erlangen-Nürnberg, March 7, 2012
- International Workshop on Packing Problems, School of Physics, Trinity College Dublin, September 3, 2012

---

<sup>1</sup>also published with minor changes in: Frank Rietz, Ralf Stannarius: A new experiment with convection rolls in granular media, in: M. Nakagawa, S. Luding (Ed.): *Powders and Grains 2009*, AIP Conference Proceedings 1145, 741 (2009).

### Poster

- Gordon Research Conference, Granular & Granular-Fluid Flow, Waterville, ME, June 22-27, 2008
- Statistical mechanics of static granular media, Lorentz-Center, Leiden, July 6-10, 2008
- Dynamics Days Europe, Goettingen, August 31-September 4, 2008
- DPG Spring Meeting, Dresden, March 24, 2009
- APS March Meeting, Boston, February 27, 2012 (presented by Ralf Stannarius)
- DPG Spring Meeting, Berlin, March 28, 2012

### Movie

- DFD Meeting, Gallery of Fluid Motion, Minneapolis, MN, November 22-24, 2009  
Accessible via: Arxiv: <http://arxiv.org/abs/0910.4897>; Cornell University: <http://ecommons.cornell.edu/handle/1813/14105>;  
Youtube: <http://www.youtube.com/watch?v=4nnEGEjGWik>; New Journal of Physics: <http://dx.doi.org/10.1088/1367-2630/14/1/015001>; or: <http://www.youtube.com/watch?v=gO2u1pPo70o>

### Stimulated projects

- Andy Hirsch: Kugelpackung und Antiferromagnetismus unter Frustration<sup>2</sup>, student project, Dept. of Nonlinear Phenomena, University Magdeburg, 2010/11
- Prashant Vipul: Convective rolls in granular materials, student project, Indian Institute of Technology New Delhi, Advisor: Balaji Srinivasan, 2010/11
- Robert Prusas: 2D Granulate – Scheiben in einer flachen drehenden Zelle<sup>3</sup>, student project, Dept. of Nonlinear Phenomena, University Magdeburg, since 2011, ongoing

### Discussions in scientific media

- Stirred, not shaken: Research Highlight, Nature 452, 4 (2008).
- M. Buchanan: Drum roll, Nature Physics 7, 741 (2011).
- G. Seiden, P. J. Thomas: Complexity, segregation, and pattern formation in rotating-drum flows, Reviews of Modern Physics 83, 1323 (2011).

### Reception in popular media

- WIRED MAGAZINE: Baffling patterns form in scientific sandbox  
<http://www.wired.com/wiredscience/2009/10/bead-cloud-mystery>
- ORF SCIENCE: Kugelhaufen mit Eigenleben<sup>4</sup>  
<http://science.orf.at/stories/1631256>
- GEOLOGY BLOG: Ten things we don't know about sand: Number 2  
[http://throughthesandglass.typepad.com/through\\_the\\_sandglass/2009/11/ten-things-we-dont-know-about-sand-number-2.html](http://throughthesandglass.typepad.com/through_the_sandglass/2009/11/ten-things-we-dont-know-about-sand-number-2.html)
- SOFTPEDIA NEWS: Beads behave unexpectedly in boxes  
<http://news.softpedia.com/news/Beads-Behave-Unexpectedly-in-Boxes-125599.shtml>

---

<sup>2</sup>translation: Sphere packing and antiferromagnetism under frustration

<sup>3</sup>translation: 2D granulates – Experiments in a flat rotating cell

<sup>4</sup>translation: Pebble bed with own life

- **TECHNOLOGY REVIEW: The unexpected behaviour of beads in a box**  
<http://www.technologyreview.com/blog/arxiv/24319>
- **THE UNIVERSITY OF WAIKATO: Beyond cornflakes**  
<http://sci.waikato.ac.nz/physicsstop/2009/11/beyond-cornflakes.shtml>
- **ENTANGLED STATES (RELIGIOUS NEWS): The puzzle of the beads in a box**  
<http://entangledstates.org/2009/10/28/the-puzzle-of-the-beads-in-a-box>
- **RUSSIAN NEWS: Ученые сняли фильм о зернах в коробке<sup>5</sup>**  
<http://lenta.ru/news/2009/10/29/beads>
- **WIKIPEDIA: Granular convection**  
[http://en.wikipedia.org/wiki/Granular\\_convection](http://en.wikipedia.org/wiki/Granular_convection)

## A.2 Sphere packings

Whereas the thesis is related to pattern formation and flow in granular media the following contributions are not directly related to them. However they also concern problems in granular media focusing three-dimensional packing issues of spheres known under the term ‘Random Close Packing’. Research started at the Center for Nonlinear Dynamics, Austin, TX and is continuing at the Max-Planck-Institute for Dynamics and Self-Organization, Goettingen, Germany. Advisor is Matthias Schröter. The results are worth another thesis and will be published in the near future. So far one related methodical paper was published.

### Paper

- Joshua A. Dijksman, Frank Rietz, Kinga A. Lőrincz, Martin van Hecke, and Wolfgang Losert: Refractive index matched scanning of dense granular materials, *Review of Scientific Instruments* 83, 011301 (2012).

### Talks

- APS Fluid Meeting, Minneapolis, November 22, 2009
- DPG Spring Meeting, Regensburg, March 23, 2010
- Pardim10, MPIPES, Dresden, June 2, 2010
- Dept. of Computational Physics for Engineering Materials, ETH Zurich, November 17, 2010

### Poster

- Dynamics Days Goettingen, September 2008
- Gordon Conference, Waterville, Maine, USA, June 20-25, 2010
- DPG Spring Meeting, Dresden, March 17, 2011

### Further attended workshops

- Workshop on Sphere Packing and Amorphous Materials, ICTP Trieste, July 25-29, 2011
- Workshop on Collective Dynamics and Pattern Formation in Active Matter Systems, MPIPES Dresden, September 12-16, 2011

---

<sup>5</sup>translation: Scientists made a movie about granulate in a box



# B Acknowledgement

x-ray measurements:	Jürgen Goldschmidt, Andreas Hilbig, InnoProfile project NaWiTec, Max Neudecker
bead size measurements:	Sabine Schlüsselburg
friction measurements:	Sonia Uterman
shear cell measurements:	Peter Müller, Sebastian Kleinschmidt
setup and and many suggestions:	Thomas John
density measurements:	Bernd Ebenau
help with literature:	Hendrik Hohmann
help with C <sup>++</sup> :	Ulf Schaper
help with video processing:	Stefan Scharfenberg
help with experiments:	David Fischer
coloring of beads:	Ralf-Peter Hitzschke (Sigmund-Lindner GmbH)
vacuum equipment:	Wolfram Knapp, Uwe Richter (Ferrotec GmbH)
setup:	Christian Warnke, Nico Fricke
reading manuscripts:	Jesse Gryn, Gabriel Seiden, James Third Tanja Ostapenko, Christoph Gögelein Say Hwa Tan, Matthias Schröter
construction of cells and related parts:	Jürgen Weissenborn and his team
hints and help:	Tamas Börzsönyi, Dirk Pietschmann, Torsten Trittel
experiments with discs:	Robert Prusas
without category:	Tilo Finger
rescue of a hard disc:	Jörg Schulenburg
administrative support:	Ines-Ute Grodrian, Birgit Leßner, Annette Lidzba
boss:	Ralf Stannarius

## *B Acknowledgement*

# Bibliography

- [1] A. Awazu: Size segregation and convection of granular mixtures almost completely packed in a thin rotating box, *Phys. Rev. Lett.* 84, 4585 (2000).
- [2] T. M. Knowlton, J. W. Carson, G. E. Klinzing, W.-C. Yang: The importance of storage, transfer, and collection, *Chemical Engineering Progress* 90, 44 (1994).
- [3] M. Gerlach: Die Altenburger Tracht ist die schönste, *Thüringer Allgemeine*, May 16 (2001).
- [4] M. Budhu, R. Gobin: Instability of sandbars in grand canyon, *Journal of Hydraulic Engineering* 120, 919 (1994).
- [5] I. Livingstone, G. F. S. Wiggs, C. M. Weaver: Geomorphology of desert sand dunes: a review of recent progress, *Earth Science Reviews* 80, 239 (2007).
- [6] B. J. Ennis, J. Green, R. Davies: The legacy of neglect in the U.S., *Chemical Engineering Progress* 32, April (1994).
- [7] J. K. Prescott, J. W. Carson: Analyzing and overcoming industrial blending and segregation problems, A. D. Rosato, D. L. Blackmore (eds.): *IUTAM symposium on segregation in granular flows: proceedings of the IUTAM symposium held in Cape May, NJ, U.S.A.*, 89 (2000).
- [8] F. J. Muzzio, T. Shinbrot, B. J. Glasser: Powder technology in the pharmaceutical industry: the need to catch up fast, *Powder Technology* 124, 1 (2002).
- [9] Jenike & Johanson, Inc.: <http://jenike.com/Solutions/segblend.html>
- [10] G. Zinkl: Entmischungsprobleme in Griff, *Chemie Technik* No.3, 44 (2001).
- [11] G. S. Riley: An examination of the separation of differently shaped particles, *Powder Technology* 2, 315 (1968/69).
- [12] D. Reguera, A. Luque, P. S. Burada, G. Schmid, J. M. Rubí, P. Hänggi: Entropic splitter for particle separation, *Physical Review Letter* 108, 020604 (2012).
- [13] Powder research to promote competitive manufacture of added-value food ingredients. Strategic document for research in food powders. Project implemented with the support of the European Commission 5th Framework Programme (2003).
- [14] E. Tijskens, E. Dintwa, J. Loodts, P. van Liedekerke, M. van Zeebroeck, P. Verboven, H. Ramon: Granular matter applications in agriculture, R. García-Rojo, H.J. Herrmann, S. McNamara (eds.): *Powders and Grains 2005*, 1167 (2005).
- [15] D. Berzi, J. T. Jenkins, M. Larcher: Debris flows: recent advances in experiments and modeling, *Advances in Geophysics* 52, Chapter 2, 103 (2010).
- [16] T. Shinbrot, N.-H. Duong, L. Kwan, M. M. Alvarez: Dry granular flows can generate surface features resembling those seen in Martian gullies, *PNAS* 101, 8542 (2004).
- [17] C. H. Rycroft, G. S. Grest, J. W. Landry, M. Z. Bazant: Analysis of granular flow in a pebble-bed nuclear reactor, *Physical Review E* 74, 021306 (2006).
- [18] P. W. Cleary, G. Metcalfe, K. Liffman: How well do discrete element granular flow models capture the essentials of mixing processes, *Applied Mathematical Modelling* 22, 995 (1998).
- [19] C. Seife: Can the laws of physics be unified?, *Science* 309, 5731, 82, (2005).
- [20] O. Pouliquen: Velocity correlations in dense granular flows, *Physical Review Letters* 93, 248001 (2004).
- [21] GDR MiDi: On dense granular flows, *European Physical Journal E* 14, 341 (2004).
- [22] P. Richard, M. Nicodemi, R. Delannay, P. Ribière, D. Bideau: Slow relaxation and compaction of granular systems, *Nature Materials* 4, 121 (2005).
- [23] V. Trappe, V. Prasad, L. Cipelletti, P. N. Segre, D. A. Weitz: Jamming phase diagram for attractive particles, *Nature* 411, 772 (2001).
- [24] A. J. Liu, S. R. Nagel: Jamming is not just cool any more, *Nature* 396, 21 (1998).
- [25] G. D'Anna, G. Gremaud: The jamming route to the glass state in weakly perturbed granular media, *Nature* 413, 407 (2001).

## Bibliography

- [26] J. M. Ottino: Granular matter as a window into collective systems far from equilibrium, complexity, and scientific prematurity, *Chemical Engineering Science* 61, 4165 (2006).
- [27] I. Aranson, L. Tsimring: Patterns and collective behavior in granular media: theoretical concepts; in: *Review of Modern Physics* 78, 641 (2006).
- [28] I. Aranson, L. Tsimring: *Granular patterns*, Oxford University Press (2009).
- [29] J. Kakalios: Granular physics or nonlinear dynamics in a sandbox, *American Journal of Physics* 73, 8 (2005).
- [30] G. H. Ristow: *Pattern formation in granular materials*, Springer, Berlin (2000).
- [31] H. M. Jaeger, S. Nagel: Granular solids, liquids, and gases, *Review of Modern Physics* 68, 1259 (1996).
- [32] J. Duran: *Sands, powders, and grains: an introduction to the physics of granular materials*, Springer, New York (2000).
- [33] P. Ball: *Nature's patterns: flow*, Oxford University Press (2009).
- [34] G. Seiden, P. J. Thomas: Complexity, segregation, and pattern formation in rotating-drum flows, *Reviews of Modern Physics* 83, 1323 (2011).
- [35] H. A. Makse, S. Havlin, P. R. King, H. E. Stanley: Spontaneous stratification in granular mixtures, *Nature* 386, 379 (1997).
- [36] H. A. Makse, S. Havlin, P. C. Ivanov, P. R. King, S. Prakash, H. E. Stanley: Pattern formation in sedimentary rocks: connectivity, permeability, and spatial correlations, *Physica A* 233, 587 (1996).
- [37] S. Morris, E. Bodenschatz, D. S. Cannell, G. Ahlers: Spiral defect chaos in large aspect ratio Rayleigh-Bénard convection, *Physical Review Letters* 71, 2026 (1993).
- [38] M. C. Cross, P. C. Hohenberg: Pattern formation outside of equilibrium, *Review of Modern Physics* 65, 851 (1993).
- [39] P. Manneville: Rayleigh-Bénard convection, thirty years of experimental, theoretical and modeling work, I. Mutabazi, J. E. Wesfreid, E. Guyon (eds.): *Dynamics of spatio-temporal cellular structures, Henri Bénard centenary review*, Springer, 41 (2005).
- [40] G. W. Simon, N. O. Weiss: Convective structures in the sun, *Monthly Notices of the Royal Astronomical Society* 252, Sept. 1, 1P (1991).
- [41] A. Kudrolli: Size separation in vibrated granular matter, *Reports on Progress in Physics* 67, 209 (2004).
- [42] N. Mohabuth, N. Miles: The recovery of recyclable materials from Waste Electrical and Electronic Equipment (WEEE) by using vertical vibration separation, *Resources, Conservation and Recycling* 45, 60 (2005).
- [43] V. Folli, A. Puglisi, L. Leuzzi, C. Conti: Shaken granular lasers, *Physical Review Letters* 108, 248002 (2012).
- [44] J. R. de Bruyn, B. C. Lewis, M. D. Shattuck, H. L. Swinney: Spiral patterns in oscillated granular layers, *Physical Review E* 63, 041305 (2001).
- [45] K. M. Aoki, T. Akiyama, Y. Maki, T. Watanabe: Convective roll patterns in vertically vibrated beds of granules, *Physical Review E* 54, 874 (1996).
- [46] T. S. Komatsu, S. Inagaki, N. Nakagawa, S. Nasuno: Creep motion in a granular pile exhibiting steady surface flow, *Physical Review Letters* 86, 1757 (2001).
- [47] W. B. Krantz, K. J. Gleason, N. Caine: Patterned ground, *Scientific American*, Dec., 44 (1988).
- [48] M. A. Kessler, A. B. Murray, B. T. Werner: A model for sorted circles as self-organized patterns, *Journal of Geophysical Research* 106, 13287 (2001).
- [49] P. Cuéllar, S. Georgi, M. Baeßler, W. Rucker: On the quasi-static granular convective flow and sand densification around pile foundations under cyclic lateral loading, *Granular Matter* 14, 11 (2012).
- [50] T. Dewers, P. Ortoleva: The role of geochemical self-organization in the migration and trapping of hydrocarbons, *Applied Geochemistry* 3, 287 (1988).
- [51] P. J. Ortoleva: *Geochemical self-organization*, Oxford University Press, chapter 14 (1994).
- [52] H. Ramberg: Instability of layered systems in the field of gravity. II, *Physics of the Earth and Planetary Interiors* 1, 448 (1968).
- [53] P. Heinemann: Das größte Giftgrab der Welt, *Die Welt*, July 24 (2007).

- [54] J. M. Ottino, D. V. Khakhar: Mixing and segregation of granular materials, *Annual Review of Fluid Mechanics* 32, 55 (2000).
- [55] Y. Ôyama: Studies on mixing of solids. Mixing of binary system of two sizes by ball mill motion, 179th Report Ôkôchi Research Laboratory, Institute of Physical Chemical Research 37, No.951, 17, (translated from Japanese), (1939).
- [56] W. L. Vargas, S. K. Hajra, D. Shi, J. J. McCarthy: Suppressing the segregation of granular mixtures in rotating tumblers, *AIChE Journal* 54, 3124 (2008).
- [57] S. K. Hajra, T. Bhattacharya, J. J. McCarthy: Improvement of granular mixing of dissimilar materials in rotating cylinders, *Powder Technology* 198, 175 (2010).
- [58] A. J. Marsh, D. M. Stuart, D. A. Mitchell, T. Howes: Characterizing mixing in a rotating drum bioreactor for solid-state fermentation, *Biotechnology Letters* 22, 473 (2000).
- [59] M. A. I. Schutyser, F. J. Weber, W. J. Briels, R. M. Boom, A. Rinzema: Three-dimensional simulation of grain mixing in three different rotating drum designs for solid-state fermentation, *Biotechnology and Bioengineering* 79, No.3, 284 (2002).
- [60] T. Kohav, J. T. Richardson, D. Luss: Axial dispersion of solid particles in a continuous rotary kiln, *AIChE Journal* 41, 2465 (2004).
- [61] Metallurgy, *Encyclopedia Britannica*, 9th ed. (1902).
- [62] M. B. Donald, B. Roseman: Mechanisms in a horizontal drum mixer, *British Chemical Engineering* 7, 749 (1962).
- [63] K. M. Hill, J. Kakalios: Reversible axial segregation of binary mixtures of granular materials, *Physical Review E* 49, R3610 (1994).
- [64] K. M. Hill, J. Kakalios: Reversible axial segregation of rotating granular media, *Physical Review E* 52, 4393 (1995).
- [65] K. M. Hill, A. Caprihan, J. Kakalios: Bulk segregation in rotated granular material measured by Magnetic Resonance Imaging, *Physical Review Letters* 78, 50 (1997).
- [66] M. Schröter, K. E. Daniels: Granular segregation in dense systems: the role of statistical mechanics and entropy, arXiv:1206.4101v1 (2012).
- [67] L. Sanfratello, E. Fukushima: Experimental studies of density segregation in the 3D rotating cylinder and the absence of banding; *Granular Matter* 11, 73 (2009).
- [68] H. P. Kuo, Y. C. Hsiao, P. Y. Shih: A study of the axial segregation in a rotating drum using deformable particles, *Powder Technology* 166, 161 (2006).
- [69] O. Zik, D. Levine, S. G. Lipson, S. Shtrikman, J. Stavans: Rotationally induced segregation of granular materials, *Physical Review Letters* 73, 644 (1994).
- [70] T. Elperin, A. Vikhansky: Mechanism of the onset of axial segregation in a rotating cylindrical drum filled with bidisperse granular mixtures, *Physical Review E* 60, 1946 (1999).
- [71] I. S. Aranson, L. S. Tsimring: Dynamics of axial separation in long rotating drums, *Physical Review Letters* 82, 4643 (1999).
- [72] I. S. Aranson, L. S. Tsimring, V. M. Vinokur: Continuum theory of axial segregation in a long rotating drum, *Physical Review E* 60, 1975 (1999).
- [73] P. Richard, N. Taberlet: Recent advances in DEM simulations of grains in a rotating drum, *Soft Matter* 4, 1345 (2008).
- [74] O. Pouliquen, R. Gutfraind: Stress fluctuations and shear zones in quasistatic granular chute flows, *Physical Review E* 53, 552 (1996).
- [75] T. Finger, A. Voigt, J. Stadler, H. G. Niessen, L. Naji, R. Stannarius: Coarsening of axial segregation patterns of slurries in a horizontally rotating drum, *Physical Review E* 74, 031312 (2006).
- [76] S. J. Fiedor, J. M. Ottino: Dynamics of axial segregation and coarsening of dry granular materials and slurries in circular and square tubes, *Physical Review Letters* 91, 244301 (2003).
- [77] Z. S. Khan, W. A. Tokaruk, S. W. Morris: Oscillatory granular segregation in a long drum mixer, *EPL* 66, 212 (2004).
- [78] S. Das Gupta, D. V. Khakhar, S. K. Bhatia: Axial segregation of particles in a horizontal rotating cylinder, *Chemical Engineering Science* 46, 1513 (1991).
- [79] M. Nakagawa: Axial segregation of granular flows in a horizontal rotating cylinder, *Chemical Engineering Science* 49, 2540 (1994).

## Bibliography

- [80] H. P. Kuo, P. Y. Shih, R. C. Hsu: Coupled axial-radial segregation in rotating drums with high fill levels, *AIChE Journal* 52, 2422 (2006).
- [81] S. Inagaki, K. Yoshikawa: Traveling wave of segregation in a highly filled rotating drum, *Physical Review Letters* 105, 118001 (2010).
- [82] K. Choo, T. G. A. Molteno, S. W. Morris: Traveling granular segregation patterns in a long drum mixer, *Physical Review Letters* 79, 2975 (1997).
- [83] K. Choo, M. W. Baker, T. C. A. Molteno, S. W. Morris: Dynamics of granular segregation patterns in a long drum mixer, *Physical Review E* 58, 6115 (1998).
- [84] K. M. Hill, N. Jain, J. M. Ottino: Modes of granular segregation in a noncircular rotating cylinder, *Physical Review E* 64, 011302 (2001).
- [85] W. Losert, M. Newey, N. Taberlet, P. Richard: Segregation transients in a tumbler flow, R. García-Rojo, H. J. Herrmann, S. McNamara (eds.): *Powders and Grains 2005*, 845 (2005).
- [86] L. Naji, R. Stannarius: Axial and radial segregation of granular mixtures in a rotating spherical container, *Physical Review E* 79, 031307 (2009).
- [87] P. Chen, B. J. Lochman, J. M. Ottino, R. M. Lueptow: Inversion of band patterns in spherical tumblers, *Physical Review Letters* 102, 148001 (2009).
- [88] T. Kawaguchi, K. Tsutsumi, Y. Tsuji: MRI measurement of granular motion in a rotating drum, *Particle & Particle Systems Characterization* 23, 266 (2006).
- [89] H. Yada, T. Kawaguchi, T. Tanaka: Relation between segregation patterns and granular flow modes in conical rotating drum, *Flow Measurement and Instrumentation* 21, 207 (2010).
- [90] A. W. Alexander, T. Shinbrot, F. J. Muzzio: Granular segregation in the double-cone blender: transitions and mechanisms, *Physics of Fluids* 13, 578 (2001).
- [91] S. Manickam, R. Shah, J. Tomei, T. L. Bergman, B. Chaudhuri: Investigating mixing in a multi-dimensional rotary mixer: experiments and simulations, *Powder Technology* 201, 83 (2010).
- [92] H. P. Kuo, P. C. Knight, D. J. Parker, J. P. K. Seville: Solids circulation and axial dispersion of cohesionless particles in a V-mixer, *Powder Technology* 152, 133 (2005).
- [93] E. Clément, J. Rajchenbach, J. Duran: Mixing of a granular material in a bidimensional rotating drum, *EPL* 30, 7 (1995).
- [94] S. K. Hajra, S. V. Khakhar: Radial segregation of ternary granular mixtures in rotating cylinders, *Granular Matter* 13, 475 (2011).
- [95] J. L. Turner, M. Nakagawa: Particle mixing in a nearly filled horizontal cylinder through phase inversion, *Powder Technology* 113, 119 (2000).
- [96] G. Metcalfe, T. Shinbrot, J. J. McCarthy, J. M. Ottino: Avalanche mixing of granular solids, *Nature* 374, 39 (1995).
- [97] J. J. McCarthy, T. Shinbrot, G. Metcalfe, J. E. Wolf, J. M. Ottino: Mixing of granular materials in slowly rotated containers, *AIChE Journal* 42, 3351 (1996).
- [98] S. E. Cisar, J. M. Ottino, R. M. Lueptow: Geometric effects of mixing in 2D granular tumblers using discrete models, *AIChE Journal* 53, 1151 (2007).
- [99] M. Nakagawa, A. Awazu, H. Nishimori: Axial migration of two species of particles in a horizontal cylinder, A. D. Rosato, D. L. Blackmore (eds.): *IUTAM symposium on segregation in granular flows: proceedings of the IUTAM symposium*, 163 (2000).
- [100] A. Awazu: Size segregation of granular mixtures almost completely packed in the rotating thin box, *AIP Conference Proceedings* 519, 769 (2000).
- [101] A. Awazu: Phase transition and structure formation in systems with finite number of particles with finite volume, doctoral thesis, Osaka Prefecture University (2001).
- [102] M. Nakagawa, J. L. Moss, S. A. Altobelli: Segregation of granular particles in a nearly packed rotating container: a new insight for axial segregation, H. J. Herrmann, J.-P. Hovi, S. Luding (eds.): *Physics of dry granular media*, 703, Kluwer Academic, Dordrecht (1998).
- [103] M. Nakagawa, J. L. Moss, S. A. Altobelli: MRI measurements and granular dynamics simulation of segregation of granular mixture, *Proceedings of the Fourth Microgravity Fluid Physics & Transport Phenomena*, August 12-14, Cleveland, Ohio, 258 (1998).
- [104] J. M. Knight: External boundaries and internal shear bands in granular convection, *Physical Review E* 55, 6016 (1997).

- [105] M. Schröter: Die Fingermorphologie in der Elektrodeposition, ein komplexes Grenzflächenphänomen, doctoral thesis, University at Magdeburg (2003).
- [106] BitFlow Software Development Kit: <http://www.bitflow.com/index.php/SDK>
- [107] C. Zeitnitz: WaveIO: a soundcard interface for Labview: <http://www.zeitnitz.de/Christian/waveio>
- [108] H. Ehlers, J. Heinämäki, J. Yliruusi: Particle size and packing characterization by diffusive light transmission, *Particuology* 10, 619 (2012).
- [109] M. Raffel, C. E. Willert, S. T. Wereley, J. Kompenhans: Particle Image Velocimetry. A practical guide, Springer (2007).
- [110] D. J. Cumberland, R. J. Crawford: The packing of particles, chapter 4, Elsevier Amsterdam (1987).
- [111] H. K. Pak, E. van Doorn, R. P. Behringer: Effects of ambient gases on granular materials under vertical vibration, *Physical Review Letters* 74, 4643 (1995).
- [112] R. P. Behringer E. van Doorn, R. R. Hartley, H. K. Pak: Making a rough place "plane": why heaping of vertically shaken sand must stop at low pressure, *Granular Matter* 4, 9 (2002).
- [113] Y. Nohguchi, H. Ozawa: On the vortex formation at the moving front of lightweight granular particles, *Physica D* 238, 20 (2009).
- [114] S. L. Conway, T. Shinbrot, B. J. Glasser: A Taylor vortex analogy in granular flows, *Nature* 431, 433 (2004).
- [115] R. Khosropour, J. Zirinsky, H. K. Pak, R. P. Behringer: Convection and size segregation in a Couette flow of granular material, *Physical Review E* 56, 4467 (1997).
- [116] O. Sano: Dilatancy, buckling, and undulations on a vertically vibrating granular layer, *Physical Review E* 72, 051302 (2005).
- [117] P. Evesque, J. Rajchenbach: Instability in a sand heap, *Physical Review Lett.* 62, 44 (1989).
- [118] G. Caballero, A. Lindner, G. Ovarlez, G. Reydellet, J. Lanuza, E. Clement: Experiments in randomly agitated granular assemblies close to the jamming transition, A. Coniglio, A. Fierro, H. J. Herrmann (eds.): Unifying concepts in granular media and glasses: from the statistical mechanics of granular media to the theory of jamming, 77 (2004).
- [119] P. Eshuis, D. van der Meer, M. Alam, H. J. van Gerner, Ko van der Weele, D. Lohse: Onset of convection in strongly shaken granular matter, *Physical Review Letters* 104, 038001 (2010).
- [120] M. Medved, D. Dawson, H. M. Jaeger, S. R. Nagel: Convection in horizontally vibrated granular material, *Chaos* 9, 691 (1999).
- [121] J.-P. Matas, J. Uehara, R. P. Behringer: Gas-driven subharmonic waves in a vibrated two-phase granular material, *European Physical Journal E* 25, 431 (2008).
- [122] D. I. Goldman, M. D. Shattuck, H. L. Swinney, G. H. Gunaratne: Emergence of order in an oscillated granular layer, *Physica A* 306, 180 (2002).
- [123] W. Knapp: Vacuum technology, J. A. Eichmeier, M. Thumm (eds.): Vacuum electronics, 483 (2008).
- [124] W. Chen: Experimental observation of self-localized structure in granular material, *Physics Letters A* 195, 321 (1995).
- [125] C. R. Wassgren, C. E. Brennen, M. L. Hunt: Vertical vibration of a deep bed of granular material in a container, *Journal of Applied Mechanics* 63, 712 (1996).
- [126] X.-D. Shang, X.-L. Qiu, P. Tong, K.-Q. Xia: Measured local heat transport in turbulent Rayleigh-Bénard convection, *Physical Review Letters* 90, 074501 (2003).
- [127] S. Fauve, C. Laroche, S. Douady: Dynamics of avalanches in a rotating cylinder, D. Bideau, J. Dodds (eds.): Physics of granular media, 277 (1991).
- [128] P. Vipul: Convective rolls in granular materials, student project, Indian Institute of Technology, New Delhi (2011).
- [129] ASAE: Density, specific gravity, and mass-moisture relationships of grain for storage; in: ASAE standards 1990: standards, engineering practices and data, American Society of Agricultural Engineers (1999).
- [130] J. M. N. T. Gray, B. P. Kokelaar: Large particle segregation, transport and accumulation in granular free-surface flows, *Journal of Fluid Mechanics* 652, 105 (2010).
- [131] C. C. Landreth, R. J. Adrian: Impingement of a low Reynolds number turbulent circular jet onto a flat plate at normal incidence, *Experiments in Fluids* 9, 74 (1990).

## Bibliography

- [132] R. Ramírez, D. Risso, and P. Cordero, Thermal convection in fluidized granular systems, *Physical Review Letters* 85, 1230 (2000).
- [133] D. Paolotti, A. Barrat, U. M. B. Marconi, A. Puglisi: Thermal convection in monodisperse and bidisperse granular gases: a simulation study, *Physical Review E* 69, 061304 (2004).
- [134] P. Sunthar, V. Kumaran: Characterization of the stationary states of a dilute vibrofluidized granular bed, *Physical Review E* 64, 041303 (2001).
- [135] J. Kreft, M. Schröter, J. B. Swift, H. L. Swinney: Fluidization of a vertically oscillated shallow granular layer, arXiv:0704.3852v2 (2007).
- [136] J. Lee: Heap formation in two-dimensional granular media: *Journal of Physics A: Mathematical and General* 27, L257 (1994).
- [137] K. Liffman, G. Metcalfe, P. Cleary: Granular convection and transport due to horizontal shaking, *Physical Review Letters* 79, 4574 (1997).
- [138] M. A. Naylor, M. R. Swift, and P. J. King: Air-driven Brazil nut effect, *Physical Review E* 68, 012301 (2003).
- [139] R. J. Milburn, M. A. Naylor, A. J. Smith, M. C. Leaper, K. Good, M. R. Swift, P. J. King: Faraday tilting of water-immersed granular beds, *Physical Review E* 71, 011308 (2005).
- [140] P. J. King, P. Lopez-Alvarez, H. A. Pacheco-Martinez, C. P. Clement, A. J. Smith, M. R. Smith: Instabilities in vertically vibrated fluid-grain systems, *European Physical Journal E* 22, 219 (2007).
- [141] R. M. Lueptow, A. Akonur, T. Shinbrot: PIV for granular flows, *Experiment in Fluids* 28, 183 (2000).
- [142] J. Jaimes, G. G. Joseph, E. Geffroy, B. Mena, J. R. Herrera-Velarde: Pattern formation in oscillatory granular flows, *Revista Mexicana de Física* 48, 534 (2002).
- [143] B. Painter, R.P. Behringer: Substrate interactions, effects of symmetry breaking, and convection in a 2d horizontally shaken granular system, *Physical Review Letters* 85, 3396 (2000).
- [144] E. Brown, G. Ahlers: Rotations and cessations of the large-scale circulation in turbulent Rayleigh–Bénard convection, *Journal of Fluid Mechanics* 568, 351 (2006).
- [145] H.-D. Xi, Q. Zhou, K.-Q. Xia: Azimuthal motion of the mean wind in turbulent thermal convection. *Physical Review E*. 73, 056312 (2006).
- [146] H.-D. Xi, S.-Qi Zhou, Q. Zhou, T.-S. Chan, Ke-Q. Xia: Origin of the temperature oscillation in turbulent thermal convection, *Physical Review Letters* 102, 044503 (2009).
- [147] K. Sugiyama, R. Ni, R. J. A. M. Stevens, T. S. Chan, S.-Q. Zhou, H.-D. Xi, C. Sun, S. Grossmann, K.-Q. Xia, D. Lohse: Flow reversals in thermally driven turbulence, *Physical Review Letters* 105, 034503 (2010).
- [148] A. Vasiliev, P. Frick: Reversals of large-scale circulation in turbulent convection in rectangular cavities, *Journal of Physics: Conference Series* 318, 082013 (2011).
- [149] V. Frette, J. Stavans: Avalanche-mediated transport in a rotated granular mixture, *Physical Review E* 56, 6981 (1997).
- [150] G. Juarez, J. M. Ottino, R. M. Lueptow: Axial band scaling for bidisperse mixtures in granular tumblers, *Physical Review E* 78, 031306 (2008).
- [151] T. Arndt, T. Siegmann-Hegerfeld, S. J. Fiedor, J. M. Ottino, R. M. Lueptow: Dynamics of granular band formation: Long-term behavior in slurries, parameter space, and tilted cylinders, *Physical Review E* 71, 011306 (2005).
- [152] S. B. Savage: Disorder, diffusion and structure formation in granular flows, D. Bideau, A. Hansen (eds.): *Disorder and granular media*, Elsevier, 255 (1993).
- [153] B. Levitan: Long-time limit of rotational segregation of granular media, *Physical Review E* 58, 2061 (1998).
- [154] EPICA community members: Eight glacial cycles from an Antarctic ice core, *Nature* 429, 623 (2004).
- [155] J. Braun, M. Mattia: Attractors end noise: twin drivers of decisions and multistability, *Neuroimage* 52, 740 (2010).
- [156] H. Caps, R. Michel, N. Lecocq, N. Vandewalle: Long lasting instabilities in granular mixtures, *Physica A* 326, 313 (2003).
- [157] R. Chicharro, R. Peralta-Fabi, R. M. Velasco: Segregation in dry granular systems, R. Behringer, J. Jenkins (eds.): *Powders & Grains* 97, Balkema, Rotterdam, 479 (1997).

- [158] S. Morris: private communication, Oct. (2007).
- [159] N. Taberlet, M. Newey, P. Richard, W. Losert: On axial segregation in a tumbler: an experimental and numerical study, *Journal of Statistical Mechanics: Theory and Experiment*, P07013 (2006).
- [160] M. K. Newey: Mechanisms for axial band formation in a rotating drum of granular material, doctoral thesis, University of Maryland (2006).
- [161] T. Finger: Segregationsdynamik granularer Mischungen in einer horizontalen rotierenden Röhre, diploma thesis, University of Magdeburg (2006).
- [162] C. M. Dury, G. H. Ristow: Radial segregation through axial migration, *EPL* 48, 60 (1999).
- [163] D. C. Rapaport: Simulational studies of axial granular segregation in a rotating cylinder, *Physical Review E* 65, 061306 (2002).
- [164] G. Seiden, S. G. Lipson, J. Franklin: Oscillatory axial banding of particles suspended in a rotating fluid, *Physical Review E* 69, 015301(R) (2004).
- [165] A. P. J. Breu, C. A. Kruelle, I. Rehberg: Oscillatory patterns in a rotating aqueous suspension, *European Physical Journal E* 13, 189 (2004).
- [166] E. Guyez, P. J. Thomas: Spatiotemporal segregation-pattern drift in particle-laden rimming flow, *Physical Review Letters* 100, 074501 (2008).
- [167] E. Guyez, P. J. Thomas: Effects of particle properties on segregation-band drift in particle-laden rimming flow, *Physics of Fluids* 21, 033301 (2009).
- [168] G. Schubert (department of dyeworks at Sigmund Lindner GmbH, Germany), private information concerning sol-gel coating for spheres of type ‘Siliglit 4508-187-L’; (2012).
- [169] S. Asakura, F. Oosawa: Interaction between particles suspended in solutions of macromolecules, *Journal of Polymer Science* 33, 183 (1958).
- [170] P. M. Reis, T. Mullin: Granular segregation as a critical phenomenon, *Physical Review Letters* 89, 244301 (2002).
- [171] R. D. Kamien: Entropic attraction and ordering, G. Gompper, M. Schick (eds.): *Soft Matter, Vol.3, Colloidal order: entropic and surface forces*, 1 (2007).
- [172] T. Mullin: Coarsening of self-organized clusters in binary mixtures of particles, *Physical Review Letters* 84, 4741 (2000).
- [173] Sobel operator: [http://en.wikipedia.org/wiki/Sobel\\_operator](http://en.wikipedia.org/wiki/Sobel_operator)
- [174] R. Prusas: 2D Granulate – Scheiben in einer flachen drehenden Zelle, student thesis, University of Magdeburg (2012).
- [175] L. Fejes Tóth: *Regular figures*, The Macmillan Company, New York, chapter 27 (1964).
- [176] O. U. Uche, F. H. Stillinger, S. Torquato: Concerning maximal packing arrangements of binary disk mixtures, *Physics A* 342, 428 (2004).
- [177] T. Kennedy: Compact packings of the plane with two sizes of discs, *Discrete Computational Geometry* 35, 255 (2006).
- [178] N. Jain, D. V. Khakhar, R. M. Lueptow, J. M. Ottino: Self-organization in granular slurries, *Physical Review Letters* 86, 3771 (2001).